The Journal of Microwave Power

Volume 10, No. 1, March 1975

THE INTERNATIONAL MICROWAVE APPLICATIONS JOURNAL DEVOTED TO THE INDUSTRIAL SCIENTIFIC AND MEDICAL USES OF MICROWAVE POWER

10th YEAR OF PUBLICATION

A publication of
THE INTERNATIONAL MICROWAVE POWER INSTITUTE — CANADA
— EDMONTON, LONDON, NEW YORK AND WARSAW —

THE JOURNAL OF MICROWAVE POWER

Volume 10, No. 1, March 1975

An International Journal of Industrial, Scientific and Medical Applications in the frequency range of 100 MHz - 100 GHz
Published quarterly since 1966

A Publication of THE INTERNATIONAL MICROWAVE POWER INSTITUTE

 Second Class Mail Registration No. 3059

MEMBERSHIP APPLICATION FORM*

☐ I wish to join IMPI and receive JMP and the Newsletter. Please bill me ($20).

Name .....

Address .....

.....

☐ Please enter my subscription to the Newsletter (non-members) $6.

☐ Please send me announcements on IMPI publications, symposia, and short courses

..... Signature

*** LIBRARIES: PLEASE SEE REAR COVER THIS ISSUE 10(1)**

AIRMAIL

IMPI
Box 1556
Edmonton
Alberta T5J 2N7
Canada

The Journal of Microwave Power

Volume 10, No. 1, March 1975

TABLE OF CONTENTS

Printed and published in Canada with the cooperation of IMPI-Europe. London office: IMPI-London Ltd., 89 Northwood Ave., Purley, Surrey CR2 2ES, England. New York address: (Office of the President of the Institute), Box 462, Alpine, N.J. 07620, U.S.A. This IMPI publication is supported by a generous grant from the National Research Council of Canada.

The Journal of Microwave Power
is the official publication of the
INTERNATIONAL MICROWAVE POWER INSTITUTE

The International Microwave Power Institute, a Canadian Non-Profit Charter Organization, is managed by a Board of Governors and an Executive Directorate. The Institute was founded in 1966, and subsequently granted Letters Patent by the Secretary of State for Canada, by application of Alan E. Supplee, Donald A. Dunn, James A. Jolly, John E. Gerling, William C. Brown, and W. A. G. Voss, who formed the first Board of Governors. Election of Governors and Officers and their terms of reference are as stated in the By-Laws, available upon request. The annual general meeting of the Institute is held at the time of the annual international symposium.

Responsibility for the contents of this Journal rests upon the authors and not upon the Institute, its committees, or its members. In certain cases, individual reprints of papers may be purchased from the Institute. The Journal is distributed to members as published, and it is available to libraries by special subscription. A directory of services to the microwave power industry is published by the Institute.

Information on the *Transactions of IMPI* and the *IMPI Newsletter* appear on the rear cover.

The Board of Editors acknowledge with gratitude the invaluable assistance of a large community of referees and various patrons, in particular the National Research Council of Canada and the University of Alberta. Manuscripts should be submitted, according to the publication policy given at the end of the Journal, to the Editor except in the case of invited papers, which should be sent to the corresponding Associate Editor.

Membership dues: $20/yr., includes the Journal and Newsletter.

The IMPI Newsletter is printed and published in Regina, Canada.
Senior Editor: P. Bhartia, Faculty of Engineering, The University of Saskatchewan, Regina, Saskatchewan S4S 0A2.
Airmail $6/yr. (Members free)

REGISTERED OFFICES

(For membership, circulation, publication, information and symposia)

IMPI, Box 1556, Edmonton, Canada 403-432-5147

In Europe: IMPI Ltd., (London), 89 Northwood Avenue, Purley, Surrey, CR2 2ES, U.K.

Printed and Published by IMPI in Canada at the University of Alberta.
Federal Sales Tax Exempt. Second Class Mail Registration No. 3059.

Microwave and Infra-red Effects on Heart Rate, Respiration Rate and Subcutaneous Temperature of The Rabbit*

L. Birenbaum†, I. T. Kaplan, W. Metlay, S. W. Rosenthal†, and M. M. Zaret

ABSTRACT

Microwaves (CW, 2.4 GHz) were used to irradiate the dorsal aspect of the head of unanesthetized rabbits at power levels from 0 to 80 mW/cm². Respiration rate, heart rate and subcutaneous temperature were monitored. Increases in all 3 indices resulted, with the greatest increases at the highest power levels. Respiration rate increases were 20 times greater than those in the heart rate.

CW and pulsed microwaves at 2.8 Ghz, 20 mW/cm² average power level, were used to irradiate the entire dorsal surface of the animal. No significant difference in any of the 3 indices between the CW and pulsed responses could be detected.

CW 2.4 GHz microwave and infra-red whole back irradiations were carried out at 0, 10, and 20 mW/cm² levels. Although respiration and heart rate changes were substantially the same, subcutaneous temperature increased more rapidly and rose to higher values for the infra-red case.

Introduction

The rabbit is one of the most commonly used animals for research into the biological effects of microwaves. Despite this, from published data, it is very difficult to extract answers to the relatively unsophisticated questions addressed in this study: What is a convenient sensitive indicator of physiological effect for the rabbit when it is subjected to microwave radiation? Is there a difference between the response to CW and to pulsed radiation? Does the animal respond

* Manuscript received August 21, 1974; in revised form December 18, 1974.

† Authors' affiliations: L. Birenbaum and S. W. Rosenthal—Dept. of Electrical Engineering and Electrophysics, Polytechnic Institute of New York, Graduate Center, Farmingdale, N.Y. 11735; I. T. Kaplan—Dept. of Psychology, The City College, New York, N.Y. 10031; W. Metlay—Dept. of Psychology, Hofstra University, Hempstead, N. Y. 11550; M. M. Zaret, M.D.—Dept. of Ophthalmology, N.Y.U. School of Medicine, N.Y., N.Y. 10016

This study was supported by the Office of Naval Research Contract N00014-69-C-0358 and by the Joint Services Technical Advisory Committee under Contract F44620-69-0047. Results of the first experiment were presented as part of a paper by Zaret, *et al.* at the 5th IMPI International Symposium, Oct. 1970, Scheveningen, Holland. Content of paper as a whole was presented by Birenbaum, *et al.* at the URSI Dec. 1972 meeting in Williamsburg, Virginia.

differently to microwaves than to infra-red radiation? At the 10 mW/cm^2 level, is there any clear evidence of biological effect?

In the work reported here with unanesthetized animals, three physiological indicators were employed: heart rate, respiration rate and subcutaneous temperature. One experiment at 2.4 GHz, a continuation of our earlier work, [1] exposed the dorsal surface of only the head to CW power levels of 0, 20, 40, 60, 80 mW/cm^2 in the far field to see how the three indicators responded when the animal was irradiated. A second experiment at 2.8 GHz compared the effects of exposure of the entire dorsal surface to CW and to pulsed microwaves at average incident power levels of 20 mW/cm^2. In a third experiment, the entire dorsal surface was exposed to 2.4 GHz CW microwaves at power levels of 0, 10, 20 mW/cm^2, and then, for comparison, to CW infra-red irradiation in the same environment at identical power levels.

Other investigators have reported experimental findings which, though not directly comparable with ours, do provide perspective.

Ely, *et al.* [2] subjected rabbits to whole-body (profile) irradiation at 2.88 GHz pulsed microwaves. They measured the resulting steady-state increases in rectal temperature. A level of 25 mW/cm^2 (average) was found to produce a 1°C rise; a 40 mW/cm^2 level gave a 3.5°C rise; higher levels were lethal.

Presman and Levitina [3] exposed rabbits to CW and to pulsed microwaves, and measured changes in the heart rate. Their results appeared to be quite complex. CW irradiation (2.4 GHz, 7-12 mW/cm^2) of the dorsal aspect of the head resulted in heart rate increases. Pulsed irradiation (3.0 GHz, 3-5 mW/cm^2, 0.0007 duty cycle) produced the same result, except that pulsed power was reported as being more effective than CW. On the other hand, CW irradiation of the whole back gave heart rate reductions, whereas pulsed irradiation gave no change in heart rate. According to Presman and Levitina, these observations fitted the following conceptual framework: The power densities were so low that the animals did not detect thermal stimuli; any effects noted were due to other mechanisms; CW power excited surface receptors only, but pulsed power having 1400 times the intensity during the pulse interval, perhaps penetrated deeply enough to act directly on the brain cells. Unfortunately, the reliability of this line of reasoning is faulted, since a replication of one of their CW procedures by Kaplan, *et al.* [1] gave a result completely at variance with theirs.

Schwan [4] asked the question, "Is it possible that pulsed radiation can be more effective in bringing about biological changes than continuous radiation of the same average power?" On theoretical grounds, based primarily upon insight gained from experimental pearl-chain investigations, he concluded that the answer is negative for reversible effects.

Deichmann, *et al* [5] used rats to compare the effects of microwaves and infra-red irradiation. Rectal and subcutaneous temperatures were used as indicators. With equal 300 mW/cm^2 power densities (a lethal level), infra-red induced temperature increases occurred much more slowly than their 24.6 GHz (pulsed) microwave counterparts. In another experiment, they were able to obtain the same temperature variation in both cases by raising the infra-red power density level. A microwave power level of 43 mW/cm^2 was found to be equivalent to an infra-red level about 3 times higher in the rat.

General Procedure

The procedure used in the 3 experiments described here was similar to that employed in our earlier work [1]. Each experiment was performed by first confining the animal in a wooden squeeze box (Figure 1) open at the sides and on the top. The rabbit was restrained from escaping by suitably positioned wooden dowels. Next, the animal was instrumented by inserting three curved surgical needles as electrodes for EKG recording into the skin of the left chest, right chest and left hip. A strain gauge, (Parks Electronics), consisting of a hollow 1.0 mm diameter rubber tube containing a 0.4 mm diameter mercury column, was tied around the thorax to sense respiration. Finally, a hypodermic thermistor probe (Yellow Springs model 524) was inserted subcutaneously near the midline of the lower back to measure temperature.

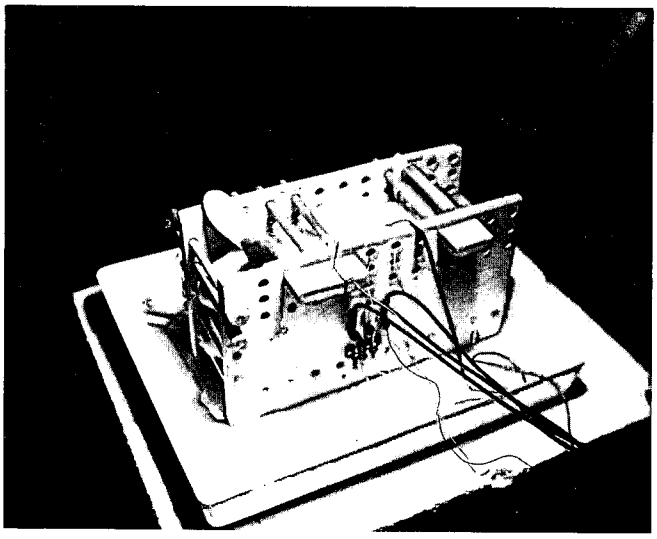

Figure 1. View of rabbit in wooden squeeze box, instrumented for exposure. Also seen are a polystyrene waste tray in which the box is placed, and a polystyrene foam block. Radiation is from above, with the electric field polarized perpendicular to the sides of the box (Replica [1]).

After instrumentation, the animal in its squeeze box was placed on a large polystyrene waste tray, and then positioned within a microwave anechoic chamber with inner dimensions $102 \times 102 \times 163$ cm high. The interior was lined with 61×61 cm CV-4 absorber panels manufactured by Emerson-Cuming. Height above the floor of the chamber was adjusted by placing foam polystyrene blocks under the tray. Ventilation occurred through an open side panel of the chamber and through an opening at the top. The animal was irradiated from above.

Each session of each experiment began with a fifteen minute acclimatization period. Then, data was collected during a 10-minute pre-irradiation period, and during a subsequent radiation period.

Exactly the same animals, two New Zealand male albino rabbits, were used in all three experiments. In the second, however, an additional experimental condition required that 2 more animals be used. Weight range was 3.5 - 4.7 kg. An interval of at least one week elapsed between successive exposures of the same animal.

Initially, before these procedures were begun, it was found that the respiration and heart rates of each animal fluctuated widely in response to the changes,

discomfort and constraints that accompanied the experimental situation. Only after many months of sham exposure did the animals become sufficiently acclimatized for these fluctuations to abate. For this reason, our experimental design was based upon the repeated use of the same animals, rather than upon the use of a very large number of different animals.

Experiment 1 - CW Microwave Irradiation of the Head

Procedure—As a source of 2.4 GHz (12.5 cm wavelength) CW microwaves, we used a magnetron-fed 20 × 15 cm rectangular aperture horn positioned at the top of the anechoic chamber, with the main lobe directed downward. Power density of 20 mW/cm^2 was set by use of a Ramcor 1250A densiometer at the level of the animal's head with the squeeze box absent. Higher power levels were set by increasing the magnetron voltage and relying on calibrated attenuators and a power meter in the monitoring line. The area of uniform illumination was considerably larger than the top of the box. The distance from the horn aperture to the top of the animal's head, 74 cm, exceeded the minimum far field distance of $2d^2/\lambda = 2(20)^2/12.5 = 64$ cm. At each power level (0, 20, 40, 60 and 80 mW/cm^2), the two subjects were each exposed twice to a 60 minute irradiation of the head. The remainder of the body was shielded by an absorber panel placed on top of the squeeze box. The animals were exposed once per week to a different power level each week in counterbalanced order.

Following the fifteen minute acclimatization period inside the anechoic chamber, the EKG, respiration and temperature were recorded at one minute intervals during both the ten-minute pre-irradiation period and during the 60 minute exposure period. Each EKG and respiration trace was 10 sec. in duration.

Results—The effects of different power levels on the respiration rate, heart rate and subcutaneous temperature are shown in Figure 2. Each point is the average of data taken during the 10 minute interval indicated on the abscissa for 2 animals, 2 exposures/animal. Straight lines through the data points were fitted using the method of least squares. For clarity, sections of the heart rate and temperature graphs were displaced vertically.

To assign a measure for the variability of the data represented by the points of Figure 2, the following procedure was used: for each physiological indicator, for each of the 5 power levels, the pre-irradiation mean was separately calculated. The standard deviation was then obtained from these 5 means for each indicator. Results were 4.6 beats/min for the heart rate; 22.4 breaths/min for respiration; 0.2°C for subcutaneous temperature.

Table 1 gives the change/minute in the three indicators during the period of irradiation. The entries are the slopes of the linear graphs, or the initial 10 minute slope of the curved graphs.

When no radiation was present (0 mW/cm^2), each of the indicators decreased with time. This was an expected finding since the animal first experienced the trauma of being shifted from its regular quarters to a squeeze box and then was allowed to recover in the undisturbed environment of the anechoic chamber. When microwave power was present, increases occurred, with the rates of increase greatest at the highest power levels. The respiration rate was much more sensitive to increases in incident power density than the

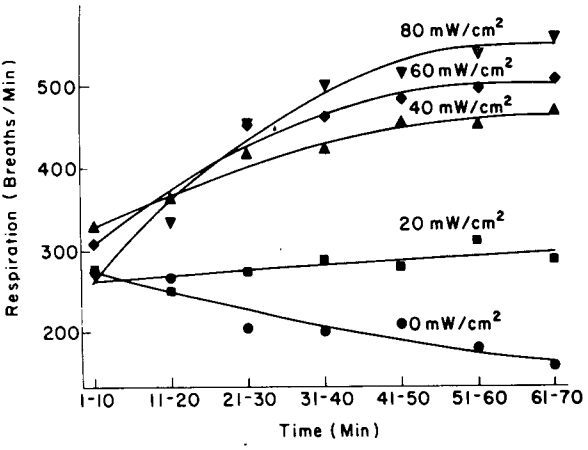

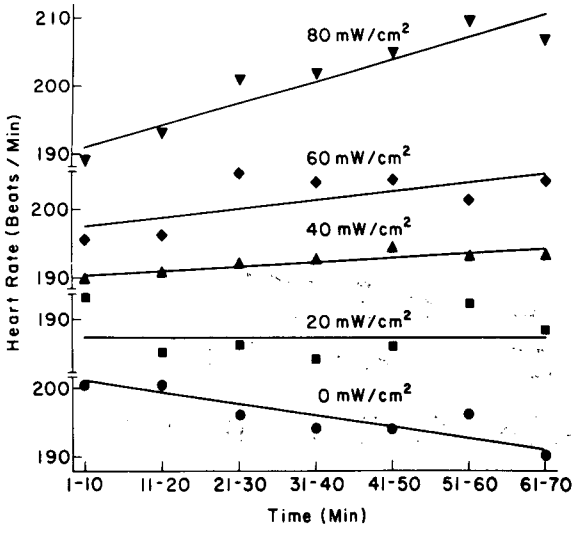

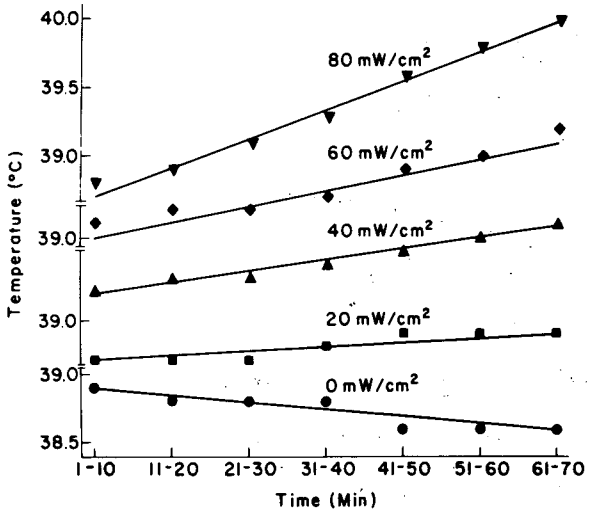

Figure 2 2.4 GHz CW irradiation of the head. Microwaves on for 1 hour after 10th minute of pre-exposure monitoring period. Each point is the average of 40 observations.

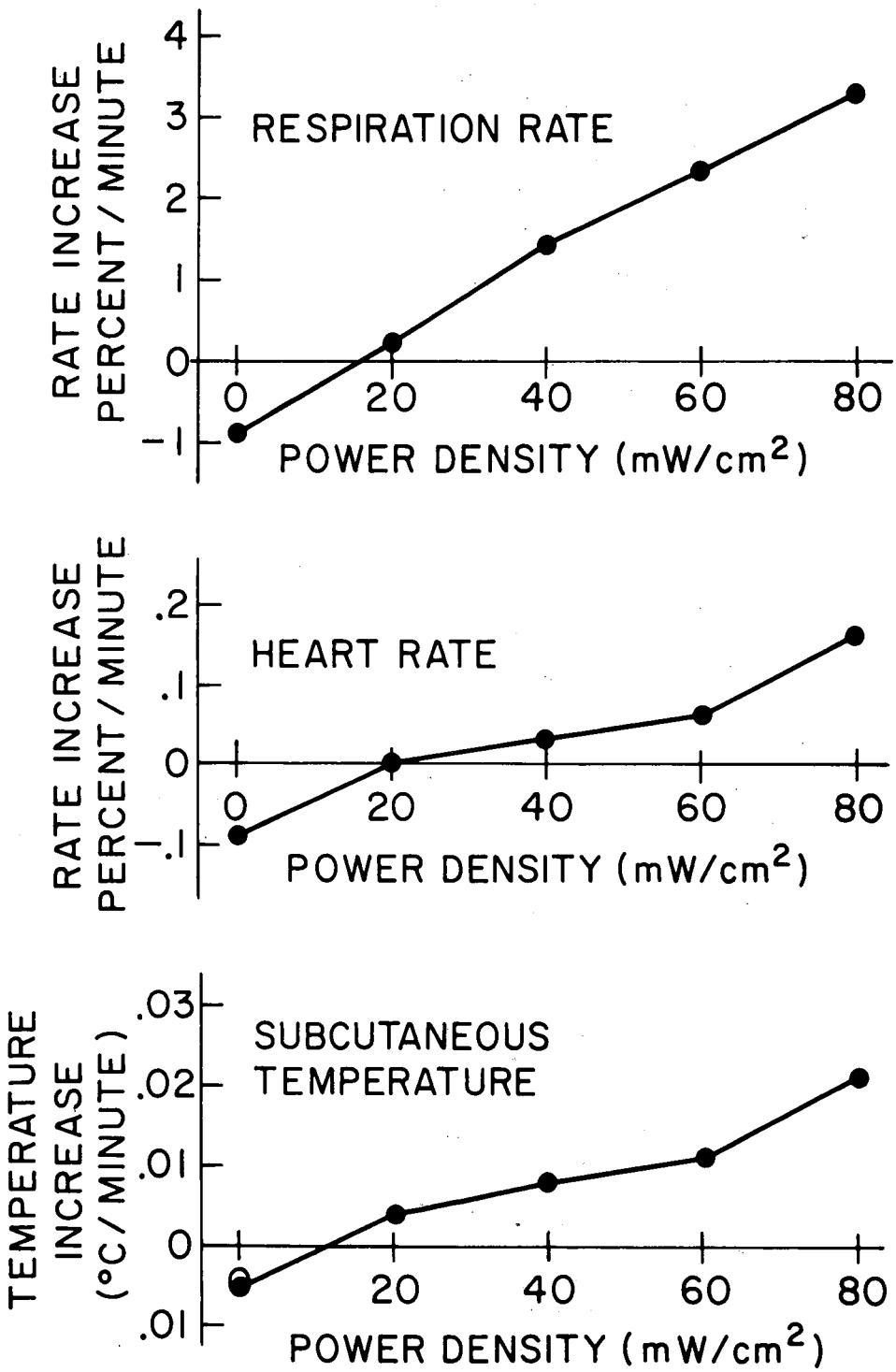

Figure 3 Response of 3 biological indicators to 2.4 GHz CW microwave irradiation of the head. Each point is the average of 4 observations (2 animals, 2 exposures/animal). Average pre-irradiation conditions were 292 breaths/min., 193.6 beats/min., 38.9°C.

heart rate. The percentage (rather than absolute) increases in these quantities are shown in Figure 3, constructed from Table 1 by dividing the entries by the average pre-irradiation respiration date (292 breaths/min.) and heart rate (193.6 beats/min.). The average pre-irradiation subcutaneous temperature was 38.9°C. Increases in this quantity represent increases in subcutaneous temperature over the whole body surface, since the thermistor temperature sensor was located in an area shielded from microwave radiation.

TABLE 1
CW MICROWAVE IRRADIATION OF THE HEAD

	Change/min of irradiation		
Power density (mW/cm^2)	Heart rate (beats/min)	Respiration (breaths/min)	Temperature (°C)
0	−0.17	−2.66	−0.005
20	0.00	0.61	0.004
40	0.06	4.13	0.008
60	0.13	6.64	0.011
80	0.32	9.39	0.021

Experiment 2 - Comparison of CW and Pulsed Irradiation

Procedure—CW power at 2.8 GHz was obtained from a QK 60 magnetron, and directed downward through the same rectangular horn as in the preceding experiment. A 2J32 magnetron was used to supply 2.8 GHz 1.3 μs wide microwave pulses, 1000/sec. The choice of frequency was dictated by availability of equipment. Average power levels of 20 mW/cm^2 were set exactly as in the preceding experiment with the Ramcor densiometer. The equipment arrangement is shown in Figure 4.

The four subjects were each exposed four times to pulsed microwaves and four times to CW in counterbalanced order. Pre-exposure time was 10 min. and exposure time was 20 min. In this experiment, the shielding absorber panel was not used, so that the entire dorsal surface was irradiated. Records were taken every two minutes throughout the 30 minute data-collecting period.

Results—In Figure 5 are shown the effects of CW and pulsed power on respiration, heart rate and temperature. During the irradiation period, the respiration and temperature increased markedly, and the heart rate remained nearly constant. To determine whether there was any real difference between the responses to CW and pulsed irradiation, Table 2 was constructed, giving the average change/min. for each indicator during irradiation for each of the four animals. Difference-t tests, when performed on this data, revealed that none of the differences between the pulsed and CW conditions even approached significance at the 0.05 level.

Experiment 3 - Comparison of Microwave and Infra-Red Irradiation

Procedure—The 2.4 GHz CW microwave equipment arrangement and procedure were the same as that of the first experiment, except that power densities of 0, 10 and 20 mW/cm^2 were used, and the shielding absorber panel was removed to permit irradiation of the entire dorsal surface.

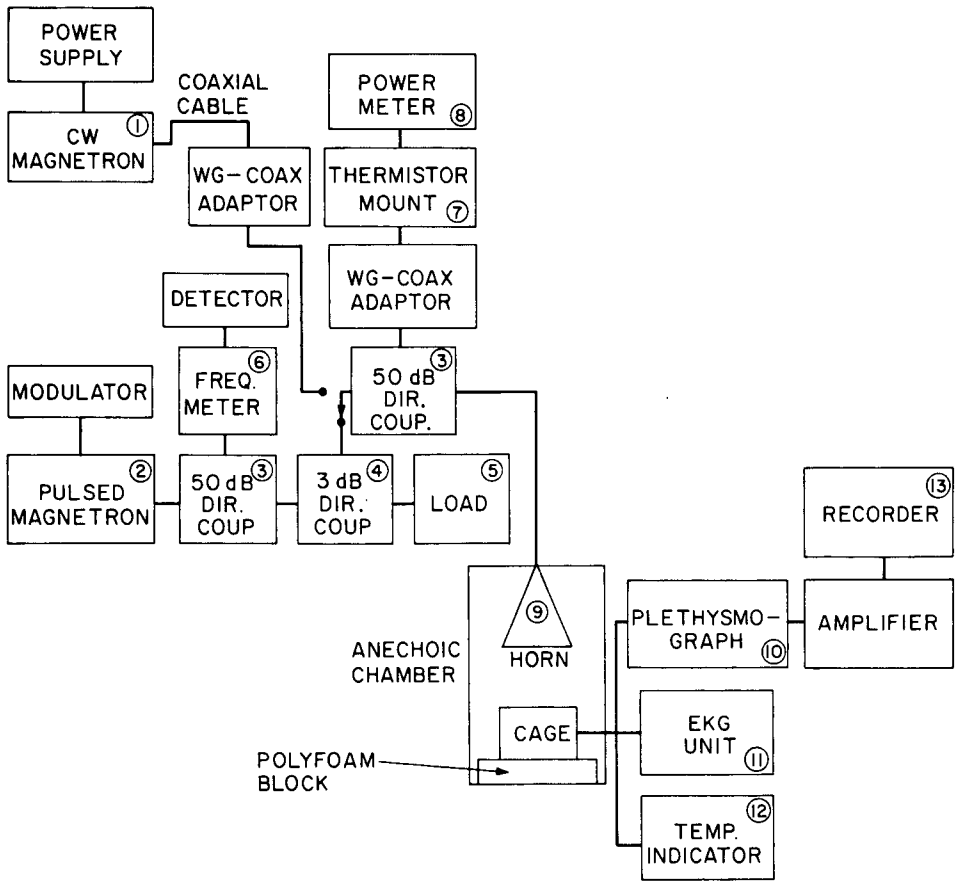

Figure 4 Equipment for CW vs. pulsed irradiation experiment at 2.8 GHz. 1. QK60. 2. 2J32. 3. Sperry 545 cross-guide. 4. FXR S610A top-wall. 5. ARF Products DA-18/U. 6., 7., 8., Hewlett-Packard 536A, 478A, 431B. 9. DeMornay-Bonardi DBL-520. 10. Parks Electronics 270. 11. Sanborn 572. 12. Yellow Springs 43TA. 13. TechniRite TR711.

TABLE 2
CW VERSUS PULSED MICROWAVE IRRADIATION AT 20 mW/cm²

	Change/min of irradiation					
	Heart Rate (beats/min)		Respiration (breaths/min)		Temperature (°C)	
Rabbit	CW	Pulsed	CW	Pulsed	CW	Pulsed
1	−0.54	0.02	4.60	5.95	0.066	0.069
2	0.01	−0.36	−0.88	5.60	0.055	0.064
3	0.05	−0.11	4.58	4.39	0.057	0.076
4	0.75	0.29	3.08	3.18	0.067	0.068

To obtain infra-red radiation, we substituted an ordinary bowl heater for the microwave horn, and set the thermal flux density by use of an Eppley thermopile and Keithley 150 A microvolt-ammeter. As an indicator of the

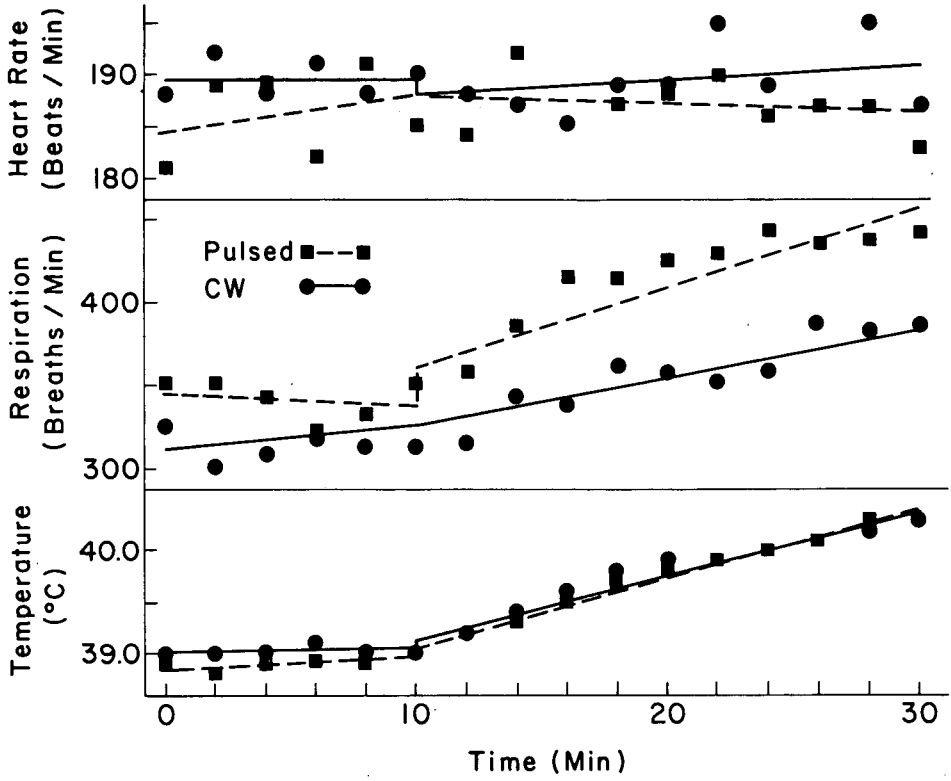

Figure 5 CW vs. pulsed irradiation at 2.8 GHz of the whole body via the dorsal surface: Microwave on for 20 minutes after 10th minute of pre-exposure monitoring period. Each point is the average of 16 observations. Average power density 20 mW/cm^2.

infra-red spectrum, we measured the temperature of the heater wires using an iron-constantan thermocouple junction. Assuming a black-body spectral distribution [6], the conditions corresponding to the 10 and 20 mW/cm^2 power densities were shown in Table 3.

TABLE 3
INFRA-RED IRRADIATION CONDITIONS

IR power density	bowl heater wire temperature	IR spectrum peak	IR bandwith lower-upper ½ power wavelengths
10 mW/cm^2	417°C	4.15 μm	2.55 – 7.60 μm
20 mW/cm^2	540°C	3.55 μm	2.17 – 6.47 μm

The two subjects were the same animals used in both preceding experiments. At each power level (0, 10, 20 mW/cm^2) each animal was exposed twice to a 60 min. irradiation. Hence, in addition to two sham exposures with no incident radiation, each animal was given a total of four microwave exposures,

and a total of four infra-red exposures. After all of the microwave work had been completed, the infra-red exposures were initiated. EKG, respiration and temperature were recorded at 5 min. intervals during both the 10 min. pre-irradiation period and the 60 min. exposure period.

Results—The effects of CW microwave radiation on respiration rate, heart rate and subcutaneous temperature are presented in Figure 6. Each data point is the average of 4 observations corresponding to 2 exposures/animal/condition. In the case of the heart rate, the graphs were vertically displaced for clarity. The effects of IR irradiation are similarly presented in Figure 7. The same data for the 0 mW/cm^2 condition was used in both figures.

In order to find a measure for the variability of the data represented by the points of Figures 6 and 7, a procedure was adopted similar to that used in experiment 1. For each of the 5 different irradiation conditions, for each indicator, the standard deviation about the mean of the pre-irradiation points at 0, 5 and 10 minutes was calculated. The 5 standard deviations so obtained were averaged for each indicator with these results: 2.5 beats/min for the heart rate; 22.3 breaths/min. for respiration, and 0.0°C for subcutaneous temperature.

Tables 4 and 5 summarize the results by giving the rates of increase and decrease (per minute) of the three indicators. The respiration rates, which decrease an average of 0.7 breaths/min. when radiation is absent, are seen to increase about 2 breaths/min. for both microwave and infra-red radiation when 20 mW/cm^2 is present. Heart rate, which decreases somewhat (about 0.1 beats/min.) without irradiation, is constant (IR) or increases (about 0.1 beats/min.) at 20 mW/cm^2. Thus, respiration and heart rates respond in substantially the same way to microwaves and infra-red. On the other hand, subcutaneous temperature increases more rapidly and reaches higher final values with IR than with microwaves. This result is consistent with the finding that IR is absorbed near the surface to a greater degree than microwaves.

TABLE 4
CW MICROWAVE IRRADIATION OF THE WHOLE BACK

	Change/min. of irradiation		
Power density (mW/cm^2)	Heart Rate (beats/min)	Respiration (breaths/min)	Temperature (°C)
0	−0.11	−0.69	0.002
10	0.02	0.30	0.011
20	0.07	2.46	0.019

TABLE 5
INFRA-RED IRRADIATION OF THE WHOLE BACK

	Change/min. of irradiation		
Power density (mW/cm^2)	Heart Rate beats/min)	Respiration (breaths/min)	Temperature* (°C)
10	−0.10	2.05	0.093
20	0.00	2.00	0.157

* During the first 10 min. of irradiation.

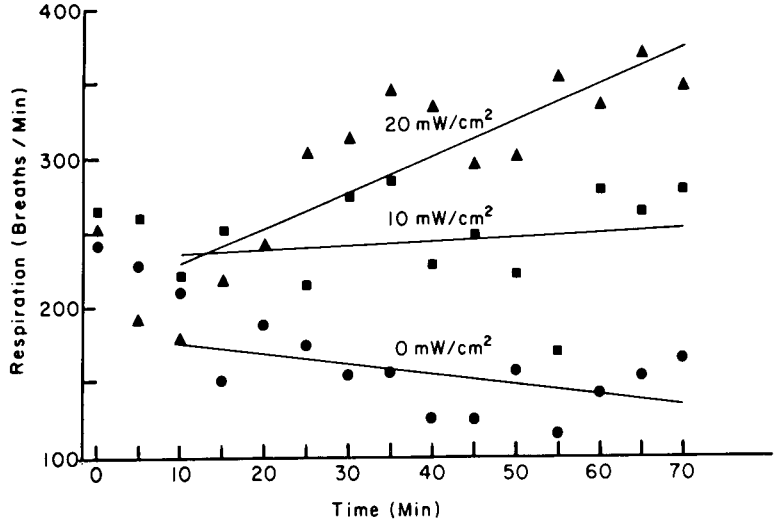

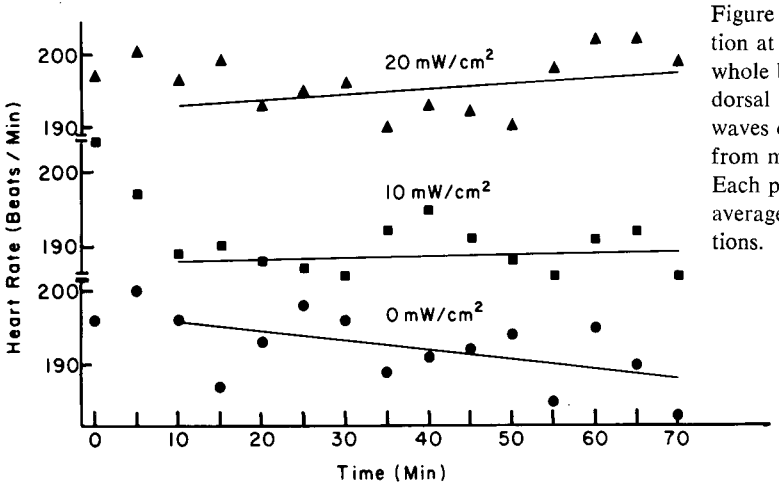

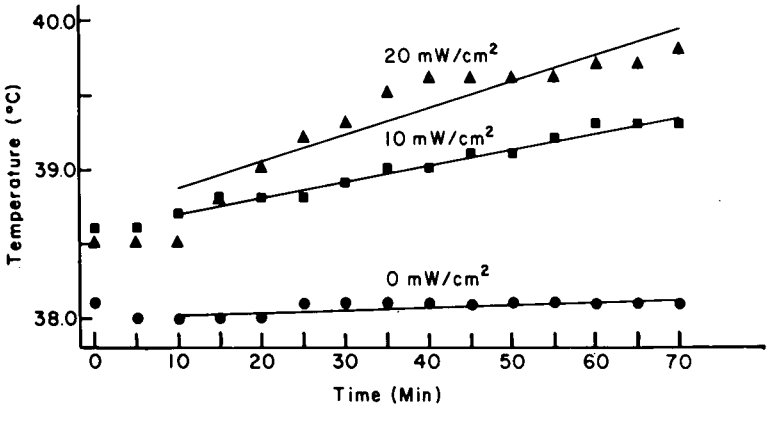

Figure 6 CW irradiation at 2.4 GHz of the whole body via the dorsal surface. Microwaves on for 1 hour from minute 10 to 70. Each point is the average of 4 observations.

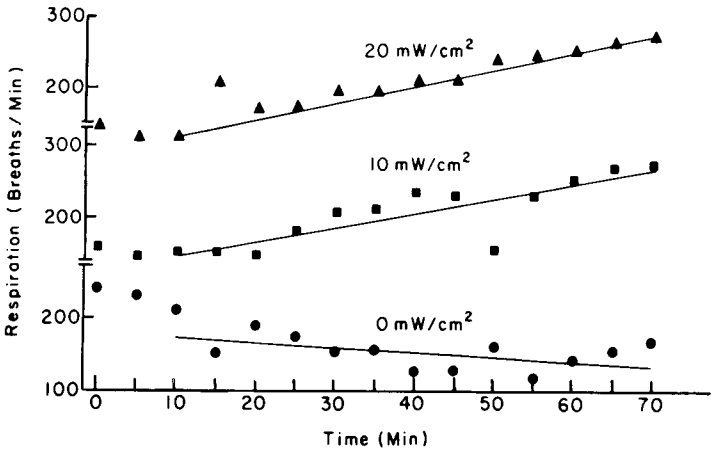

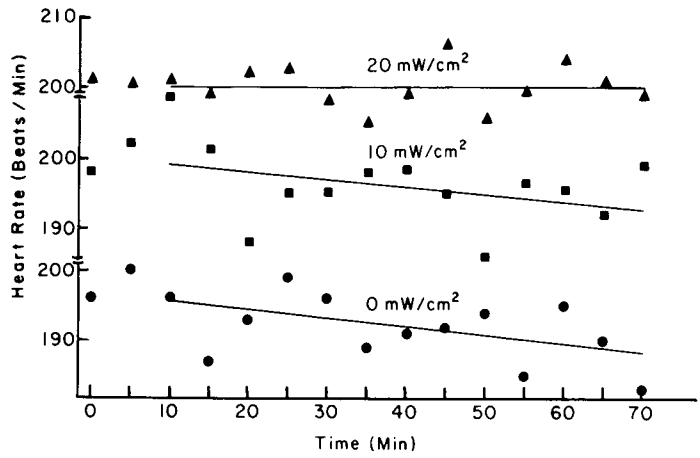

Figure 7 Infra-red CW irradiation of the whole body via the dorsal surface. Radiation on for 1 hour from minute 10 to70. Each point is the average of 4 observations.

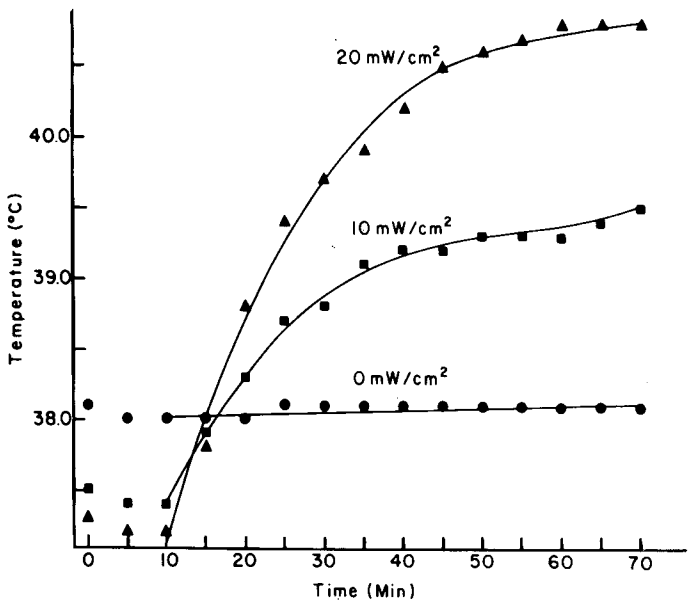

Discussion

Experiment 1—(2.4 GHz CW irradiation of the head only)—Figure 3, incorporating the results, shows that the respiration rate is very sensitive, and the heart rate relatively insensitive, to changes in the level of incident microwave radiation. Quantitatively, on a percentage basis, a rise in radiation level produced respiration rate increases at least 20 times greater than those in the heart rate. This observation is an interesting one because previous investigators in this area have utilized temperature and heart rate as indicators. None, to our knowledge, except in our own earlier study [1] has used respiration rate. The ease with which instrumentation for respiration may be accomplished, and the relative sensitivity of this indicator, should prove useful in later investigations of bioeffects of microwaves utilizing the rabbit.

Experiment 2—(2.8 GHz CW and pulsed 20 mW/cm^2 irradiation, total dorsal surface)—When responses to CW and pulsed microwaves were compared, for the same average power, no significant differences were found to exist at the 0.05 level in respiration, heart rate or temperature changes during irradiation. It is not evident that this result should have been obtained.

From one point of view, during the 1.3 μs wide pulse, the power level was pulse period/pulse width = 770 times higher than during the CW exposures, so that the fields at any given depth inside the animal were $\sqrt{770} = 28$ times greater. If 1.5 cm is taken as the depth of penetration [7], δ, at 2.8 GHz, one may calculate that during the pulse, the exponentially decaying fields penetrate an additional distance of 5 cm into the animal before they reach levels comparable with those existing during CW irradiation. Hence, one may compere "penetration depths" of 1.5 cm and 6.5 cm, for the CW and pulsed situation, into a rather small animal. The suggestions by Presman and Levitina [3] that electromagnetic field effects cause direct involvement of the central nervous system is an interesting one. However, since the responses to the two types of radiation were similar, one can assume that the dominant physiological mechanisms causing changes in the three indicators were the same for both CW and pulsed radiation under the test conditions. Hence, the responses we obtained appear to be related to the thermal burden induced by the absorbed energy and unrelated to the concept of direct alteration in electrophysiological activity.

In this experiment, of the 4 animals that were irradiated, 2 had been previously exposed to all of the conditions of experiment 1, and 2 were "new". None of the 4 showed any consistent differences in response to CW versus pulsed microwaves. In this respect, there was no difference between the set of 2 animals previously exposed, and the set exposed for the first time. Hence, this data reveals no evidence of adaptive mechanisms that might have become operative during the repeated exposures of Experiment 1.

Our data does exhibit a consistent difference between the CW and pulsed absolute respiration rates. It is present both during the 10 min. pre-irradiation monitoring period and subsequently; that is, it is independent of whether or not the animal is being irradiated. This may be due to the 120 cycle noise produced by the power transformers in the modulator unit.

Experiment 3—(2.4 GHz CW and IR irradiation, total dorsal surface)—A comparison of Figure 6 and Figure 7 reveals that heart and respiration response to CW microwaves and to IR were substantially the same, although

the subcutaneous temperature response was different. It is difficult to predict what the relative responses *should* be for a number of reasons. The reflection (or absorption) coefficients for 2.4 GHz and for IR may be entirely different. Also, the IR wavelength is so small that absorption depends on the projected area of the animal, or portion of the animal, seen by the incident beam. At 2.4 GHz, the 12.5 cm wavelength is comparable with the animal's size, resulting in an absorption profile which may differ considerably from that indicated by the projected area. This comment applies even more strongly to absorption by individual parts of the animal's body. Depth of penetration of microwaves greatly exceeds that of IR, so that energy deposition with depth is different, and therefore there is a difference in the excitation of surface receptors. Hence, relative response to IR and microwaves is not easily estimated.

There is a difference between the 0 and 10 mW/cm^2 IR respiration rate response (see Figure 7). Also, there is a difference between the 0 and 10 mW/cm^2 microwave respiration and heart rate response. Hence, 10 mW/cm^2 cannot be called an athermal level for the rabbit. *To our knowledge, the unequivocal demonstration of a physiological response to 10 mW/cm^2 has not been reported earlier.*

It is noted that time intervals between successive observations during the exposure sessions were 1, 2 and 5 min., respectively, during experiments 1, 2 and 3. While our procedures were being developed, we had observed that steady changes in the physiological indicators during irradiation were slow compared to momentary fluctuations. In fact, during 1 min. of irradiation the steady increase in heart rate was never greater than 1 beat/min., and the accompanying respiration rate increase did not exceed 10 breaths/min. The experience gained during the performance of experiment 1 showed that time between observations could be safely increased in view of the slow steady nature of the radiation-induced changes in the indicators.

Whether the wooden squeeze box by itself seriously perturbed the incident field was determined by performing an auxiliary measurement at 2.8 GHz. With the box present, and then absent, the incident power density was measured at several locations along the central axis of the box, normal to the sides, at the level of the top. The differences were of the order of 0.1 dB.

When instrumenting an experiment of this sort, the optimum procedure would be to use devices that are non-metallic, and hence not field perturbing by nature [8]. Although this was not possible here, attempts were made to minimize the extent of artifacts introduced. The EKG sensors, the three 1 cm long surgical needles, were imbedded ventrally, and hence the body of the animal served to provide shielding for the electrodes from the downward-directed microwave radiation. Connections to the respiration sensor, the 0.4 mm diameter mercury column completely encircling the thorax, were made in the ventral area, so that here again the body provided shielding for another area that might tend to have a high field concentration. The hypodermic needle temperature sensor, oriented perpendicular to the direction of the incident electric field, is discussed further below.

The significance of the subcutaneous temperature data obtained in the three experiments is not the same in each. In experiment 1, the hypodermic needle, within the tip of which was housed the thermistor temperature sensor, was shielded from the incident radiation. The local temperature increases are

therefore indicative of temperature increases over the whole body surface. In experiments 2 and 3, the needle was under an area directly irradiated and hence measured local temperature rise only. Recently, evidence has been presented [7] that there may occur local microwave field concentrations near metal probes that would tend to give rise to higher temperatures than would normally be detected. In our experiment, this effect was found to be present to the following extent: at the 20 mW/cm^2 level, turning on the microwave power resulted in an observable flicker of the needle on the readout unit, corresponding to about half of the smallest readable temperature increase (0.1°C). It is not possible to state with certainty the degree to which the temperatures observed during irradiation were influenced, and the degree to which the rates of increase were affected. One significant factor is the vascularity of the part of the animal's body near the tip. Experiments similar to those of McAfee, *et al* [9] would help to shed light on this question. In retrospect, the placing of a suitable absorbent disk on the skin area immediately above the hypodermic probe tip so that it lay in the microwave shadow of the disk could have eliminated this factor from consideration.

The graphical and tabular methods selected to display the experimental results do not show the original data points. This was made necessary by the need to present a large number of observations in a clear, concise way (4260 in experiment 1; 1536 in experiment 2; 900 in experiment 3).

The experiments described here have attempted to relate the overall systemic response of an animal to a controlled incident field. This is distinct from other investigations [7] which examine detailed questions such as whether excessive local temperature increases occur within particular tissues or organs.

It is interesting to consider the following question: Is it possible to *predict* the response of the rabbit to a complex microwave environment in a non-laboratory setting on the basis of experimental observations reported here and elsewhere? Prediction must include proper weighing of the following factors: the frequencies present; the variation of absorption with frequency; whether the animal is in the near or far field; orientation of the animal with respect to the incident fields; heat stress due to sunlight; humidity; wind velocity; ambient temperature; the physiological state of the animal; perhaps other factors. This certainly appears to be a discouragingly complex job.

In attempting to assess human response to ordinarily-found complicated microwave environments, in high-field situations, where special attention must be paid to possible injury [10 - 16], a similar evaluation must be made. Recent advances have made possible the measurement of total local power density of complex microwave fields with commercially available broadband omni-directional probes [17 - 19] and their associated equipments. Use of this instrumentation, together with an exposure standard [20], is helpful only in estimating situations of thermal hazard, but is by no means sufficient even for that: dissipation of the thermal burden may not be the only hazard.

An alternative approach is to place a test animal in the field, and to determine from its physiological response whether an immediate thermal stress hazard is present, i.e., to employ a biological dosimeter [21] rather than a technological one. Perhaps similar work with other animals to determine their thermal response thresholds would yield a range of responses which could permit one to estimate this factor for man.

References

1 Kaplan, I. T., Metlay, W., Zaret, M. M., Birenbaum, L. and Rosenthal, S. W. "Absence of heart-rate effects in rabbits during low-level microwave irradiation," IEEE Trans. MTT-*19*, No. 2, pp. 168-173, February 1971.

2 Ely, T. S., Goldman, D. E. and Hearon, J. Z. "Heating characteristics of laboratory animals exposed to ten-centimeter microwaves," IEEE Trans. Bio-Medical Eng. BME-*11*, No. 4, pp. 123-137, October, 1964.

3 Presman, A. S. *Electromagnetic Fields and Life* Plenum Press 1970, pp. 119-122.

4 Schwan, H. P. "Microwave radiation: biophysical considerations and standards criteria", IEEE Trans. Bio-Medical Eng., BME-*19*, No. 4, pp. 304-312, July 1972.

5 Deichmann, W. B., Stephens, F. H., Keplinger, M. and Lampe, K. F. "Acute effects of microwave radiation on experimental animals (24000 megacycles)" J. Occupational Medicine, *1*, pp. 369-381, July 1959.

6 Leighton, R. B. *Principles of Modern Physics*, McGraw-Hill, 1959, p. 60ff. Also General Electric Radiation Calculator GEN. 15-B9-56.

7 Johnson, C. C. and Guy, A. W. "Non-ionizing electromagnetic wave effects in biological materials and systems," Proc. IEEE, *60*, No. 6, pp. 692-718, June 1972.

8 Rozzell, T. C., Johnson, C. C., Durney, C. H., Lords, J. L. and Olsen, R. G. "A Non-perturbing Temperature Sensor for Measurements in Electromagnetic Fields", J. Microwave Power, *9*, No. 3, pp. 241-249. September 1974.

9 McAfee, R. D., Cazenavette, L. L. and Shubert, H. A. "Thermistor Probe Error in an X-Band Microwave Field", J. Microwave Power, *9*, No. 3, pp. 177-180, September 1974.

10 Hirsch, F. G. and Parker, J. T. "Bilateral lenticular opacities occurring in a technician operating a microwave generator," Am. Med. Assoc. Arch. Ind. Hyg., *6*, pp. 512-517, December 1952.

11 Shimkovich, I. S. and Shilyaev, V. G. "Cataract of both eyes which developed as a result of repeated short exposures to an electromagnetic field of high density," Vestn. Oftalmol. (Moscow), *72*, pp. 12-16, 1959.

12 Rosenthal, D. S. and Beering, S. C. "Hypogonadism after microwave irradiation," J. of the Am. Med. Assoc., *205*, No. 4, pp. 245-248, July 22, 1968.

13 Rose, V. E., Gellin, G. A., Powell, C. H. and Bourne, H. G. "Evaluation and control of exposures in repairing microwave ovens," Am. Ind. Hyg. Assoc. Jour., *30*, pp. 137-142, March-April 1969.

14 LaRoche, L. P., Zaret, M. M. and Braun, A. F. "An operational safety program for ophthalmic hazards of microwaves," Arch. Environ. Health, *20*, pp. 350-355, March 1970.

15 Zaret, M. M., Kaplan, I. T. and Kay, A. M. "Clinical microwave cataracts," Biological Effects and Health Implications of Microwave Radiation, Symposium Proceedings, U.S. Dept. of HEW Publications No. BRH/DBE 70-2, 1970.

16 Hirsch, F. G. "Microwave cataracts—a case report reevaluated," Electronic Products Radiation and the Health Physicist, U.S. Dept. of HEW Publication No. BRH/DEP 70-26, pp. 111-140, October 1970.

17 Fletcher, K. and Woods, D. "Thin-film spherical bolometer for measurement of hazardous field intensities from 400 MHz to 40 GHz," Non-Ionizing Radiation, *1*, No. 2, pp. 57-65, September 1969. (Wayne-Kerr Co., Ltd., New Malden, Surrey, England.)

18 Aslan, E. "Broadband isotropic electromagnetic radiation monitor," Conference on Precision Electromagnetic Measurements, NBS, Boulder, Colo., June 26-29, 1972. (Narda Microwave Corp., Plainview, N.Y.)

19 Hopfer, S. "An ultrabroadband probe for RF radiation measurement," Microwave Dosimetry Workshop, Georgia Inst. of Tech., Atlanta, Georgia, June 1-2, 1972. (General Microwave Corp., Farmingdale, N.Y.)

20 "Safety level of electromagnetic radiation with respect to personnel," American National Standard C95. 1-1974, ANSI, 1430 Broadway, N.Y., N.Y.

21 Zaret, M. M. "Investigation of personnel hazard associated with radio-frequency fields encountered in naval operations," Final report for ONR, Contract N00014-69-C-0358, July 1971.

Microwave Press-Setting Equipment for Pencil Manufacture*

K. Oshima†, T. Toishi†, T. Muranaka†, T. Serikawa‡ and T. Hiratsuka

ABSTRACT

A microwave heating equipment which can automate the press-setting process in pencil manufacture has been developed. This equipment has microwave output power of 4kW maximum and can make 600 to 700 gross of pencils in 8 hours. The quality of these pencils is excellent.

Introduction

In pencil manufacturing, only the drying and press-setting process of slats has remained a manual handling operation, including natural drying of 24 hours. We developed microwave heating equipment, 2450 MHz in frequency and 0 to 4.5 kW in output power, and succeeded in making this process completely automatic.

In this paper, the conventional process, the design of the new equipment and an explanation of the microwave heating equipment will be presented.

The Conventional Process

In the pencil making process, many kinds of automatic equipment have been introduced. A typical line of pencil making is illustrated in Figure 1.

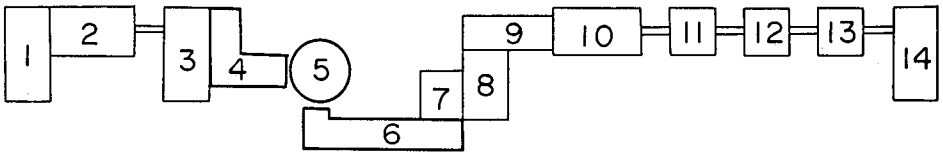

Figure 1 The new processing line for pencil making with microwave heating. (The conventional line does not include stages 4 to 6).

(1) Automatic slat feeeding machine
(2) Automatic groover
(3) Automatic lead laying and glueing macine
(4) Automatic stacking machine
(5) Microwave heating press-setting equipment
(6) Feeding conveyor for blocks
(7) Heavy-duty end cutting saw for blocks

* Manuscript received September 9, 1974; in revised form November 30, 1974.
† Tokyo Shibaura Elec. Co. Ltd.
‡ Mitsubishi Pencil Co. Ltd.

(8) Heavy-duty automatic shaping machine
(9) Pencil feeding conveyor
(10) Automatic pencil painting machine
(11) Double end cutting machine
(12) Pencil checking machine
(13) Stamping machine
(14) Automatic pencil packing machine

In this line, between the automatic lead-laying and glueing machine and the heavy end cutting saw for blocks, the drying and press-setting process has previously remained a manual handling operation which includes natural drying.

At the first stage in this process, well dried slats of incense cedar are fed to an automatic grooving machine. Nine grooves are made on one side of the slats which are 71.3 mm in width, 184 mm in length and 4.8 mm in thickness. Then an automatic machine lays pencil leads in the grooves of a slat, applies glue to another grooved slat and places it on top of the former. Usually from 40 to 50 pairs are manually forced together with a pressing jig, shown in Figure 2, at about 50 kg/cm^2 and left in a warm room to set

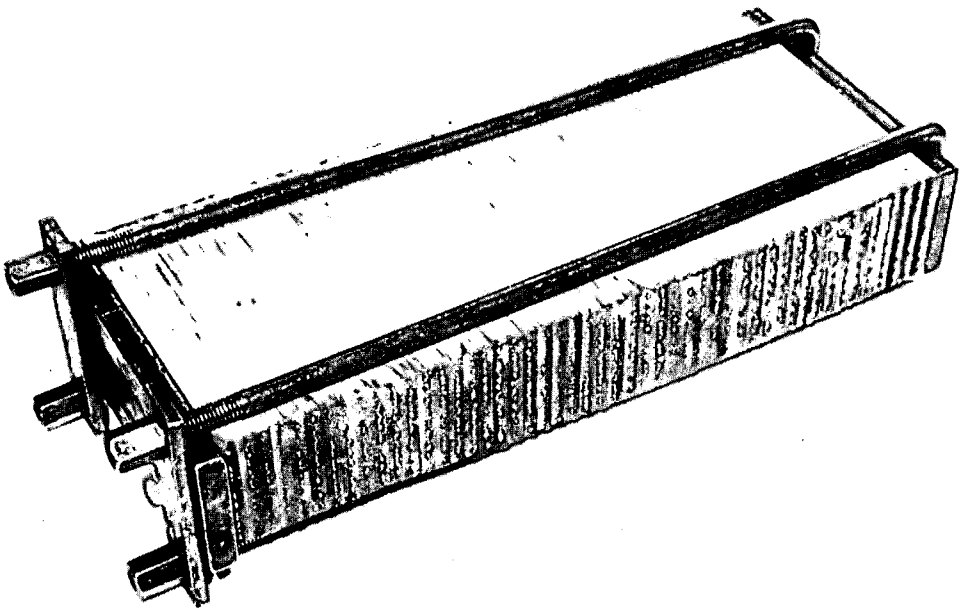

Figure 2 A manual pressing-jig to force together pencil slats.

naturally. For drying and setting, it takes about 24 hours. After this period the slats are released manually from the pressing jig, and then each complete block is cut and shaped into separate pencils by high speed machines. In steps 10 through 14 of the process, pencils are then finished and packed. Figure 3 illustrates several of the steps in pencil making.

Several types of equipment have been developed for the press-setting process, employing steam, heated air, electrically heated plates or radio frequency heating. But the results have not been satisfactory for pencil manufacturers, because of only small improvements in productivity.

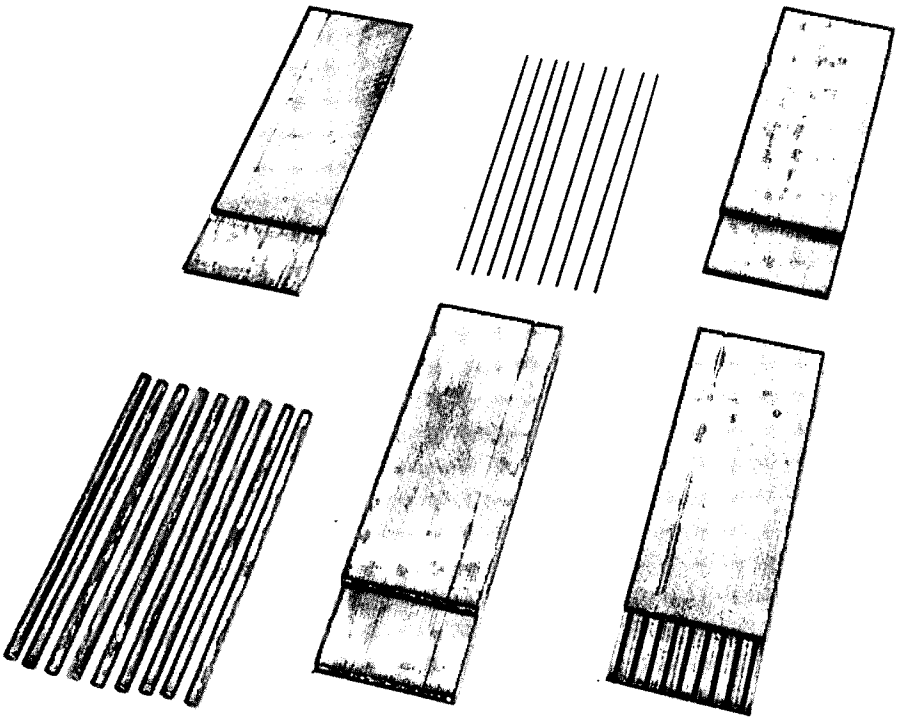

Figure 3 Steps in a pencil making process.

Preliminary Examination

The product quality using microwave heating was repeatedly examined by preliminary experiments using a small 1 kW batch type oven at 2450 MHz. 20 to 30 pairs of slats including leads were heated from room temperature to about 55°C in 1 min. The weight of each pair was about 53 g., and the weight of glue applied to each pair ranged from 0.4 to 0.7 g. Vinyl acetate and urea resin glues were used.

The strength of setting was found to be sufficient for practical use, and was increased further during a 4-min. period after microwave radiation. When the maximum temperature exceeded 80°C, urea resin glue was sometimes puffed, but no puffing was observed if the temperature was kept below 60°C.

Quality checking points are: (1) Tactile hardness, (2) Grade of touch in writing, (3) Degree of reflection of trace, (4) Abrasive rate, (5) Strength of pointed end of lead, and (6) Resistive strength against pulling out of lead.

Mitsubishi-Uni and Hi-Uni brand leads in hardness grades of H, HB and 2B were used as standards of comparison. Each group of hardness and brand includes naturally dried samples and microwave heated samples. Each cycle of the check employed 20 pieces of each hardness level. The quality checks were executed through blind tests by specialists. The results are listed in Table 1.

As shown, there are no differences in relation to three check points, which are tactile hardness, strength of pointed end of lead and resistive strength against pulling out of lead. The expression of grade of touch in writing is

TABLE 1
COMPARING OF QUALITY, MICROWAVE HEATED PENCIL WITH CONVENTIONAL ONE

Sample Hardness	brand*	Drying Condition	Tactual Hardness	grade of touch in writing	Order of Touch	degree of reflection $\bar{x}$(%)	degree of reflection $\bar{R}$(%)	abrasive rate $\bar{X}$(mm)	abrasive rate $\bar{R}$(mm)	strength of point **	resistive strength ***
H	Uni	Natural		A	4	77.53	0.35	2.76	0.13		
		Microwave	No Change	A	3	75.85	1.6	2.67	0.17	Equality	Equality
	Hi Uni	Natural		S	1	76.73	1.4	2.92	0.05		
		Microwave	No Change	S	2	76.78	1.3	3.10	0.15	Equality	Equality
HB	Uni	Natural		A	3	59.50	2.6	3.88	0.24		
		Microwave	No Change	A	4	62.38	3.5	3.83	0.43	Equality	Equality
	Hi Uni	Natural		S	1	64.55	1.6	3.81	0.07		
		Microwave	No Change	S	2	71.00	0.8	3.77	0.20	Equality	Equality
2B	Uni	Natural		A′	4	41.63	1.4	4.40	0.61		
		Microwave	No Change	A	3	40.70	1.3	4.30	0.37	Equality	Equality
	Hi Uni	Natural		S	2	49.88	3.2	4.47	0.19		
		Microwave	No Change	S	1	48.53	1.9	4.27	0.25	Equality	Equality

*Uni: Mitsubishi Uni brand
Hi Uni: Mitsubishi Hi Uni brand
**Strength of pointed end of lead
***resistive strength to pulling out of lead

that S and A represent high grade, A′ and A″ represent medium grade, and B, which does not appear in this table, represents low grade. All of the Hi-Uni brand are classified as grade S, and all of the microwave heated Uni-brand are classified as grade A. Among the natural dried Uni brand, two of them are grade A and one of them is A′. Concerning the order of touch in writing, microwave heated samples are sometimes excellent—but not always.

There are no significant differences in degree of reflection and abrasive rate. One of the most particular physical advantages is a decrease of warping of slats sometimes caused in the drying process. A supposed reason for this phenomena is that drying and setting of glue is finished before migration of water into the slat: microwave heats the glued layer faster than wooden parts. Our data has shown that the temperature of the glued layer and the wooden part are 55°C and 45°C, respectively, immediately after microwave radiation.

From these data it can be concluded that the quality of microwave heated pencils is as good as or superior to conventional ones.

In the case of colour pencils, if the final temperature of the lead is controlled around 45°C, the quality of products is the same as the conventional product.

Design of the Equipment

The production capacity of the microwave press-setting equipment must match the conventional line capacity. Moreover, a small setting area is preferable, as major re-arrangements should be avoided. For the first step in the design, the required microwave power was estimated. Production capacity of the line was chosen to be 40 pairs/min. Initial temperature of the pairs was assumed as 25°C in summer and 10°C in winter, and final temperature to be 55°C according to the former experiments. Then, the estimated power level required is 3.04 kW in summer and 4.56 kW in winter. These values coincide with the data of the preliminary experiments which employed a batch type oven.

A type TMU-418C Toshiba 2450 MHz microwave power generator of variable power output from 0 to 4.5 kW was chosen. To make the size of the equipment compact, an index-table type system was planned. The required stages on the table are (1) a stage for loading, (2) four stages for an oven, including the entrance and the exit portions, (3) four stages for a cooling period after radiation and (4) one stage for unloading. The total number of the stages required would be ten, but we designed a twelve head index-table for convenience of construction.

Efficient heating is the most important characteristic. It was observed experimentally that if two pile of slats are in the oven, the necessary radiation time is shorter by 10% than for one pile. Therefore, the oven was designed to admit 2 heads at one time.

Each head acts as a pressing jig. During the microwave radiation and cooling periods, each pair of slats must be held together with a pressure of 5 to 20 kg/cm^2. Then the jigs must be able to endure a peak load of about 3,000 kg. Relating to the mechanism, the allowable period of pressing or releasing time should be shorter than the index time of 50 sec. Moreover, arcing and unwanted heating must be avoided. Therefore, the construction and materials of the jigs are carefully designed, and most of the materials are of non-magnetic stainless steel. These are shown in the photographs.

Uniform heating and the prevention of leakage power are essential characteristics, and we have been successful in overcoming these problems, using two feeding points of power, microwave trapping regions with absorbing materials at the entrance and exit portions of the oven, and $\lambda/4$ choke construction for the rotating portion.

Description of the Equipment

Table 2 shows the main specifications of the equipment. Figure 4 is an

TABLE 2
MAIN SPECIFICATION OF THE EQUIPMENT

Term	Specification
Power input	3 phase, 200V, 50/60 Hz, 16KVA
Power output	4.5 KW
Microwave tube	Toshiba Magnetron 2M60A
Frequency	2450 $\pm$50 MHz
Coolant	water 7 ℓ/min.
Index time	about 60 sec.
Microwave radiation time	about 45 sec.
Capacity	about 240 pairs/hour (150 gross of pencils)

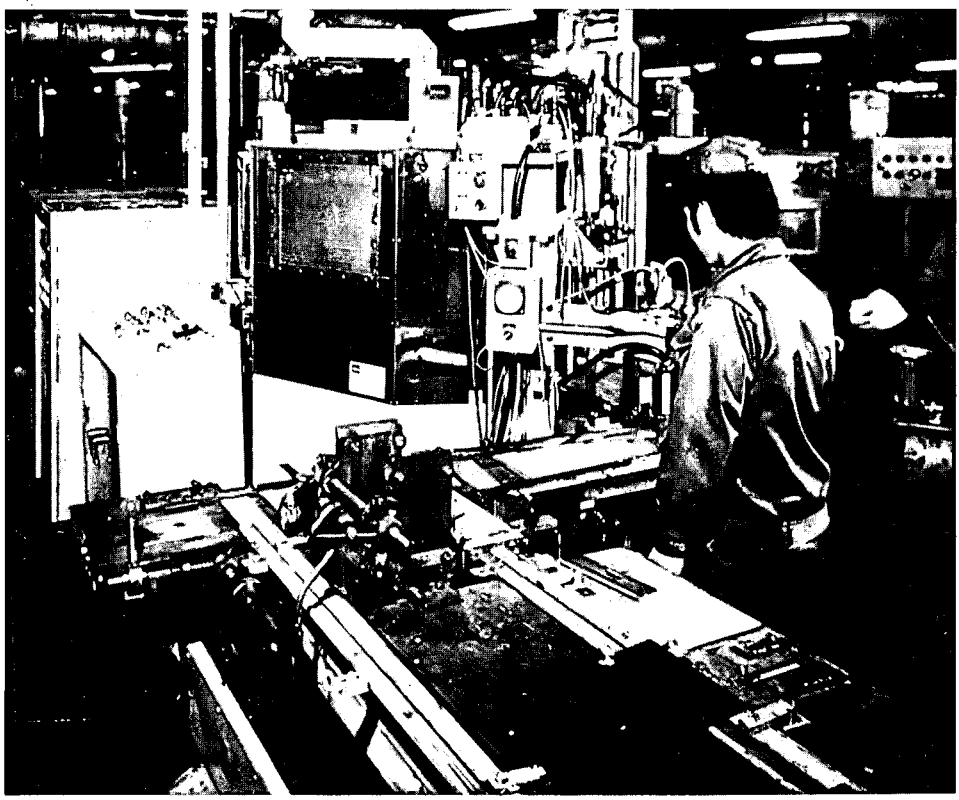

Figure 4 Overall view of the microwave press-setting equipment.

overall view of the equipment. Figure 1 symbolically depicts a new line of pencil making with a microwave press-setting equipment. Figure 5 illustrates the block diagram of the equipment, and using this figure we will explain the function of the successive stages.

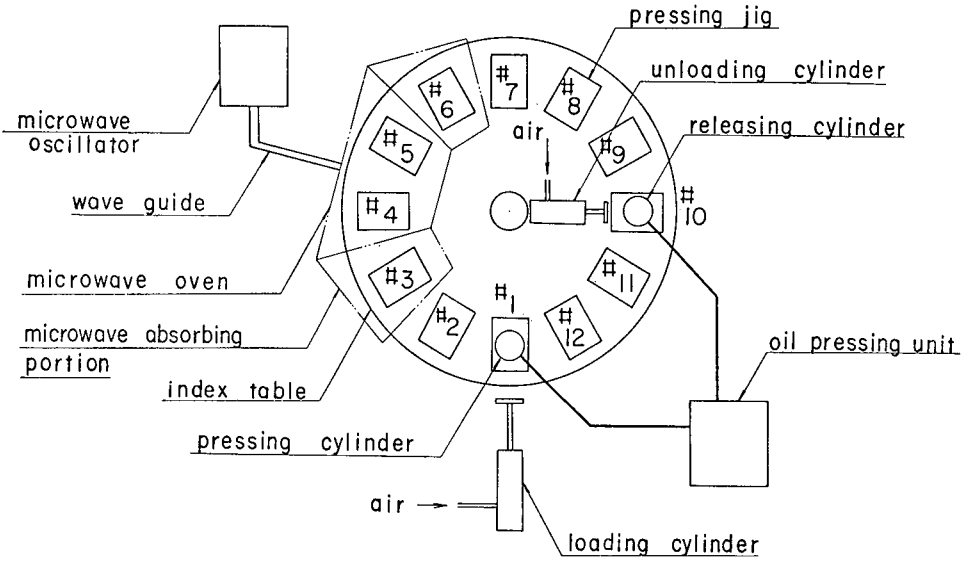

Figure 5 The block diagram of the microwave heating press-setting equipment.

Stage 1: 40 pairs of slats stacked up by automatic stacking machine are loaded into the pressing jig, and forced together by oil pressure cylinder with a load of 3 tons. The stack is held under pressure with screws; Stage 2: Idle stage; Stage 3: Entrance room to the oven. The object of this room is to trap the small amount of leakage power with absorbing material and the stack itself. There are two French window type doors at both ends of this room; Stage 4 and 5: A microwave oven, in which two stacks held in the pressing jigs are heated by microwave power; Stage 6: Exit room from the oven, similar to the entrance room; Stage 6, 7, 8 and 9: Cooling and setting region. Setting strength increases while passing through this region; Stage 10: Unloading stage. The released stack is sent to the heavy duty end cutting saw by a conveyor. As shown, the angle between the two directions of loading and unloading is 90 degrees; Stages 11 and 12: Idle stages.

In normal operation, 4.2 kW of microwave power is used. The microwave radiation time is regulated to be 47 per index, and the mechanical index time is 58 sec. Under these conditions, the productivity capacity of 246 pairs/hour (154 gross of pencils per hour) is achieved. Quality checks like the described preliminary examinations are executed to determine that all points are satisfied.

Conclusion

By the introduction of microwave heating to the drying and press-setting process of pencil manufacture, the following results are obtained: (a) process time is shortened from 24 hours to several minutes, and this is effective in improving productivity and reducing working area, (b) the manual hard labor of pressing work is eliminated, (c) a saving of two operators per line is achieved, (d) the quality of pencils is as good as or superior to conventional ones, and (e) operation and machine maintenance are simple.

Effect of 2450 MHz Microwave Radiation on Horseradish Peroxidase*

H. M. Henderson, K. Hergenroeder, and S. S. Stuchly†

ABSTRACT

Solutions of horseradish peroxidase were subjected to 2450 MHz CW microwave radiation over an absorbed power density range of 62.5 to 375 W/cm³ for time periods of 5, 10, 20, 30 and 40 minutes. The enzyme samples were placed in a specifically designed waveguide applicator, and strict temperature control (25°C ± 1 to 2°C) was maintained by circulation of the coolant carbon tetrachloride. Our findings indicate that, in our experimental conditions, there is a significant inactivation of the enzyme only for absorbed power densities greater than 125 W/cm³ for 20 minutes, or at power densities above 60 W/cm³ for periods greater than 20 minutes. It is concluded that the dosages of microwave radiation required to achieve significant inactivation of the enzyme at 25°C are very high, and therefore any practical utilization of microwave power for inactivation of peroxidase at room temperature appears to be doubtful at the present time.

Introduction

The enzyme peroxidase (donor: H_2O_2 oxidoreductase, EC 1.11.1.7)[1], universally distributed in plant tissues [16], is of particular interest to food technologists, due to its high thermostability, its ability to regenerate its activity, and its probable involvement in the production of off-flavours in food material. It is thought to be involved in undesirable oxidative changes in flavouring components in stored vegetables [20, 10].

Confirmation of the absence of peroxidase activity is the most frequently-used biochemical index for the effectiveness of the blanching procedure during the processing of fruits and vegetables [14]. Blanching is a form of rapid sterilization in which fruits and vegetables are subjected to boiling water or steam for a short interval of time, which treatment is normally sufficient to inactivate all enzymes present. Inactivation of peroxidase is taken to indicate a loss of activity of all other enzymes present in a given sample of food. The considerable stability of peroxidase to heat is exemplified by an experiment

* Manuscript received September 23, 1974; in revised form January 13, 1975.

† Department of Food Science and Department of Agricultural Engineering, University of Manitoba, Winnipeg, Manitoba R3T 2N2, Canada.

1 EC 1.11.1.7 is the number of peroxidase in the enzyme classification table of the Enzyme Commission of the International Union of Biochemistry.

described by Reed [20]. When an enzyme preparation was held at 85°C, one-half of the original activity was retained after 32 minutes at this temperature. The corresponding time for 145°C was 0.4 minutes. Thermal inactivation studies have been undertaken on peroxidase in green beans and turnips [24], peas [17], sweet corn [23], and horseradish [11].

There is considerable current interest in the use of microwave radiation in dry blanching techniques, as a possible alternative to the traditional methods of steam or hot water blanching of fruits and vegetables [19]. Dry blanching procedures may minimize undesirable changes in flavour and texture, may reduce the amount of waste effluents, and may result in greater retention of nutritive value in the product [18]. If microwave is to be employed for blanching, then it is desirable to know the effect of this type of radiation on enzymes significant in food. Copson [7] demonstrated that pectin methyl esterase in orange juice concentrate was inactivated in a microwave applicator. Studies have been undertaken to investigate the effects of 2450 MHz microwave radiation on *Bacillus subtilis* α-amylase [12], on lysozyme and trypsin [13], at a frequency of 2.8 GHz on the human serum enzymes lactate dehydrogenase, acid phosphatase and alkaline phosphatase [2], and at a frequency of 60 MHz on a number of food enzymes [15]. The effect of 2450 MHz microwave radiation on peroxidase has been studied in potatoes [6, 5], and also (915 MHz) in corn-on-the-cob [8] and in brussels sprouts [9], but not in model systems.

It is the purpose of the present study to determine the effect of 2450 MHz microwave radiation *per se* on aqueous solutions of horseradish peroxidase at room temperature.

Experimental

Enzyme

Horseradish peroxidase, a lyophilized (freeze-dried), soluble, partially-purified (RZ = 1.09 – 1.14)[2] preparation, was obtained from Worthington Biochemical Corporation, Freehold, New Jersey. Solutions (2.0 μg. enzyme/ml. distilled water) were made up immediately prior to use, and the activity confirmed before and after microwave experiments, to provide baseline data.

Determination of enzyme activity

The method employed was a modification of that described by Birecki *et al.* [4]. The reaction mixture composition was: hydrogen peroxide, 8.2×10^{-5}M, in 0.05M citric acid – 0.1M Na_2HPO_4 buffer, pH 4.2, 2.8 ml.; o-dianisidine dihydrochloride, 6.8×10^{-4}M, 0.1 ml.; enzyme, 0.1 ml. (0.2 μg.). In the reference mixture, the hydrogen peroxide was omitted. The progress of the reaction at 30°C was followed by continuous determination of the increase in absorbance at 470 nm in a Unicam SP 800 recording spectrophotometer. The specific activity of the enzyme was calculated as the increase in absorbance at 470 nm per minute per 0.2 μg. enzyme.

Control enzyme samples were run in the microwave equipment for the same periods of time and at the same temperature as the test runs, but in the absence of microwave radiation.

2 RZ = Reinheitszahl = ratio of A_{403}/A_{275} = a spectrophotometric criterion of purity of a preparation of peroxidase, an iron-porphyrin enzyme. Absorbance at 403 nm (the Soret band) is characteristic of all porphyrins, and that at 275 nm is due to the protein.

Experimental equipment

A schematic diagram of the experimental set-up is shown in Figure 1. The set-up consists of a microwave power generator, a waveguide applicator, a cooling system with temperature monitoring and control, and a waveguide load.

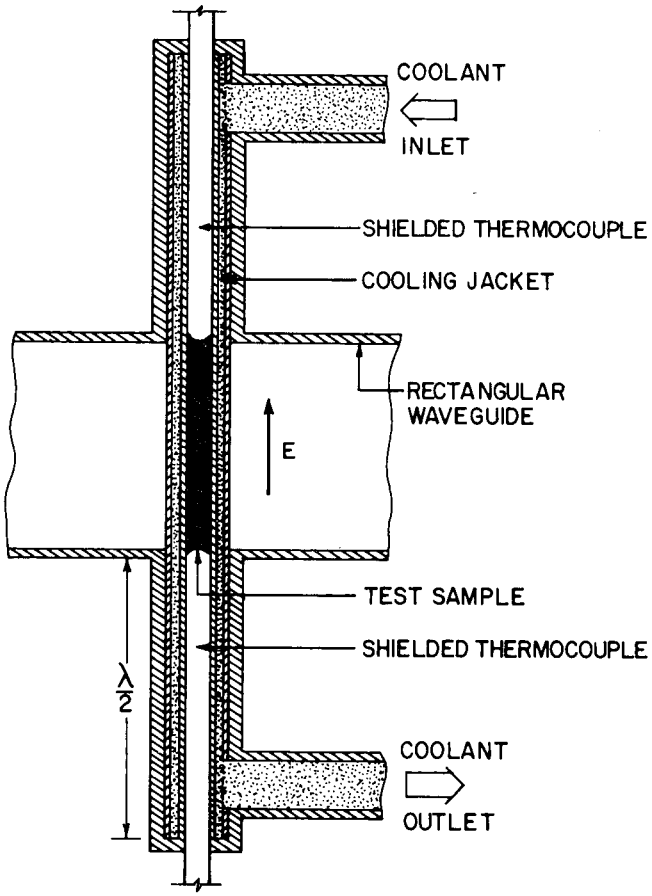

Figure 1 Schematic illustration of the equipment.

The waveguide applicator [22] is of a transmission type and consists essentially of a section of a standard rectangular waveguide WR 340 with a cylindrical sample container located in the center of the waveguide parallel to the electric field as shown in Figure 2. The sample is contained in a section of a 3/16″ ID Teflon tube terminated by two shielded thermocouples which form $\lambda/2$ (λ is the free space wavelength) coaxial stubs on both sides of the actual sample container. The volume of the sample is 0.8 ml $\pm$ 0.04 ml. The thermocouples remain in direct thermal contact with the sample without being heated directly by microwave power flowing through the applicator. The sample container is surrounded by a cooling jacket consisting of a section of a 7/16″ ID Teflon tube carrying the low loss coolant. The microwave power dissipated in and reflected from a cylindrical dielectric sample located in the centre of the rectangular waveguide (Figure 2), can be calculated analytically [3]. For a water sample (at 25°) of diameter 3/16″ located in the centre of a standard WR 340 rectangular waveguide operating in the fundamental mode of a frequency of 2450 MHz, 52% of the incident power is absorbed in the sample while 48%

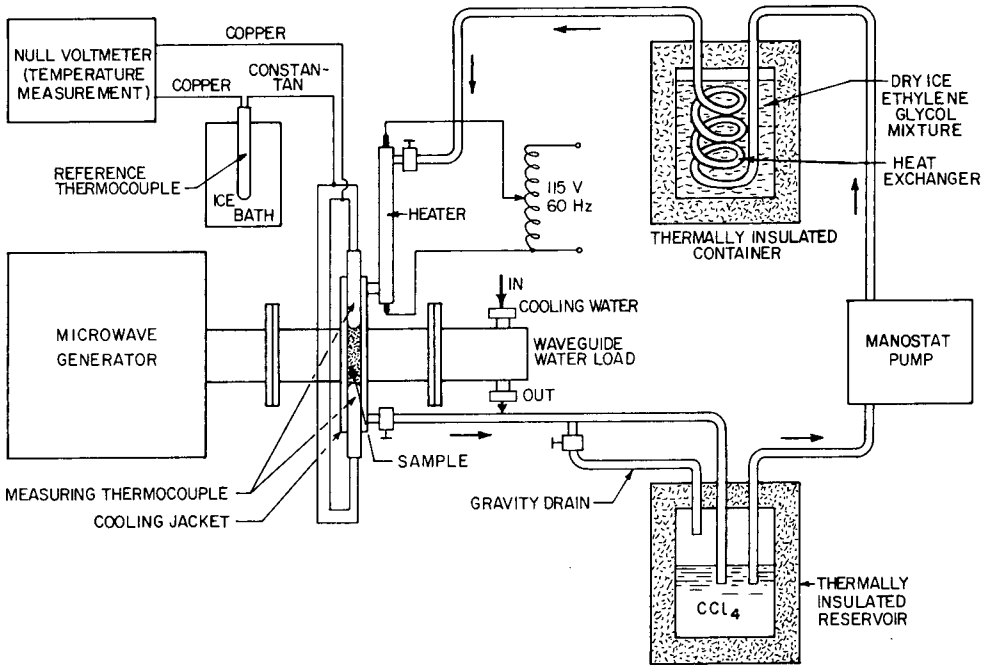

Figure 2 The waveguide applicator. λ represents the wavelength in the dielectric loaded coaxial line.

is reflected or transmitted to the load. These numbers agree well with the experiments. Since the sample is contained between the broad walls of the waveguide there are no idle pockets of the test substance in the applicator, in other words the whole sample is being irradiated, and since the electric field throughout the sample is, for all practical purposes, position independent, the microwave power dissipated throughout the sample is also position independent. This applicator offers several inherent advantages in studying the effects of microwave radiation on biological substances, namely the temperature of the sample can be accurately monitored during the irradiation and kept constant at a desired level, independently of the amount of microwave power dissipated in the sample. Since a relatively large part of the microwave power flowing through the applicator is dissipated in the sample very large power densities absorbed in the sample,of the order of kW/cm^3, are possible. The microwave power is dissipated uniformly throughout the sample and the value of microwave power actually dissipated in the sample can be monitored during the experiment.

The cooling and temperature control system is designed to maintain the temperature of the sample at 25°C during the exposure to microwave radiation. The system consists of a heat exchanger, an electric heater, a reservoir and a pump all connected in series as shown in Figure 1, and the two thermocouples measuring the sample temperature with reference to an ice-bath temperature. The coolant was carbon tetrachloride[3] cooled by circulation through

3 Carbon Tetrachloride was selected because of its low dielectric losses at microwave frequencies ($\epsilon' = 2.17$, $\tan\delta = 0.0004$ at 2450 MHz) and excellent cooling properties (H. L. Basset, "High power microwave window", 1974 Microwave Power Symposium, Milwaukee, Wisc.). Microwave power dissipated directly in the coolant was found to be negligible.

the heat exchanger consisting of a copper coil placed in a mixture of dry ice and ethylene glycol. Circulation of the coolant through the cooling system was maintained with a Manostat Varistaltic pump, of a pumping capacity of 300 - 4000 ml/min. The electric heater, of a capacity of 300 W adjacent to the waveguide applicator and fed from the 60 Hz line through the variable transformer, was employed to control the temperature of the coolant which passed through the cooling jacket of the waveguide applicator before returning to the reservoir. The gravity drain enabled the carbon tetrachloride to be removed from the cooling jacket, during the time required to change samples between experiments. The thermocouples, copper-constantan with a 3/16″ OD stainless steel shield, were connected in parallel to measure the average temperature of the sample. The difference in thermal EMF's between the measuring thermocouples and a reference thermocouple located in an ice-bath was measured by an HP 419A DC null voltmeter.

Microwave power was generated by a Philips YJ 1420 magnetron operating at a frequency of 2.45 GHz with a power output adjustable continuously from 50 to 600 W. The part of microwave power passing through the applicator (not dissipated in the sample) was absorbed by a Varian EW 3-WL 3 waterload.[4]

The cooling system shown in Figure 1 allows control of the temperature of the sample during the irradiations and measurement of the microwave power *dissipated* in the sample. The coolant flowing continuously in the system in the direction shown in Figure 1 is first cooled in the heat exchanger and then heated by a 60 Hz heater and finally passes through the cooling jacket of the sampler holder as shown in Figure 2, and is heated indirectly by microwave power dissipated in the sample. Keeping the flowrate of the coolant constant and adjusting the 60 Hz power dissipated in the heater for any given microwave power level (dissipated in the sample) one can obtain an equilibrium for any desired temperature of the sample at any given microwave power level. The actual microwave power *dissipated* in the sample was measured during the irradiation by measuring the difference between the 60 Hz power delivered to the heater in the absence of microwave power and during irradiation. It was assumed that the thermal losses between the heater and the applicator were negligible. The technique employed has been widely used for measurement of high microwave power by so-called balanced calorimetry.

Results

Peroxidase samples were subjected to microwave radiation of a power density range of $62.5 - 375$ W/cm^3 over time periods of 5, 10, 20, 30 and 40 minutes. The temperature of each sample was maintained within ± 1 to 2°C at an average value of 25°C, with extreme values ranging between 13°C and 33°C over the whole course of the work. The results are shown in Figure 3. Similar solutions of horseradish peroxidase had previously been shown, in the authors' laboratory, to be stable after being held in a water bath at 30°C for four hours. Exposure to microwave radiation for 5 min. results in a steadily decreasing activity, with a loss of approximately 20% on exposure to 375 W/cm^3 for this length of time. A similar result was obtained for a period of 10 minutes ,with 35% inactivation of the enzyme on exposure to 375 W/cm^3. For

4 VSWR of the waterload is 1.3 at 2.45 GHz which is equivalent to 2% of the power reflected.

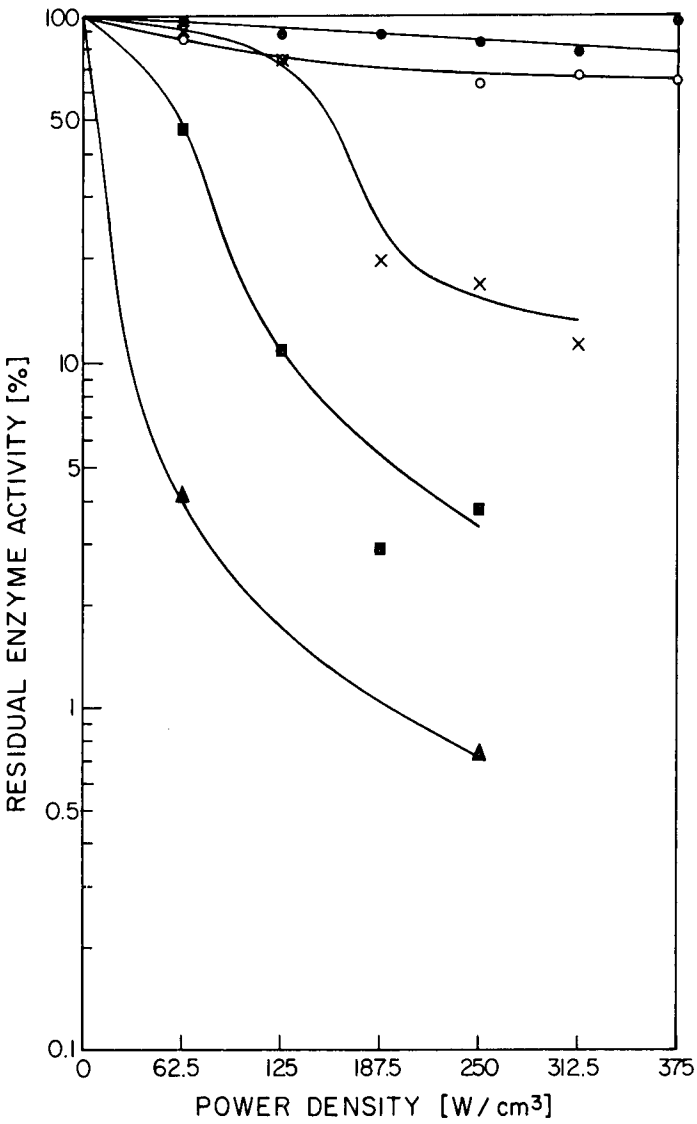

Figure 3 Effect of 2450 MHz microwave radiation on peroxidase activity: ●, 5 min. exposure to microwave radiation; ○, 10 min. exposure; X, 20 min. exposure; ■, 30 min. exposure; ▲, 40 min. exposure.

an exposure time of 20 min., there was 24% enzyme inactivation at 125 W/cm³ radiation, but at greater power densities, enzyme inactivation increased markedly with 80.6% inactivation at 187.5 W/cm³ and 88.7% at 312.5 W/cm³. Inactivation was more marked on exposure to microwave radiation for 30 minutes, increasing to 96.2% at 250 W/cm³. For an exposure period of 40 minutes, only two valid results could be obtained, which however suggested that there was considerable, but not total, inactivation at 62.5 and at 250 W/cm³. Experimental limits were determined by the fact that radiation reflected from the waveguide applicator activated a cut-out safety mechanism within the generator.

In no instance was there complete inactivation of the enzyme. It had previously been demonstrated in the authors' laboratory that similar peroxidase

solutions were not totally inactivated after being held in a sealed glass tube in an oil bath at 145°C for 2 minutes.

Discussion

A number of studies have been undertaken to determine the effect of microwave radiation on aqueous solutions of enzymes. In no instance did the microwaves have any effect on enzyme activity, aside from thermal effects. Kamat and Laskey [12] studied the effect of 2450 MHz microwave radiation on aqueous solutions of *Bacillus subtilis* α-amylase. They were unable to demonstrate any enzyme inactivation in samples irradiated at an incident power density of 106.8 mW/cm^2 for 15 minutes, and in untreated controls, all of which samples were maintained at a temperature range of $16 - 38$°C. The enzyme was significantly inactivated (62.78%) when the temperature of the solutions was 63.7 ± 11.1°C during irradiation. Exposure of enzyme solutions to 72.0 ± 1.6°C in a water bath for 15 minutes resulted in 96.51% inactivation. Lopez and Baganis [15] demonstrated the effect of radio-frequency energy at 60 MHz on a number of food enzymes, including peroxidase, *in vitro* and in apple juice, milk and sweet potato extract. There was no enzyme inactivation on exposure to radio-frequency energy at 20°C. These workers concluded that R–F energy *per se* at 60 MHz did not have any significant effect on the enzymes studied, apart from thermal effects. Langley *et al.* [13] studied the effects of 2450 MHz microwave radiation on lysozyme and trypsin. In their series of experiments, the enzyme solutions were circulated by a pump, between a reservoir and the heating apparatus. Experiments were undertaken at varying temperatures and time periods, with microwave radiation at power levels of 100 to 200 watts, and with conventional heating. No statistically significant differences in enzyme inactivation could be demonstrated between microwave power absorption and conventional heating methods. Belkhode *et al.* [2] studied the effects of 2.8 GHz microwave radiation on *in vitro* samples of human serum lactate dehydrogenase and acid and alkaline phosphatases. The samples were irradiated at incident power densities of between 400 and 1000 mW/cm^2, at temperatures of 35°C, 46.7°C and 49.7°C for time periods of 4.5 or 18.5 minutes. These workers demonstrated thermally-induced inactivation of all three enzymes, but there was no evidence for nonthermal effects.

Rosen [21] discussed the effects of microwaves on food and related materials, and concluded that the overwhelming majority of reported effects of microwaves on biological material is of thermal origin. Proper temperature control is difficult to achieve in microwave experiments, and is especially important since a rise of only a few degrees can completely obfuscate the results. Also, Rosen explains, quantum energies of microwaves fall short by several orders of magnitude of breaking chemical bonds. The quantum energy of microwave radiation is 1.2×10^{-5}eV, whereas the bond energy required even for the cleavage of weak hydrogen bonds is 0.1eV. Therefore the quantum energy of microwave radiation is too low to break hydrogen bonds, which largely contribute to the structure and function of native proteins, unless the molecule were to absorb a number of quanta simultaneously. The chances of this occurring are very remote.

Our experimental conditions are such that the enzyme sample is stationary within the field of microwave radiation, with the thermocouples placed at each

end of the sample. The sample is entirely surrounded during microwave treatment by circulating carbon tetrachloride, functioning as a coolant to minimize sample overheating. We have endeavoured to fulfill two important conditions essential for this type of work to have meaningful results, namely a small test volume and cross-section [1], and strict temperature control [21].

There was no evidence of local heating of the sample because the experiment was very slow, and in a vertical sample container cooled from outside which was used in the experiments one would expect an immediate heat exchange (towards thermal equilibrium) if there were any temperature gradients within the sample.

Our findings indicate that, in our experimental conditions, there is a significant inactivation of the enzyme only at absorbed power densities greater than 125 W/cm^3 for 20 minutes, or at power densities above 60 W/cm^3 for periods greater than 20 minutes. These represent very high levels of microwave energy density and although the temperature of the sample was macroscopically kept constant at 25°C it is conceivable that the destruction of the enzyme may be due to local heat denaturation of the protein molecules within the sample. No satisfactory explanation of the observed effects is available at this time.

Although it was demonstrated that it is possible to obtain significant inactivation of the enzyme even at room temperature (25°C) the doses of microwave radiation required to achieve this effect are very high (of the order of 50 W hr/cm^3), and therefore any practical utilization of microwave power for inactivation of peroxidase at room temperature seems doubtful at the present time.

Acknowledgements

The authors wish to express their thanks to Mr. A. L. Schellenberg and Mr. J. Putnam for assistance in equipment construction. This work was supported by the National Research Council of Canada.

References

1 Bassett, H. L., Ecker, H. A., Johnson, R. C. and Sheppard, A. P. (1971). New techniques for implementing microwave biological-exposure systems. IEEE Transactions of Microwave Theory and Techniques. Vol. MTT-19, No. 2, pp. 197-204.

2 Belkhode, M. L., Muc, A. M. and Johnson, D. L. (1974). Thermal and athermal effects of 2.8 GHz microwaves on three human serum enzymes. J. Microwave Power *9*, 23-29.

3 Bhartia, P. (1973). Private communication.

4 Birecki, M., Bizien, H. J. and Henderson, H. M. (1971). Effect of culture, storage and variety on polyphenol oxidase and peroxidase activities in potatoes. Amer. Potato J. *48*, 255-261.

5 Chen, S. C., Collins, J. L., McCarty, I. E. and Johnston, M. R. (1971). Blanching of white potatoes by microwave energy followed by boiling water. J. Food Sci. *36*, 742-743.

6 Collins, J. L. and McCarty, I. E. (1969). Comparison of microwave energy with boiling water for blanching whole potatoes. Food Technol. *23*, 337-340.

7 Copson, D. A. (1954). Microwave irradiation of orange juice concentrate for enzyme inactivation. Food Technol. *8*, 397-399.

8 Dietrich, W. C., Huxsoll, C. C., Wagner, J. R. and Gaudagni, D. G. (1970a). Comparison of microwave with steam or water blanching of corn-on-the-cob. 2. Peroxidase inactivation and flavor retention. Food Technol. *24,* 293-296.
9 Dietrich, W. C., Huxsoll, C. C. and Gaudagni, D. G., (1970b). Comparison of microwave, conventional and combination blanching of brussel sprouts for frozen storage. Food Technol. *24,* 613-617.
10 Eskin, N. A. M., Henderson, H. M. and Townsend, R. J. (1971). Biochemistry of foods. Academic Press, New York. 240 pp.
11 Joffe, F. M. and Ball, C. O. (1962). Kinetics and energetics of thermal inactivation and the regeneration rates of a peroxidase system. J. Food Sci. *27,* 587-592.
12 Kamat, G. P. and Laskey, J. W. (1970). Enzyme inactivation in vitro with 2450 MHz microwaves. Radiation Bio-Effects, summary report, U.S. Department of Health, Education and Welfare, Publ. No. BRH/DBE 70-7.
13 Langley, J. B., Yeargers, E. K., Sheppard, A. P. and Huddleston, G. K. (1973). Effects of microwave radiation on enzymes. Paper presented at the Symposium on Microwave Power, Loughborough, England.
14 Lee, F. A. (1958). The blanching process. Advan. Food Res. *8,* 63.
15 Lopez, A. and Baganis, N. A. (1971). Effect of radio-frequency energy at 60 MHz on food enzyme activity. J. Food Sci. *36,* 911-4.
16 Paul, K. G. (1963). Peroxidases. *In* 'The Enzymes' (P. D. Boyer, H. Lardy, and K. Myrbäck, eds.), 2nd Ed., Vol. 8, p. 227. Academic Press, New York.
17 Pinsent, B. R. W. (1962). Peroxidase regeneration and its effect on quality in frozen peas and thawed peas. J. Food Sci., *27,* 120-6.
18 Proctor, B. E. and Goldblith, S. A. (1948). Radar energy for rapid food cooking and blanching, and its effect on vitamin content. Food Technol. *2,* 95-104.
19 Ralls, J. W., Maagdenberg, H. J., Yacoub, N. L. and Mercer, W. A. (1972). Reduced waste generation by alternative vegetable blanching systems. Proc. 3rd. Nat. Symp. on Food Processing Wastes, New Orleans, La. U.S. Environmental Protection Agency, No. EPA-R2-72-018, pp. 25-70.
20 Reed, G. (1966). Enzymes in Food Processing. Academic Press, New York.
21 Rosen, C. G. (1972). Effects of microwaves on food and related materials. Food Technol. *26* (7), 36-40, 55.
22 Stuchly, S. S. and Rzepecka, M. A. (1974). A waveguide applicator for irradiation of samples at controlled temperatures, to be published.
23 Yamamoto, H. Y., Steinberg, M. P. and Nelson, A. I. (1962). Kinetic studies on the heat inactivation of peroxidase in sweet corn. J. Food Sci. *27,* 113-119.
24 Zoueil, M. E. and Esselen, W. B. (1959). Thermal destruction rates and regeneration of peroxidase in green beans and turnips. Food Res. *24,* 119-133.

Time Domain Measurements of the Dielectric Properties of Frozen Fish*

M. Kent†

ABSTRACT

Measurements of the dielectric properties of frozen cod have been carried out in the temperature range 0 to −30°C. The technique used was a variation of Time Domain Spectroscopy, (TDS), known as the total reflection method, which employs the complete reflected pulse from a sample terminated in a 50 Ω load. The effective bandwidth in the frequency domain was typically 3 to 100 MHz for these measurements although certain preliminary measurements were made up to 3 GHz. Changes with time were observed, particularly in the loss tangent, as was expected from previous measurements at 10 GHz. Such changes took place over periods of weeks.

Introduction

To some extent the work reported here is complementary to earlier studies in the frequency domain published by Bengtsson *et al.*, [1]. Those studies concerned the dielectric properties of frozen foodstuffs including fish, at different temperatures within the range −30°C to +10°C and at frequencies of 10, 35, 100 and 200 MHz. The work described in this paper differed from the earlier work in the following respects: (1) it involved the use of the relatively new technique of Time Domain Spectroscopy (TDS); (2) the use of TDS enabled the conductive losses to be separated easily from the dispersive losses; (3) a novel form of sample cell was developed to accommodate the expansion of freezing materials; and (4) the dielectric parameters had been seen to be time dependent at higher frequencies and this was further investigated. The frequency range covered by this work was roughly as in Bengtsson *et al.* but with some extension to lower frequencies.

Methods and Materials

TDS measurement of the complex dielectric properties of materials by means of time domain analysis of the response to a step pulse can be traced as far back as Hopkinson [6]. More recently such techniques have been extended into the microwave region by many authors, including Fellner-Feldegg [3], Loeb *et al.* [11], and Iskander and Stuchly [7]. The basic principles of this technique have been treated in some depth by a number of authors and

* Manuscript received September 12, 1974; in revised form December 18, 1974.
† Torry Research Station, 135 Abbey Road, Aberdeen, Scotland AB9 8DG.

a recent review by van Gemert [18] is recommended for those unfamiliar with these principles.

In van Gemert's review, the variation known as thin sample, or total reflection TDS, is discussed. This was first introduced by Fellner-Feldegg [4] but has since been generalized by Clerk *et al.* [16]. This is the technique employed for the work described here.

Time domain reflectometry (TDR) was used to measure the scattering parameters (S_{11} or S_{12}) of a sample filled section of transmission line terminated with the characteristic impedance of the empty line. The equation relating S_{11} to the complex permittivity, ϵ^*, is (see for example van Gemert [18]);

$$S_{11} = \frac{(1-\epsilon^*)\,[1-\exp(-j\omega\ell\sqrt{\epsilon^*}/c)]}{(1+\sqrt{\epsilon^*})^2-(1-\sqrt{\epsilon^*})^2\,\exp(-j2\omega\ell\sqrt{\epsilon^*}/c)} \quad (1)$$

where ℓ is the sample length, ω is the angular frequency and c is the speed of light *in vacuo*. Thus using a standard sampling oscilloscope the time domain response of a dielectric sample to an incident step pulse was recorded. The measurement time window was chosen such that all multiple reflections within the sample had effectively taken place. S_{11} was then calculated for each frequency from the ratios of the Fourier transforms of the reflected and incident pulses. By the use of the Samulon [15] technique of analysis, the truncation errors due to taking a finite time window are avoided since a form of the first derivative of the waveforms is used in the Fourier transform.

For conductive materials the response is as shown in Figure 1. Van Gemert

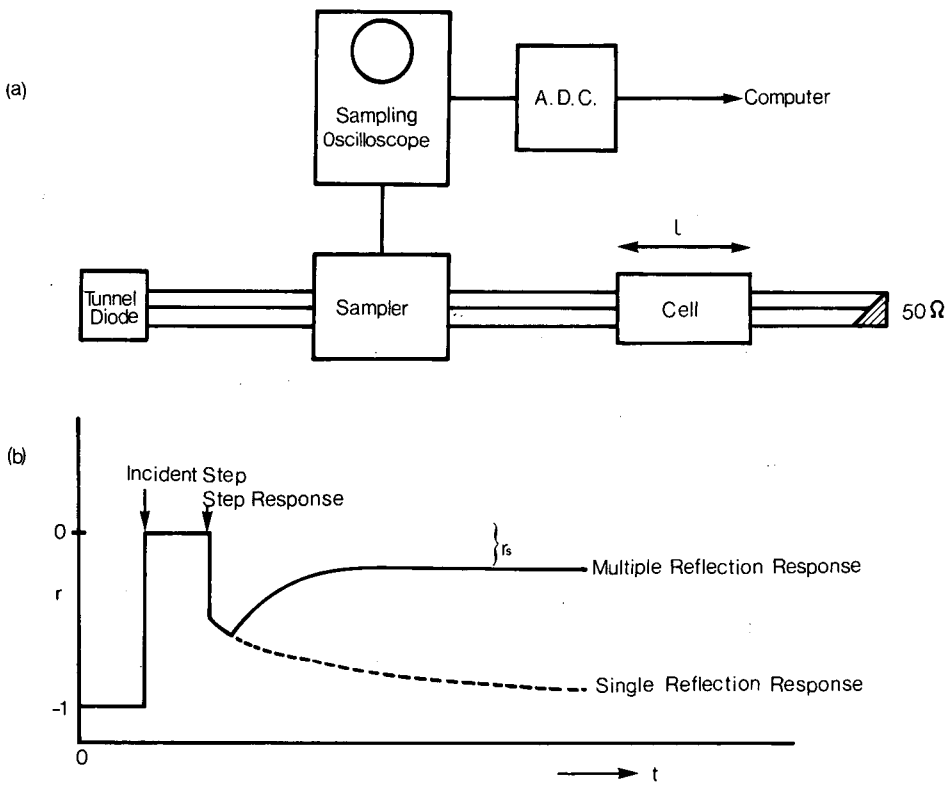

Figure 1 (a) schematic diagram of TDS equipment,
(b) typical thin sample response to an incident step pulse.

[18] and Fellner-Feldegg [4] have shown that the offset in r_s, the measured reflection coefficient as $t \to \infty$, is a function of sample length and of dc conductivity and hence may be used to calculate the latter. This will be discussed later.

Data handling—Successive scans of the time window were digitised at 1000 time intervals and transmitted to an IBM 1130 computer where the data from each scan were stored in individual files on magnetic disk. Up to 100 scans were so accommodated although the disk capacity was much larger. In order to improve the signal to noise ratio, signal averaging was carried out in the following manner.

The maximum slope of each response was found and its location used as a reference point. All the scans were then pooled in such a way that each point of maximum slope occurred at the same location in the 'averaged' data file. The same procedure was applied to the response from a short circuit placed in approximately the same position as the sample. This reflected pulse was used to calculate the frequency spectrum of the incident step. The necessary Fourier transformation of the data was achieved by using Samulon's [15] approach. S_{11} was then calculated for a number of frequencies, equispaced in the log frequency range, as has already been described, by taking the ratio at each frequency of incident and reflected components. As the maximum slope had been used to ensure removal of some pulse jitter it was also used in effect to provide a time reference for the two spectra. Some phase error resulted from this but in the frequency range covered by these experiments this was not significant.

In addition, the base line variations due to interference from the pulse used to drive the step generating tunnel diode were subtracted from both step responses before Fourier transformation was applied.

The asymptotic finite value of the step response when dealing with conductive samples (Figure 1) was used to calculate the dc specific conductivity σ. The expression used for the calculation was that given by van Gemert [18];

$$\lim_{t \to \infty} r_s(t) = -\sigma \ell / (\sigma \ell + 2c\epsilon_o) , \qquad (2)$$

where σ = specific conductivity ($\Omega^{-1}.m^{-1}$), and ϵ_o = permittivity of free space (Farad. m^{-1}).

The total relative complex permittivity at angular frequency ω is $\epsilon^* = \epsilon' - j\epsilon_t''$, where $\epsilon_t'' = \epsilon''_{dispersive} + (\sigma/\epsilon_o\omega) = \epsilon'' + \epsilon_\sigma''$ was calculated from the transcendental equation (1), S_{11} being known from the measurements. Since no solution in terms of ϵ^* exists in closed form for this expression, it was solved numerically using a Newton-Raphson iterative technique, as discussed by Hamming, [5].

Each set of measurements usually covered between 1 and 2 decades of frequency. Data collection occupied some 2 min. and subsequent handling and calculation during Fourier transformation took between 5 and 10 min. The Fourier analysis itself was performed in about 30 sec. for each frequency of interest. Algorithms such as Loeb's [12] or the Cooley and Tukey [2] type were not used since arbitrary discrete frequencies were required rather than a set of frequencies related by some power of 2.

Sample Cell—The most common difficulty with any dielectric measurements in coaxial line is that of constructing a cell to contain the sample.

Often this is achieved by simply filling sections of coaxial line with whatever dielectric is to be studied, terminating liquids or powders with some form of reflectionless window or bead. In addition to the mechanical problem of dismantling such devices in order to fill them, whenever aqueous systems are to be studied at temperaturees below the freezing point, some means must be found of accommodating the expansion of the sample which takes place on freezing. The solution to this problem was found by using a section of slab-line as shown in Figure 2. In this type of transmission line most of the field

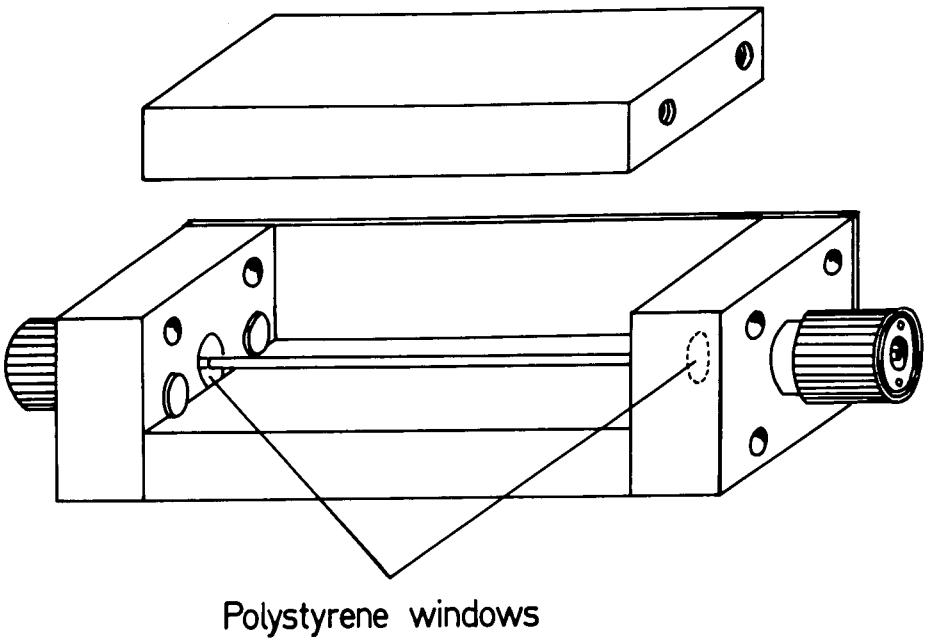

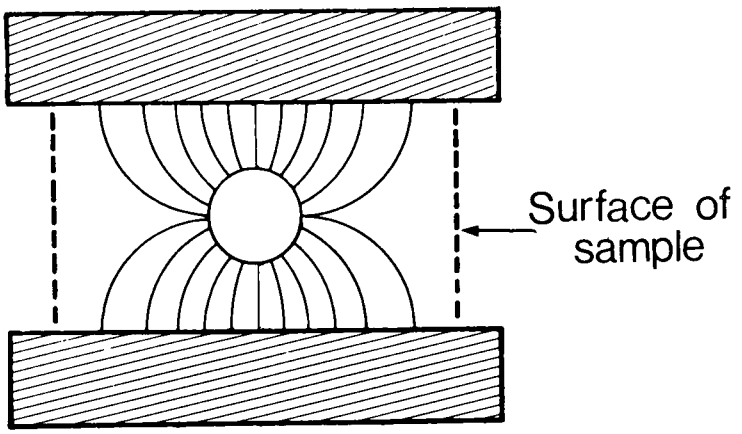

Figure 2 Modifications to slab line or triplate 'slotted' line to enable its use as a sample cell. Lower diagram shows field configuration in a cross section of the line.

is concentrated in the region between the centre conductor and the ground planes. Consequently the nature of the surface exposed at the edges of these planes is unimportant. It is in this region that expansion can be allowed to occur, or, in the case of liquids, a meniscus allowed to form. The first of the lines used was merely a modified section of a simple commercially available slotted line. The modification consisted of the provision of the dielectric windows at the junction of slab line and coaxial line to define the sample faces and to prevent leakage of any sample into the connectors. This 50 Ω line was 177 mm long and was based on 7 mm coax line dimensions.

Further versions of this kind of cell were constructed based on General Radio type GR 900, 14 mm coaxial line (Figure 3). The cells available had lengths of 5, 10, 50, 100 and 177 mm, the latter being the modified slotted line.

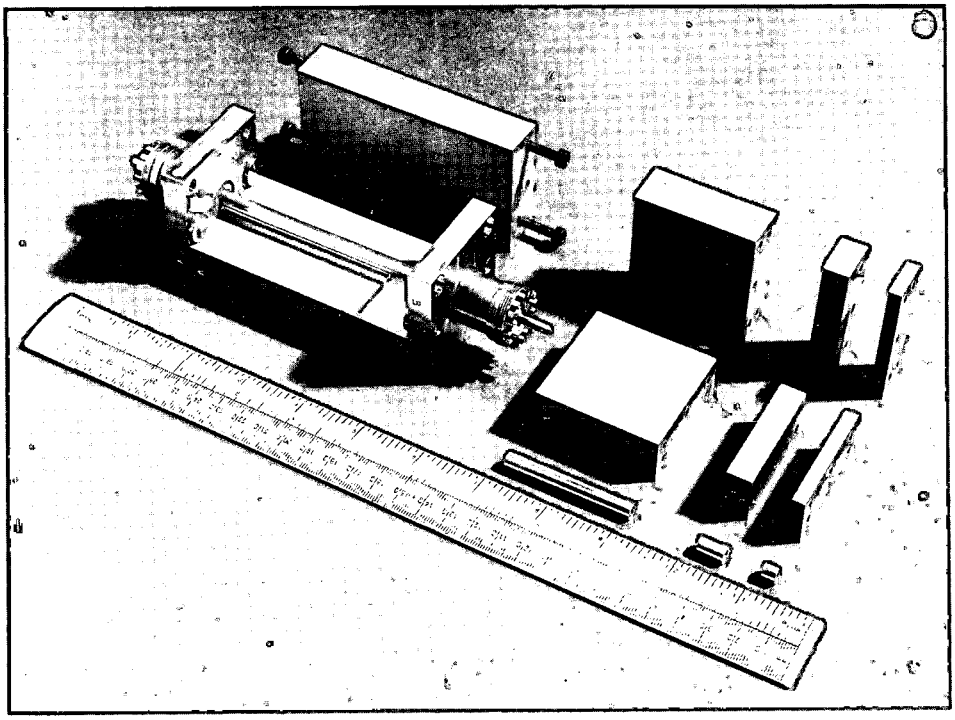

Figure 3 Slab line cell based on 14 mm line. The various lengths constructed are shown.

Because of the absence of any significant fields at the exposed surface of the samples it was possible to insert a thermocouple into the sample with negligible effect on the sample's reflection characteristics.

Materials—The slab line cell and the general technique were tested using the alcohols n-octanol ($C_8H_{18}O$; Fisher Scientific), n-butanol ($C_4H_{10}O$; May & Baker) ethanol (C_2H_6O; HM Customs & Excise) and n-propanol (C_3H_8O; May & Baker) for which some published dielectric data exist. These liquids were contained in the slab line by sealing one open side which thus created a base for the sample container. The liquids could then be poured in through the other open side.

The principal material studied in these experiments was the frozen flesh of cod *(Gadus morhua).* Samples were prepared by mincing the flesh before freezing. The slab line cell with one ground plane removed as in Figure 3 was filled with this minced material so that no air gaps were present. The detached plane was then replaced firmly on the sample and bolted into position, the correct ground plane separation being maintained by metal spacers. After placing a thermocouple in the sample as previously described, the cell was sealed with several layers of adhesive tape and placed within a thin polythene bag. The whole assembly was then immersed in a low temperature bath allowing freezing to take place *in situ.* All samples were of previously unfrozen, fresh fish, typically of 81% water, less than 1% fat and 0.1% NaCl. The density of flesh at sub zero temperatures is about 950 kg m^3 decreasing on freezing from 1050 kg m^3.

Temperature Control—The temperature of the bath was maintained constant within $\pm 0.5°C$ with a combination of refrigeration and heating. The coolant in the bath was a water and ethylene glycol based antifreeze solution. The fact that the samples were sealed in the slab line prevented either escape of moisture from the sample or leakage of the coolant into the sample. It is important to note that no shrinkage occurs away from the walls of the cell as the temperature is lowered.

Errors—The assessment of the errors involved in this technique is difficult. Although the individual contributions to the error are known, the overall effect on the final result cannot in general be expressed in the form of error graphs, as for example Iskander and Stuchly [7] have done for the lumped capacitance method. The errors in ϵ' are dependent on both the magnitude of ϵ' and ϵ'' as well as the product of frequency and sample length. Also, since equation (1) needs to be solved numerically, there is also an error resulting from the tolerance limits set by the iterative process.

The major possible sources of error are detailed below;

1. dimensional tolerance of sample cell: $\pm 0.5\%$
2. sampling oscilloscope time scale accuracy: $\pm 3\%$
3. tolerance of line impedance: $\pm 0.5\%$
4. accuracy of S_{11} determination from transformation of experimental results: $\pm 0.3\%$
5. timing errors: (not significant below 1 GHz)
6. temperature fluctuation: $\pm 0.5°C$
7. errors associated with digital Fourier analysis. These have been discussed fully by Nicolson [13]. They can be made negligible by keeping the frequency well below the Nyquist frequency and removing truncation error by the use of Samulon's [15] method. Although this has been considered to lead to errors (Nicolson [14]) they are not significant.
8. system noise: minimised by signal averaging but contributing to 4 above
9. iteration tolerance error: reduced by making tolerance limits narrower. Total error likely in ϵ^* is in this case $\pm 1\%$.

Estimates of the total maximum possible errors made by inserting relevant values of the above error sources into equation (1) shows that typically ϵ' may be determined within $\pm 6\%$ and ϵ'' to within $\pm 12\%$. The conductivity accuracy is in absolute terms about ± 6 μ-mhos.cm^{-1}. These figures worsen

for large conductivities when the shift of the base line becomes comparable to the height of the reflected pulse. Also at the higher frequencies as the sample electrical length approaches a quarter wavelength, considerable errors result as indeed they do in frequency domain methods, the iteration procedure tending to find multiple roots. The problem of high frequency accuracy is further added to by timing errors.

For each set of measurements made the errors were calculated for the values of permittivity and loss at the extremes of the frequency band. These are the error bars shown in Figures 4 - 7.

Results and Discussion

Alcohols—To test the validity of the use of a slab line cell with the total reflection TDS technique a number of alcohols were studied at room temperature as has been described.

A plot of ϵ' and ϵ'' versus frequency for n-octanol is shown in Figure 4. At least from this the data appeared self-consistent. The various parameters, high frequency permittivity ϵ_∞, static permittivity, ϵ_s, and relaxation time, τ, for the other alcohols used are shown in Table 1. Also in Table 1 are the results published by van Gemert [17] on the same liquids. As will be seen quite good agreement exists between the sets of data, the major discrepancies occurring in the determination of ϵ_∞. This is also reflected in the values of τ obtained from the Argand diagram. However the precision appeared sufficiently accurate to permit this method to be employed to study frozen biological materials such as fish flesh.

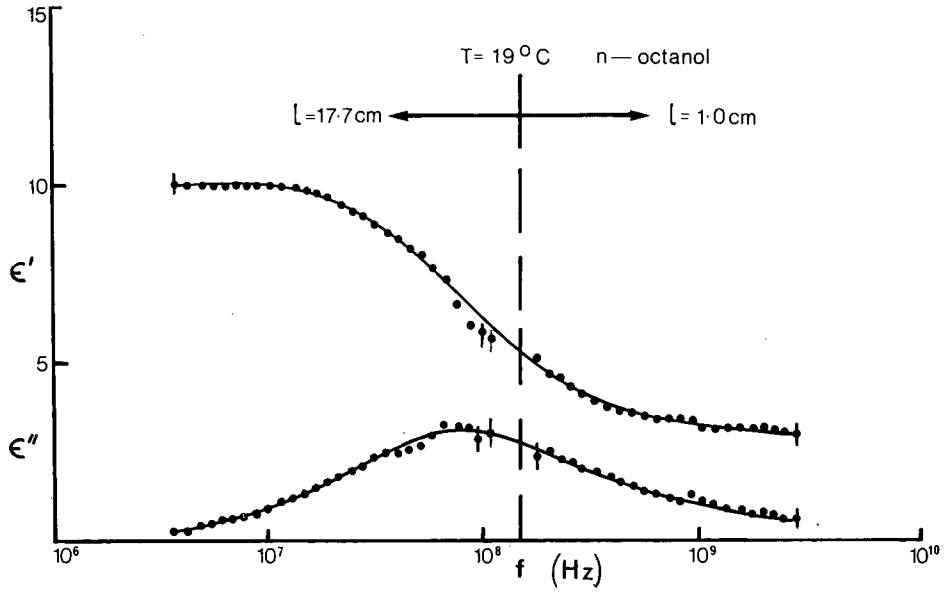

Figure 4 Complex permittivity and loss ϵ' and ϵ'' versus frequency for n-octonal at 19°C.

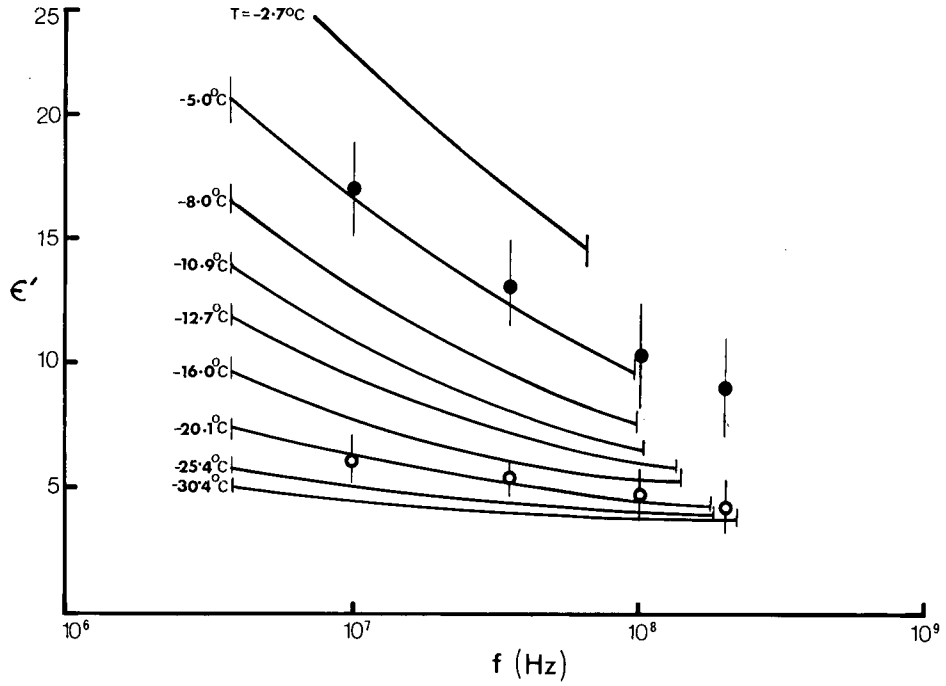

Figure 5 ϵ' versus frequency for frozen cod flesh at various temperatures below 0°C. Error bars calculated for extremes of frequency range. Plotted points are from Bengtsson *et al.* (1963); open circles −25°C, closed circles −5°C.

TABLE 1

Substance	T°C	ϵ_∞	ϵ_s	τ(ps)
Ethanol	2.0	4.7	28.3	332
	19.0	*5.0*	*25.3*	*187*
	24.0	4.55	24.75	176
Propanol	19.8	4.22	21.3	404
	20.0	*3.9*	*21.3*	*371*
	25.9	4.25	20.6	322
Butanol	19.2	3.3	17.1	543
	21.0	*3.7*	*17.6*	*496*
	22.5	3.3	17.4	513
Octanol	*20.0*	*3.1*	*10.0*	*1750*
	*20.0	*3.05	*10.35	*1750

The values in italics are current work, others are from van Gemert [17].
* Lebrun, A., [10].

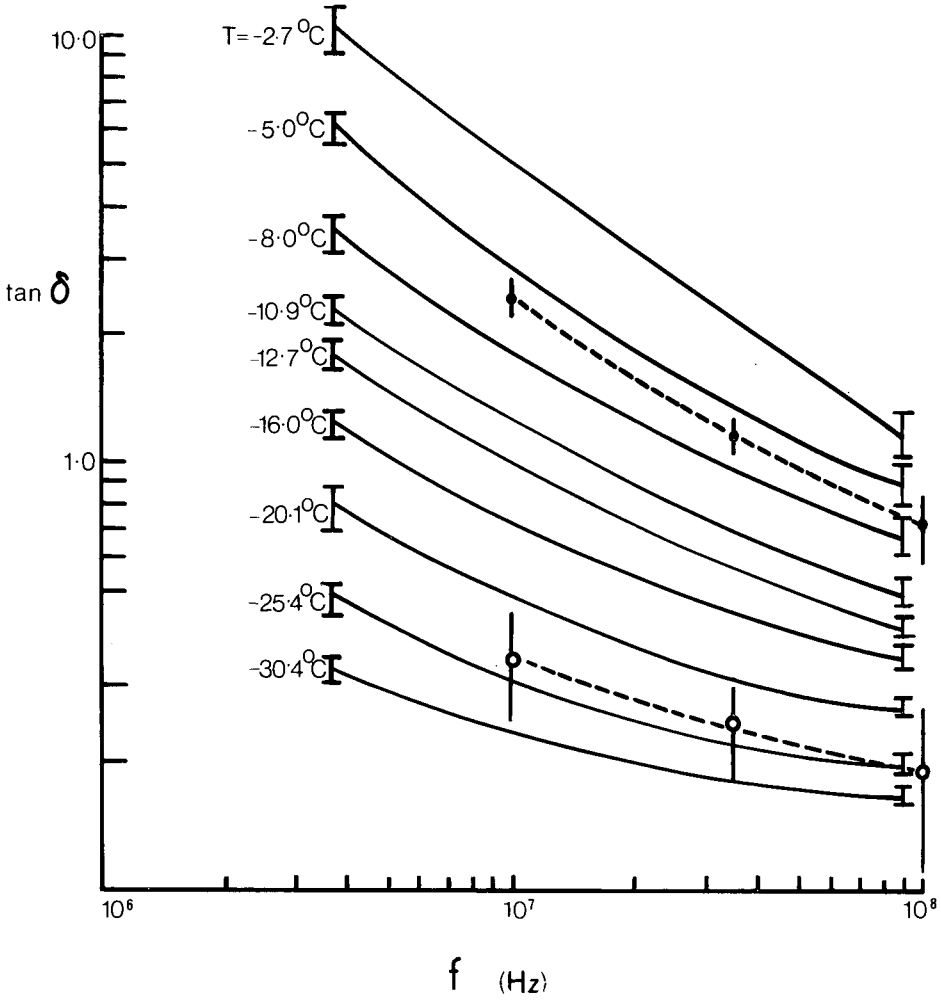

Figure 6 Tan δ versus frequency for cod flesh at various temperatures below 0°C. Error bars are calculated standard errors for extremes of frequency range. Plotted points and dotted lines from Bengtsson *et al.*, (1963): open circles −25°C, closed circles −5°C.

Fish muscle—The reason for undertaking the study of frozen fish muscle was partly to examine the time dependence of the various states of water at sub zero temperatures. It has already been noted that at 10 GHz a considerable change takes place in the microwave absorption properties. This change is seen as a fall in the attenuation factor, α, over periods of between a few days to several weeks depending on the temperature (Kent [9]). Such observations had been attributed to a gradual accretion of ice from the remaining liquid states. However confidence in this explanation was limited by a lack of information on the properties at other frequencies. In particular, confirmation of the above findings would be provided by changes being observed in (1) the real part of the complex permittivity, and (2) dispersive loss, since any conductivity changes would not have been expected to be sufficient to explain all the change at 10 GHz.

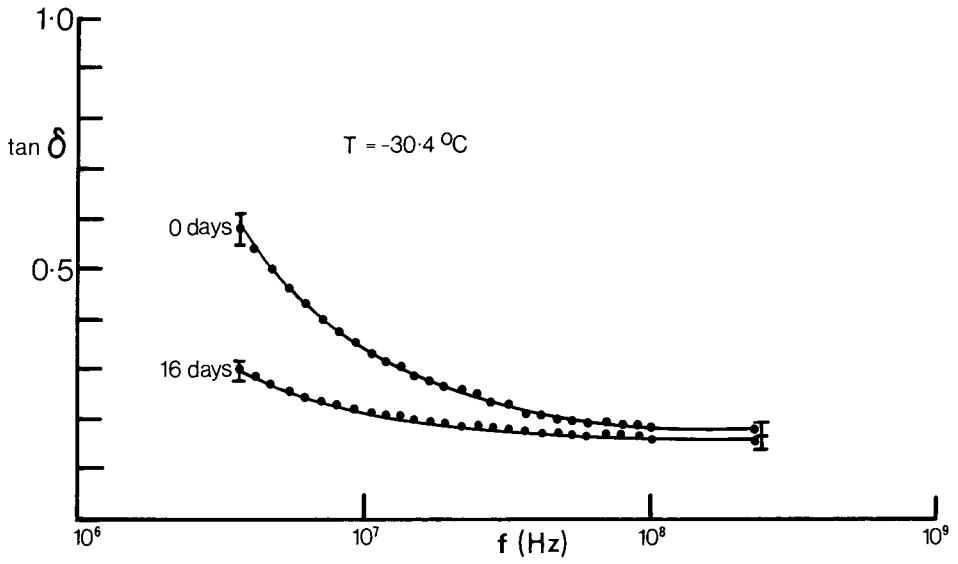

Figure 7 The effect of time on loss tangent spectrum of frozen cod flesh at −30.4°C.

For freshly frozen muscle at 10 GHz and −10°C the conductive contribution to the loss factor can be calculated from the conductivity measurements (Jason, Private Communication [8]) shown in Figure 8. These calculations yield a value of $\epsilon''_{\delta} \sim 0.01$. If this fell by a factor of 50% say, a very large proportion indeed, the change in ϵ'' at 10 GHz would at most only be ~5%. ϵ'' at this frequency is estimated to be $\sim 0.1 \rightarrow 0.2$ and, as is well known the conductivity loss component is inversely proportional to frequency. The total change observed in α at 10 GHz is typically in excess of 10% so even in the presence of conductivity changes the dispersive loss must also change.

Although the work of Bengtsson *et al.*, [1] showed no significant changes in the dielectric properties of frozen cod with storage time, it should be mentioned that changes had been observed in frozen meat. The lack of changes in the fish can be explained in two ways. Firstly, the period over which a comparison of the samples was made did not start until 2 days after freezing during which time a significant proportion of the change would have taken place. Secondly, the samples were warmed from −30°C to −10°C for measurement which by melting some of the ice would have tended to mask any changes that had occurred at the lower temperature. However, in those data, despite the statistical analysis, a trend may be seen which is downwards with time.

By making measurements of the permittivity spectrum at regular intervals during the first few days or weeks of frozen storage, after apparent temperature equilibrium had been achieved, very large changes indeed were noted (Figure 7). Both ϵ' and ϵ'' were seen to fall at all frequencies above 3 MHz but particularly striking was the large change in conductivity. The absolute value of conductivity is extremely dependent on the state of the muscle prior to freezing and hence is not very informative, but the large changes, post freezing, are worthy of note. As explained above, however, the contribution that such

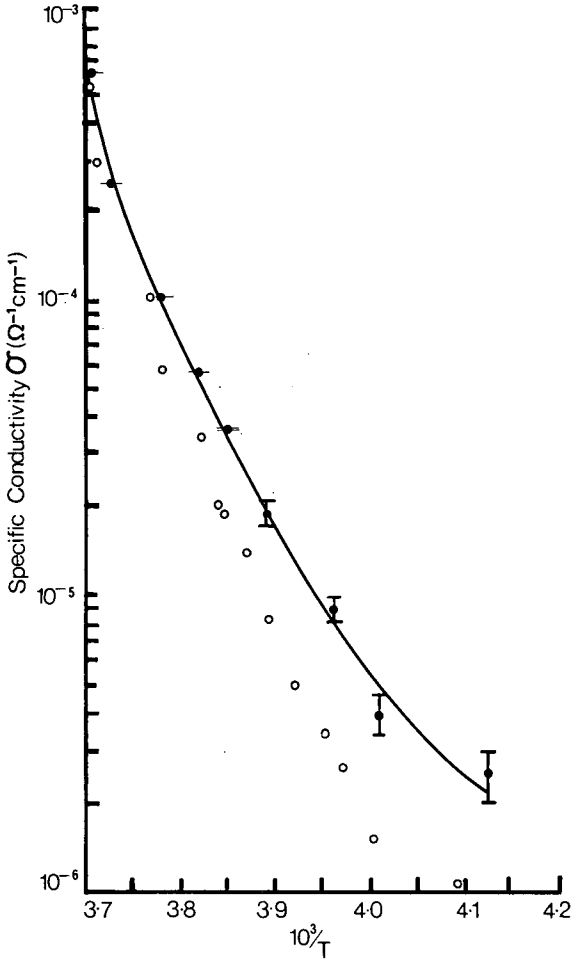

Figure 8 DC conductivity after equilibration versus $10^3/T$. Open circles represent data collected by 2 terminal dc measurements. (Jason, Private Communication [8]).

a change as this would make to measurements at 10 GHz must be slight though still measurable. It is to be noted also that the dispersive loss is seen to fall, perhaps a further indication that water is being converted to ice. Figures 5 and 6 show the equilibrated values of permittivity and loss at different temperatures.

The dipolar components, contributing to the dielectric spectrum in the frequency range covered by this experiment, are probably all configurations of water substance intermediate in rotational freedom between liquid and solid. That no distinct relaxation occurs is evident from the loss spectrum itself which shows no peaks. This is as one would expect from the heterogeneous nature of the system. The gradual decrease in the dielectric parameters is something which would arise if some of the water involved in the high frequency permittivity was gradually changing state to ice.

Conclusions

The results obtained on frozen cod muscle confirm that the marked time dependence observed previously in α at 10 GHz is seen at lower frequencies. This strengthens the argument that it can be attributed to slow changes in the internal partition of ice and water within the muscle structure.

References

1 Bengtsson, N. E., Melin, J., Remi, K. and Söderlind, S. (1963), 'Measurement of the dielectric properties of frozen and de-frosted meat and fish in the frequency range 10-200 MHz' J. Sci. Fd Agric. *14,* 592-604.

2 Cooley, J. W. and Tukey, J. W. (1965), 'An algorithm for the machine calculation of complex Fourier series', Math. Comput., *19,* 297-301.

3 Fellner-Feldegg, H., (1969), 'The measurement of dielectric in the time domain' J. Phys. Chem. *73,* 616-623.

4 Fellner-Feldegg, H., (1972), 'A thin sample method for the measurement of permeability, permittivity and conductivity in the frequency and time domain' J. Phys. Chem., *76,* 2116.

5 Hamming, R. W., (1962), 'Numerical methods for scientists and engineers' p. 82, McGraw-Hill, New York.

6 Hopkinson, J., (1901), Original Papers, *2,* p. 119 Cambridge Univ. Press, London.

7 Iskander, M. F., and Stuchly, S. S., (1972), 'A time domain technique for measurement of the dielectric properties of biological substances', IEEE, trans. *IM21,* 425-429.

8 Jason, A. C., (Torry Research Station, Private Communication).

9 Kent, M., (1974), 'Fish muscle in the frozen state: time dependence of its dielectric properties' J. Fd. Sci. Tech. (to be published).

10 Lebrun, A., (1955), 'Some techniques for the study of dielectric properties of solid and liquid substances. Application to the case of some normal saturated alcohols' Ann. Phys., *10,* 16.

11 Loeb, H. W., Young, G. M., Quickenden, P. A. and Suggett, A. (1971), 'New methods for measurement of complex permittivity up to 13 GHz and their application to the study of dielectric relaxation of polar liquids including aqueous solutions' Ber. Bunsenges. Phys. Chem., *75,* 1155-1165.

12 Loeb, H. W., (1972), "Efficient data transformation in time domain spectrometry' IEEE trans., *IM21,* 166-168.

13 Nicolson, A. M., (1968), 'Broad band microwave transmission characteristics from a single measurement of the transient response' IEEE trans., *IM17,* 395-402.

14 Nicolson, A. M. (1973), 'Forming the fast Fourier transform of a step response in time domain metrology' Electronics Letters, *9,* 317-318.

15 Samulon, H. A., (1951), 'Spectrum analysis of transient response curves' Proc. IRE. *39,* 175-186.

16 Clark, A. H., Quickenden, P. A. and Suggett, A., (1974) 'Multiple Reflection Time Domain Spectroscopy' J. Chem. Soc., Faraday Trans. II, *70,* 1847-1862.

17 van Gemert, M. J. C., (1972), 'Time domain reflectometry as a method for the examination of dielectric relaxation phenomena in polar liquids' Doctorate Thesis, University of Leiden.

18 van Gemert, M. J. C. (1973), 'High frequency time domain methods in dielectric spectroscopy' Philips Res. Repts., 28, 530-572.

A Portable Microwave Phase Detector*

T. Kardiçali†

ABSTRACT

Microwave phase-shift measurements play an important role in a number of industrial applications. Unfortunately, instruments and methods currently available for phase measurements are either very sophisticated or rather involved. For this reason, an automatic portable low-cost microwave phase detector was developed. A single-sideband modulator provides audio frequency substitution within a microwave bridge, the phase measurement being then carried out by electronic means. Application to the measurement of reflection phase-shift is described in this paper.

Introduction

Several microwave measurement techniques require a fast and accurate determination of the phase of a signal. For instance, reflection measurements were developed to determine physical material properties such as the dielectric constant, which is strongly affected by water content, and to measure small displacements or surface irregularities. Alternate means to determine phase-shift include slotted line measurements, which are very tedious and time-consuming, or elaborate instruments like automatic network analyzers, which are bulky and costly. It appeared that a small, if possible portable, low-cost microwave phase-meter would be a most valuable tool in a number of studies connected with the measurement of material properties. This device could typically be narrow-band and should give a sufficient accuracy. The device described in this article was designed to operate at 9.35 GHz (X-band). The accuracy obtained to-date is of the order of $\pm 1°$. Although this instrument was originally intended for measurement of reflections, it can just as well be used, by changing the waveguide connections, to measure transmission phase-shift.

Specifications

The frequency of 9.35 GHz is often encountered in the measurement of material properties. Power levels of the order of 10 mW are easily generated by using either Gunn or IMPATT type diodes. For these reasons, the phase detector described in this article is designed to operate in conjunction with a 9.35 GHz low power oscillator. For the measurements of distance considered, the precision desired is of the order of ± 0.1 mm, corresponding at the operating frequency to a phase accuracy of about $\pm 1°$.

* Manuscript received May 23, 1974; in revised form October 10, 1974.

† The author is with the Chaire d'Electromagnétisme et d'Hyperfréquences, Ecole Polytechnique Fédérale le Lausanne, 16 Chemin de Bellerive, CH-1007—Lausanne/Switzerland.

For accurate measurements of material properties, on the other hand, the precision should be higher, since phase-shift inaccuracies introduce significant errors in the permittivity, in particular affecting the imaginary part (losses) [1, 2]. For this application, a precision of $\pm 0.1°$ should be sought, a value which is not directly attainable by standard measurement techniques.

Principle of Operation

Phase-shift measurements utilize interference techniques: it is necessary to compare the signal one wishes to measure with a reference [8]. Automatic instrument operation is achieved here by a phase-bridge and an audio frequency substitution. The principle of operation is shown in Figure 1, in which the unknown signal e is modulated ($b\ell$) and then compared with the reference signal b. The signals in the arms e and b are proportional to the functions of time:

$$E_e \sim \sin(\omega t + \phi)$$
$$E_b \sim \sin(\omega t) \qquad (1)$$

with $\omega = 2\pi f$, f corresponding to the RF frequency. The signal e to be measured goes through a single-sideband modulator fed by an audio generator [9]. The effect of this device is to shift the RF angular frequency in the arm e by ω_m, the angular frequency of the audio generator. If the SSBSC modulator suppresses completely the carrier and the second sideband, the time dependence of the output signal will be:

$$E_{b\ell} \sim \sin[(\omega + \omega_m)t + \phi] \qquad (2)$$

The unknown phase ϕ is conserved during the transformation. This signal is then mixed with the reference signal in a balanced mixer, giving finally an audio signal, (the difference of the arguments of E_e and $E_{b\ell}$);

$$V_s \sim \sin(\omega_m t + \phi)\ . \qquad (3)$$

This audio output signal V_s goes through a passive filter, an amplifier and a phase comparator, which displays the time difference separating the signal V_s from the reference signal supplied by the audio oscillator.

Main Sources of Errors

(a) *Second Sideband Residual Signal*

This error is mostly due to the difference between the four diodes of the 2 balanced modulators and dimensional tolerances. In the previous section, an ideal performance of the SSBSC modulator was assumed. However, it is not possible in practice to suppress completely the second sideband which gives rise to a signal with an $\omega - \omega_m$ angular frequency. The output signal E_b will then have the form:

$$E_{b\ell} \sim \sin[(\omega + \omega_m)t + \phi] + \epsilon \sin[(\omega - \omega_m)t + \phi] \qquad (4)$$

where $\epsilon << 1$ is the ratio of the second sideband residual signal to the first sideband signal. After mixing and detection the audio output signal will become:

$$V_s \sim \sin(\omega_m t + \phi) - \epsilon \sin(\omega_m t - \phi) \cong \sin(\omega_m t + \phi + \Delta\phi)\ . \qquad (5)$$

The presence of the residual sideband produces an error $\Delta\phi$ on the phase ϕ, which is approximately given by the following expression (Figure 2):

$$\Delta\phi \cong \text{arc sin } \epsilon\ (\sin 2\phi) \text{ if } \epsilon << 1. \qquad (6)$$

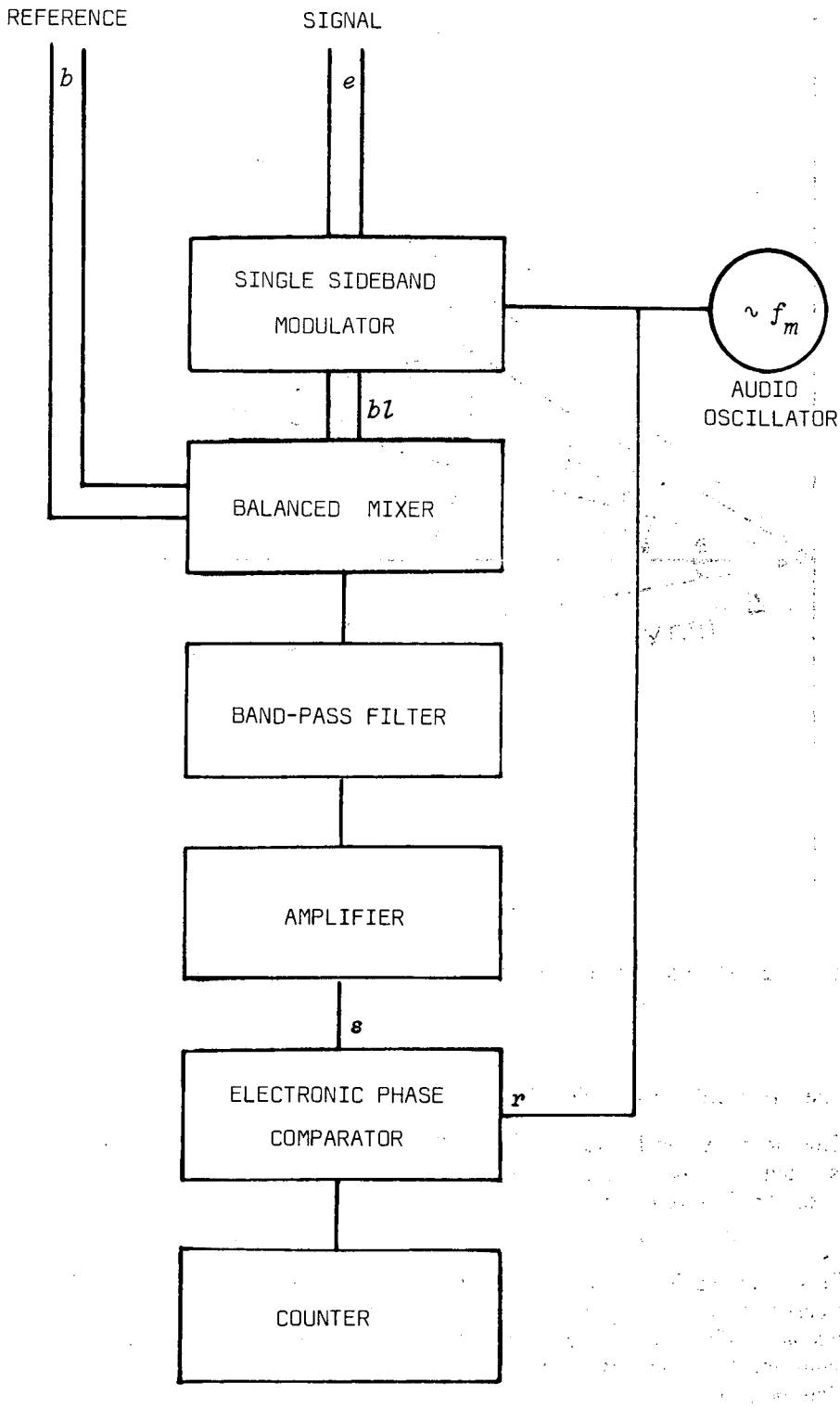

Figure 1 Block diagram of the microwave phase detector.

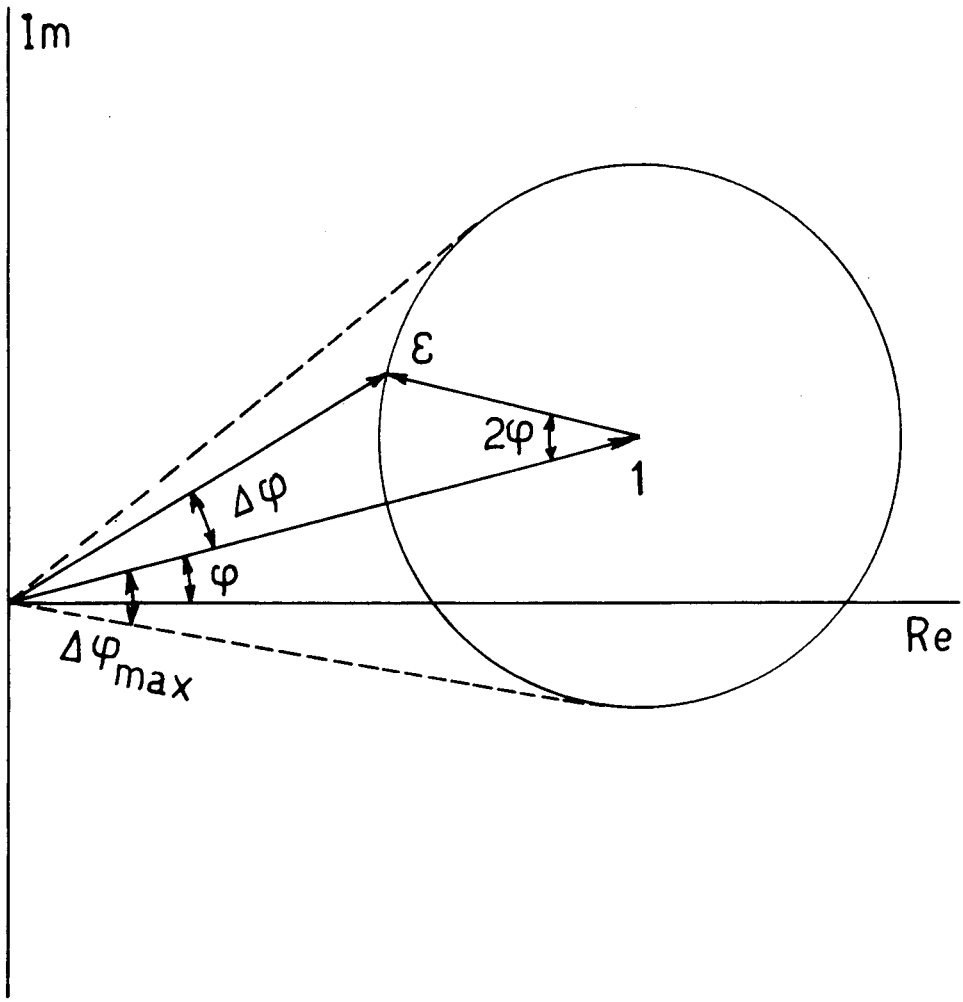

Figure 2 The effect of the residual second sideband in the complex plane.

The error $\Delta\phi$ varies with ϕ and vanishes when $\phi = \pm n\frac{\pi}{2}$ $(n = 0, 1, \ldots)$. This property can be used when small variations of the phase are involved, which is often the case in the measurement of materials. The maximum value of the error $\Delta\phi$ is given by:

$$|\Delta\phi| \leqq \Delta\phi \text{ max} = \text{arc sin } \epsilon . \tag{7}$$

This relationship is presented in Figure 3. To obtain $\pm 0.1°$ precision in the measurement of the phase angle it would be necessary to decrease the residual sideband 55dB below the main sideband. The suppression of the residual sideband must be 35 dB if the desired precision is $\pm 1°$, which still requires a high performance modulator.

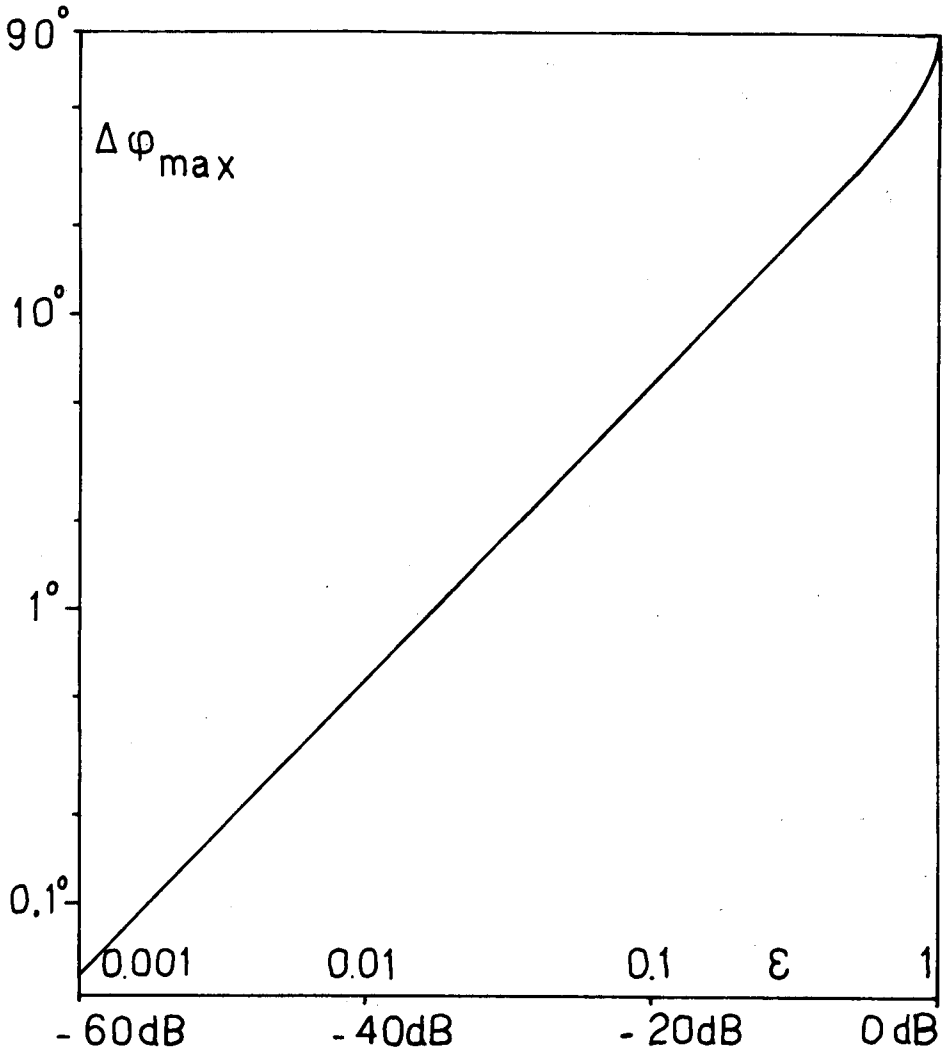

Figure 3 Maximum error as a function of the relative amplitude ϵ of the second sideband.

(b) *Temperature Variation*

The difference in path length [3] between the reference and the measurement channels is too small for a change in temperature to cause any significant error ($<< 1°$).

(c) *Harmonics of the audio signal and residual carrier component*

The suppression of the residual carrier component is not perfect and intermodulation products appear in the modulator and in the mixer. After detection, a constant voltage (carrier) and audio signals $n \times f_m$ appear, both of which are eliminated by the band-pass filter.

(d) *Noise*

The effect of noise becomes important when the amplitude of the audio output signal is very low. Sensitivity to noise can be reduced by using a narrow band-pass filter centered on f_m and an audio oscillator with very high-stability. This effect can be almost completely suppressed when the following conditions are satisfied in the balanced mixer [4]:

— The detectors follow a square low.
— The differential phase shift is the same in the two arms of the modulator for the unknown signal and the reference. This condition is satisfied if $f_m << f$.
— The coupling coefficient is exactly 3dB and the diodes have identical conversion efficiencies.
— The oscillator noise is small compared to the oscillator output, so that the product of noise and signal can be neglected.

Experimental Realization

The method used here to build the SSBSC modulator combines the signals produced by two balanced modulators, fed by the audio oscillator in phase quadrature with the same amplitude. The principle of operation is shown in Figure 4, which uses the following trigonometric relation:

$$\sin\ [(\omega + \omega_m)t + \phi] = \sin\ (\omega t + \phi)\ \cos\ \omega_m t + \cos\ (\omega t + \phi)\ \sin\ \omega_m t \qquad (8)$$

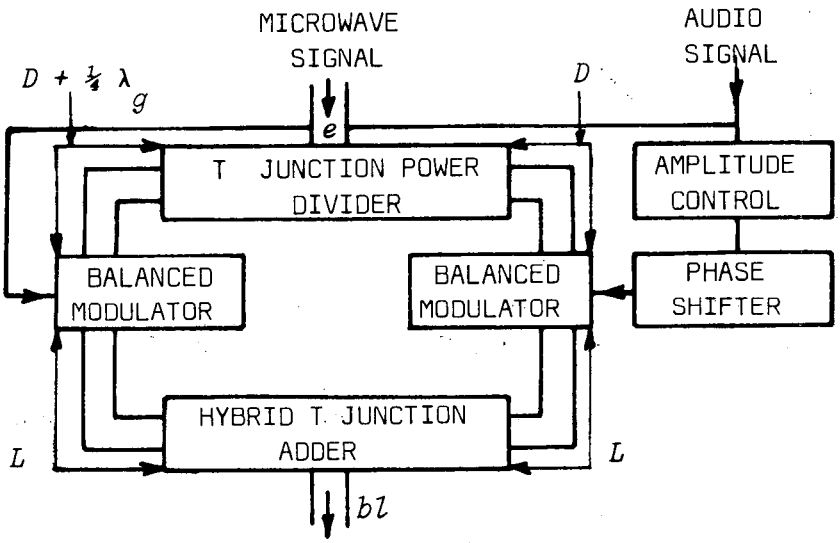

Figure 4 Block diagram of the single-side band modulator.

In each balanced modulator, a matched pair of diodes is used. By adjusting independently the level and the phase of the shifted RF signal in one arm of the modulator bridge by means of an electronic control circuit, it is possible to suppress almost completely the carrier and the unwanted sideband signals, compensating possible unbalances. This is carried out by observing the resulting signal on a spectrum analyzer (after heterodyning) or determining the

variation of the amplitude of the demodulated signal when the phase ϕ is varying. In the reflection measurements a movable short circuit is used: the maximum and the minimum of the detected signal are respectively proportional to $1 + \epsilon$ and to $1 - \epsilon$. If the amplitude remains constant while the phase is varied between ϕ to $\phi + 360°$ (movable short-circuit), the instrument is well calibrated.

The output audio signal obtained goes through a band-pass filter and a 30dB gain amplifier in order to compare it with the fixed reference signal generated by the audio oscillator. The two sine waves are first transformed into square waves and the pulses are then formed by a high-pass-filter. The two inverters connected to a nand gate realize a storage circuit (Flip-Flop) which gives a pulse, the width of which varies with the passage through zero of the unknown signal V_s. This time difference can be determined by measuring it with an electronic counter or by pulse integration (Figure 5).

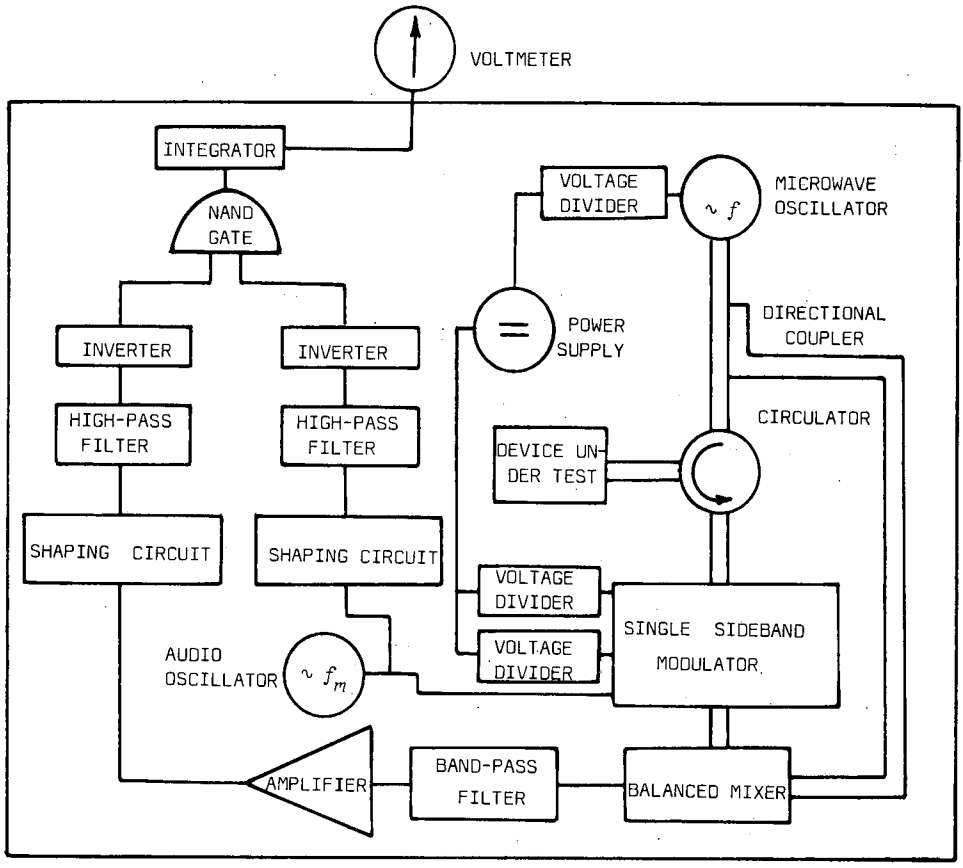

Figure 5 Block diagram of the audio circuit.

Application to Distance Measurements

The complete instrument for reflection phase measurements is composed of the described phasemeter, a Gunn diode generator, a 20dB directional

coupler, a circulator, an open-ended tunable waveguide and waveguides needed to assemble the bridge (Figure 6).

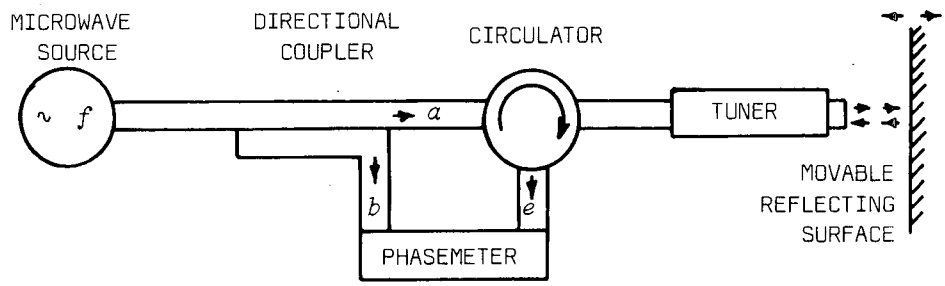

Figure 6 Distance measurement equipment.

Another source of error appearing in this setup is due to the finite isolation of the circulator (in the bridge presented here the isolation of the circulator is 32dB at the frequency of interest): a leakage signal with constant amplitude and phase is added to the signal to be measured. The apparent effect due to the leakage signal is similar to the one due to residual side band signal. The maximum variation of the phase is given by the equation (7) in which $\epsilon << 1$ represents the ratio of the leakage signal to the signal V_s. The spurious signal is cancelled by means of an opposing signal of same amplitude, this compensation being done by adjusting the screws of the tuner until the audio output is as low as possible when the open-ended waveguide is radiating into free space.

The effect of the temperature variations can become important here if the circulator is not adequately temperature-compensated. For operation over a broad range of temperatures it might be preferable to replace it with a directional coupler having very high directivity. In this case the sensitivity will decrease, while the error on the phase shift will be practically negligible.

Measurement results are presented in Figure 7. Curve A shows the error caused by the residual second sideband due to the unbalance between the four diodes (the two balanced modulators are in this case fed by two audio signals of the same amplitude in phase quadrature). After the tuning adjustments were made the curve B is obtained which presents a linear relationship agreeing with the theory [5, 6] and with measurements on a slotted line [7].

Conclusion

The instrument described here meets completely the desired requirements for operation once the calibration is done to suppress the leakage signal and the second sideband signal. It permits measuring the phase shift between 2 electromagnetic signals within a 100 MHz bandwidth centered at the nominal frequency of 9.35 GHz. Present dimensions of the instrument are $150 \times 100 \times 300$ mm including the electronic circuitry. Although portable, the device is still bulky and further size reduction by using microstrip circuits should be considered.

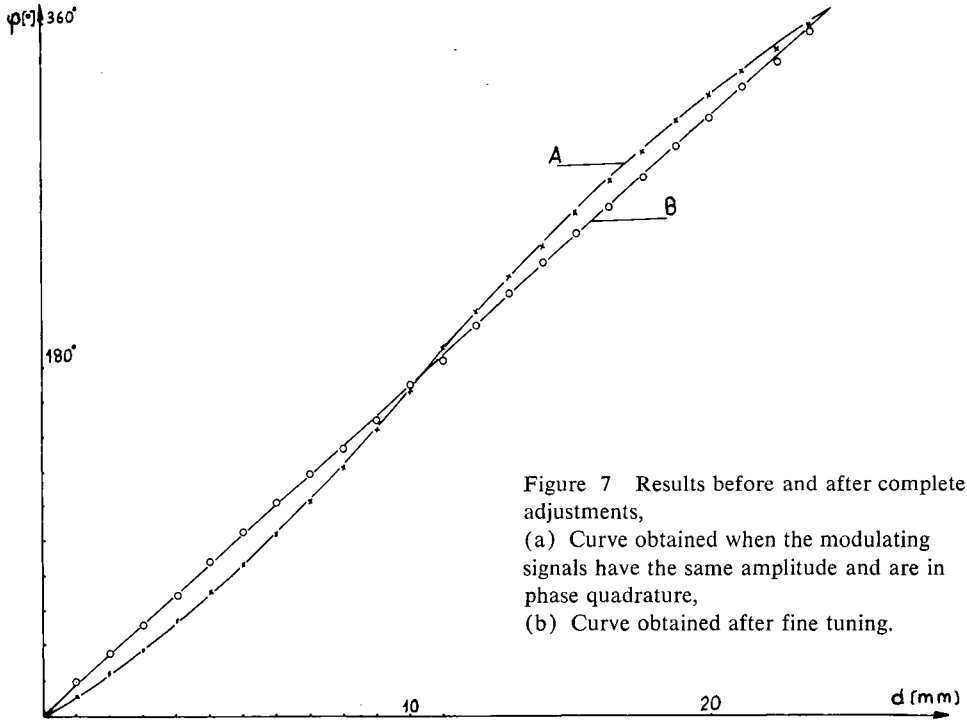

Figure 7 Results before and after complete adjustments,
(a) Curve obtained when the modulating signals have the same amplitude and are in phase quadrature,
(b) Curve obtained after fine tuning.

Acknowledgements

The author wishes to thank Prof. F. E. Gardiol for many interesting discussions and suggestions and Mr. O. Janz for his excellent mechanical realization of the modulator and mixer assembly.

References

1 Decréton, M. C. and Gardiol, F. "Simple non destructive method for the measurement of complex permittivity", *Conference CPEM 74 on Precision Electromagnetic Measurements,* London, pp. 113-115, July 1974.

2 Gardiol, F. "Nomograms save time in determining permittivity", *Microwaves,* 12, (11), pp. 68-70, November 1973.

3 Brooker P. G. and Beynon, J. E. D. "A 10 GHz Single sideband modulator with 1KHz frequency shift", *IEEE Trans.* MTT-19 pp. 829-834, October 1971.

4 Lange, J. "Oscillator noise cancellation in hybrid Mixers", *IEEE Trans.* MTT-16 (6) pp. 368-369, June 1968.

5 El-Moazzen, Y. S. and Shafai, L. "Mutual coupling between parallel plate waveguides", *Trans. 1973 G-MTT International Microwave Symposium,* Boulder, Colorado, pp. 281-283, June 1973.

6 Decréton, M. C. and Andriamiharisoa, V. "Effect of a conducting plate in the near-field region of an open-ended waveguide", *5th Colloquium on Microwave Communication,* Budapest, ET-97/108, June 1974

7 Ramachandraiah, M. and Gardiol, F. "A non contracting method for the measurement of small displacements" *IMPI Microwave Power Symposium Summaries,* Ottawa, pp. 48-51, May 1972.

8 Dyson, J. D. "The measurement of phase at VHF and microwave frequencies", *IEEE Trans.* MTT-14, p. 410, Sept. 1966.

9 Schwartz, M. "Information, Transmission, Modulation and Noise", *McGraw Hill Book Co.* New York, pp. 218-223, 1970.

Electromagnetic Fields and Skin Wound Repair*

C. Romero-Sierra†, S. Halter†, J. A. Tanner‡, M. W. Roomi† and D. Crabtree‡

ABSTRACT

Experiments were conducted to compare the effect on wound healing of treatment with saline, or histamine diphosphate alone or combined with the application of electromagnetic (EM) fields. Surgical incisions in the skin of the dorsum of 240 rats were treated with either saline or histamine; one-half of the animals treated with each chemical were exposed to a VHF (27 MHz) EM field for 15 minutes. Surgical incisions were also made in the skin of the right scapular region in 10 dogs; one-half of the animals were treated with saline and the other half with histamine and a VHF field for 30 minutes.

Histamine treatment in conjunction with EM field exposure proved most efficient in improving wound healing (rate of healing, tensile strength, minimized scar tissue); saline treatment plus EM field exposure, histamine alone and saline alone were successively less effective. The medical efficacy of EM field treatment is demonstrated, and it is noted that the greatest effort occurs within 12 hours of treatment.

Introduction

Experimental studies of the interaction of radio frequency fields with birds, in connection with the development of a bird deterrent for airports, led to the discovery that electromagnetic energy in the non-ionizing frequency range stimulates and enhances the production of collagen in tissue. This prompted an investigation of the possible beneficial action of controlling collagen generation in the process of wound repair.

The efficiency and rate of wound healing may be enhanced by chemical and physical stimulants. Previous experiments by the authors [1] indicated that the application of histamine to a fresh wound followed by exposure of the wound to an electromagnetic (EM) field accelerated the healing process.

Using an identical experimental technique, a comparison has been made of the healing processes in four sample specimen groups. Two groups of rats were treated with saline (applied to incisions), and two groups were treated with histamine. One group of each pair treated with chemicals served as a control,

* Invited paper; first received December 2, 1974.

† Department of Anatomy, Queen's University, Kingston, Canada.
‡ Control Systems Laboratory, Division of Mechanical Engineering, NRC, Ottawa.

while the other was exposed to an EM field. In this manner, the effect on wound healing of the saline and histamine treatments alone could be compared as well as the effects produced by the EM field. A comparative evaluation was made of the healing process at 12, 24, and 72 hours.

Adjunct to the histological evaluation of healed wounds, a preliminary study was initiated on the mechanical characteristics of the healing process. A pilot experiment was conducted on dogs to compare the tensile strength of normally healed and VHF treated wounds after a period of five days.

Materials and Methods

Procedure with Rats

Incisions 1.5 cm in length were made in the backs of 240 Sprague-Dawley rats, each weighing between 200 gm and 300 gm. The wounds were pretreated by applying two drops of either saline or histamine diphosphate (1.0 mg per ml) to the incisional area. One-half of the saline group and one-half of the histamine group were then exposed to a VHF (27 MHz) field for 15 minutes during which time the edges of the wound were apposed by manual pressure After 12, 24 and 72 hours the tissues were removed and examined by light microscopy. (Details of the experimental procedure are given in Reference [1].)

Procedure with Dogs

Ten beagle dogs used in this study were 9 - 11 months old and weighed between 9 and 12 kg. The right foreleg was clipped and cleaned with 70% alcohol. Thiopental sodium (Diamond Laboratories Inc., Desmoines, Iowa) was administered (5% solution at a rate of 1 ml per 2 kg body weight) intravenously. When fully anesthetized the dog was intubated and supplied with oxygen at a rate of 50 - 100 ml/min. The scapular area was then clipped and shaved and a single incision 2.5 cm in length made in the skin. The depth of the incision was such as to cut both the epidermis and dermis leaving underlying fascia intact.

In five of the dogs (controls) the wound was treated with saline only and in the remaining five histamine was applied followed by VHF irradiation. The edges of the wound were carefully apposed and held together for 30 min. At the end of the operation the tube was withdrawn and the dog was given 1 ml of Innoval-Vet (Pitman-Moore, Don Mills, Ontario).

After a period of five days the dogs were anesthetized again and a sample of skin was taken from the wounded area. Templates were constructed to mark out the area of skin to be excised. A specimen 1 cm wide crossing the central part of the wound was prepared from each excised sample for tensiometric analysis. It was placed in a specially designed chuck for mounting in an Instron tensile testing macine. The chuck assembly constituted a transportable specimen holder which prevented the specimen from being prestressed while being mounted in the Instron machine. The active part of the specimen under tension measured 1.0 cm by 1.3 cm.

Specimens were tested to destruction and the peak value of the tension noted. Strain was applied at a constant rate of 1.25 cm/min.

Observations

Rats After 12 Hours

After 12 hours the incisional area of the control rats treated only with saline was observed to be filled with acute inflammatory cells, predominantly polymorphonuclear leukocytes. The fibrin network at the base of the wound was loosely woven and there was no specific orientation of the fibres.

In rats treated with histamine alone the incisional gap appeared smaller than in those treated with saline. The cellular infiltrate again consisted predominantly of acute inflammatory cells, although more macrophages and fibroblasts were present than in the previous control group treated with saline. There was extensive dilation of blood vessels and as in the control group treated with saline, the fibrin was loosely woven with no specific orientation of the fibres.

In each rat treated with saline and exposed to an EM field the wound area was difficult to identify after 12 hours. The presence of acute inflammatory cells enabled the gap to be identified in only a few areas. The fibrin network of these incisions appeared more compact than in either test group and the fibrin was oriented parallel to the sides of the wound.

In the test group treated with histamine and exposed to an EM field the wound area was even more difficult to identify. Identification was possible in some areas because of the presence of a foreign body, such as a piece of hair, whereas in other areas it was seen as a thin line of acute inflammatory cells.

Rats After 24 Hours

At 24 hours the observations described in the earlier report [1] were confirmed (see Figures 1, 2, 3 and 4). These include, (i) a smaller incisional gap, (ii) less infiltration of white blood cells, and (iii) more fibroblasts and macrophages and more of a fibrin base in the test group of rats treated with saline and EM field as compared to the controls treated only with saline. In addition, more fibrin was observed in the base of the wounds of both groups of histamine-treated rats, the most being observed in the test group treated with histamine and EM field. The histamine-treated groups, both control and test, had fewer white blood cells in the incisional area but a greater number of fibroblasts.

In the control group treated with saline, Figure 1, the fibrin base was observed to be largely amorphous in nature but beginning to form an organized reticulum. The fibres appeared to be only loosely associated. However, the fibrin base of the histamine control group appeared very granular in consistency, with little evidence of fibre formation.

A very interesting fibrin pattern was observed after 24 hours in the test group treated with saline and EM field. The individual components of the fibrin base appeared to be oriented parallel to the edges of the incision, and were densely packed together. In the test group treated with histamine and EM field, it was very difficult in places to locate the incision. The only sign of inflammation and repair was a thread-like collection of mononuclear cells. In other areas resorbing blood clots could be seen but the extensions of the

Figure 1 Transverse Section of a Wound from a Rat Pretreated Only With Saline, (Control Group No. 1). The Fibrin Base has a Loose Reticular Pattern. (1200 X).

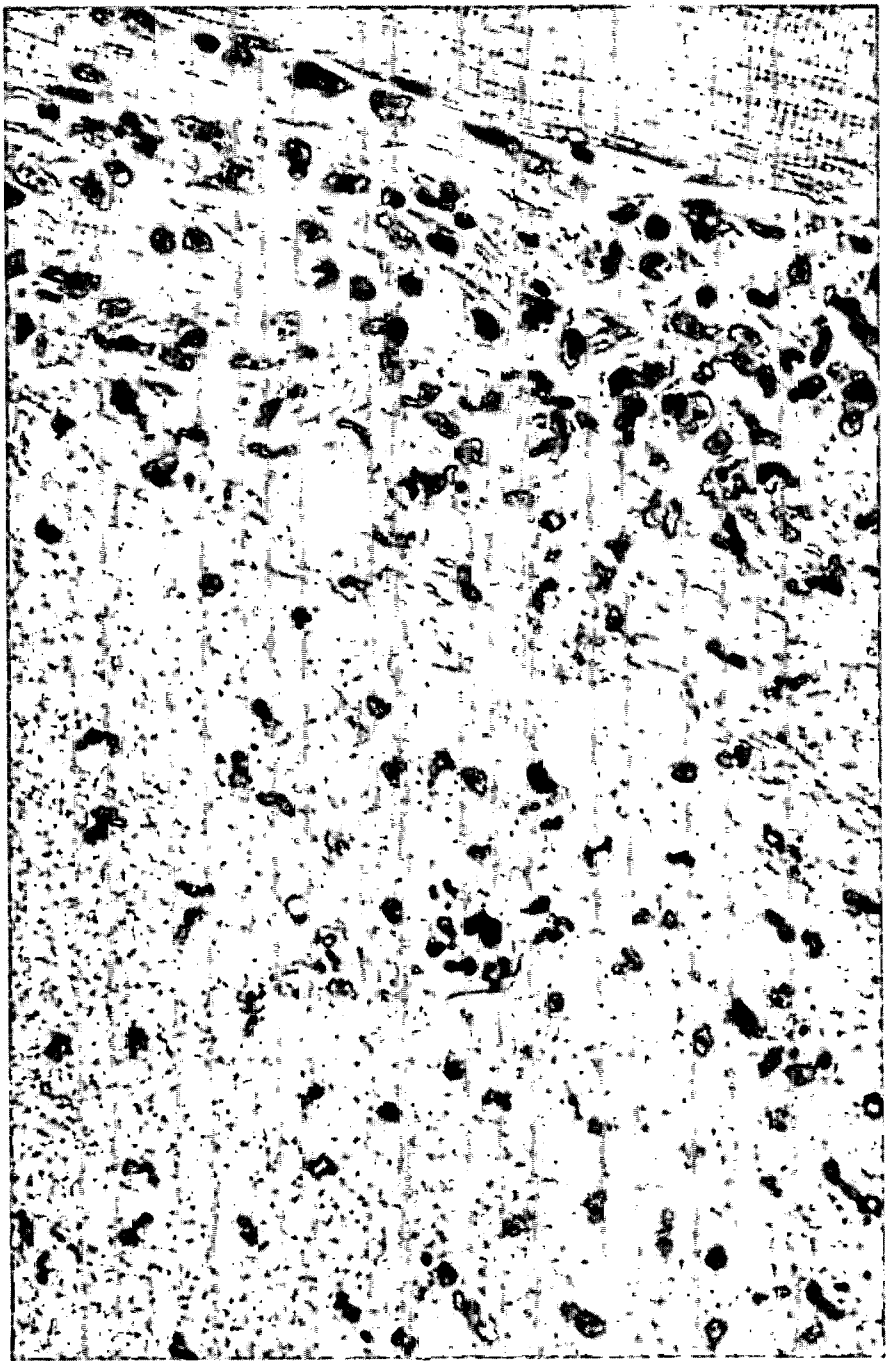

Figure 2 Transverse Section of a Wound from a Rat Pretreated With Histamine, (Control Group No. 2). Showing the Granularity of the Fibrin Base. (1200 X).

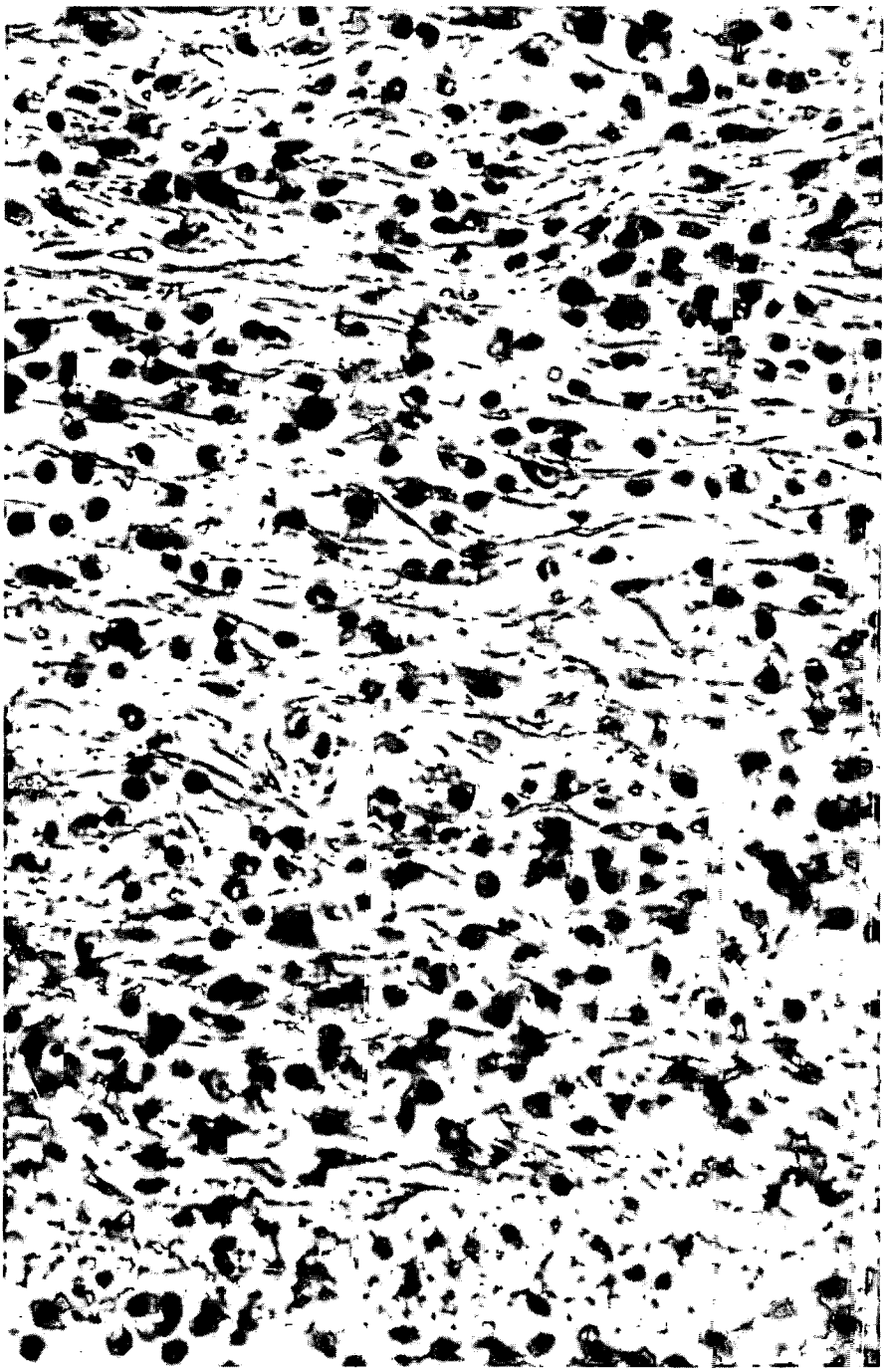

Figure 3 Transverse Section of a Wound from a Rat Treated with Saline and EM Field, (Test Group No. 3). Showing the Parallel Orientation of the Fibrin Fibres. (Most of the Cells in the Infiltrate are Mononuclear Cells and Fibroblasts). (1200 X).

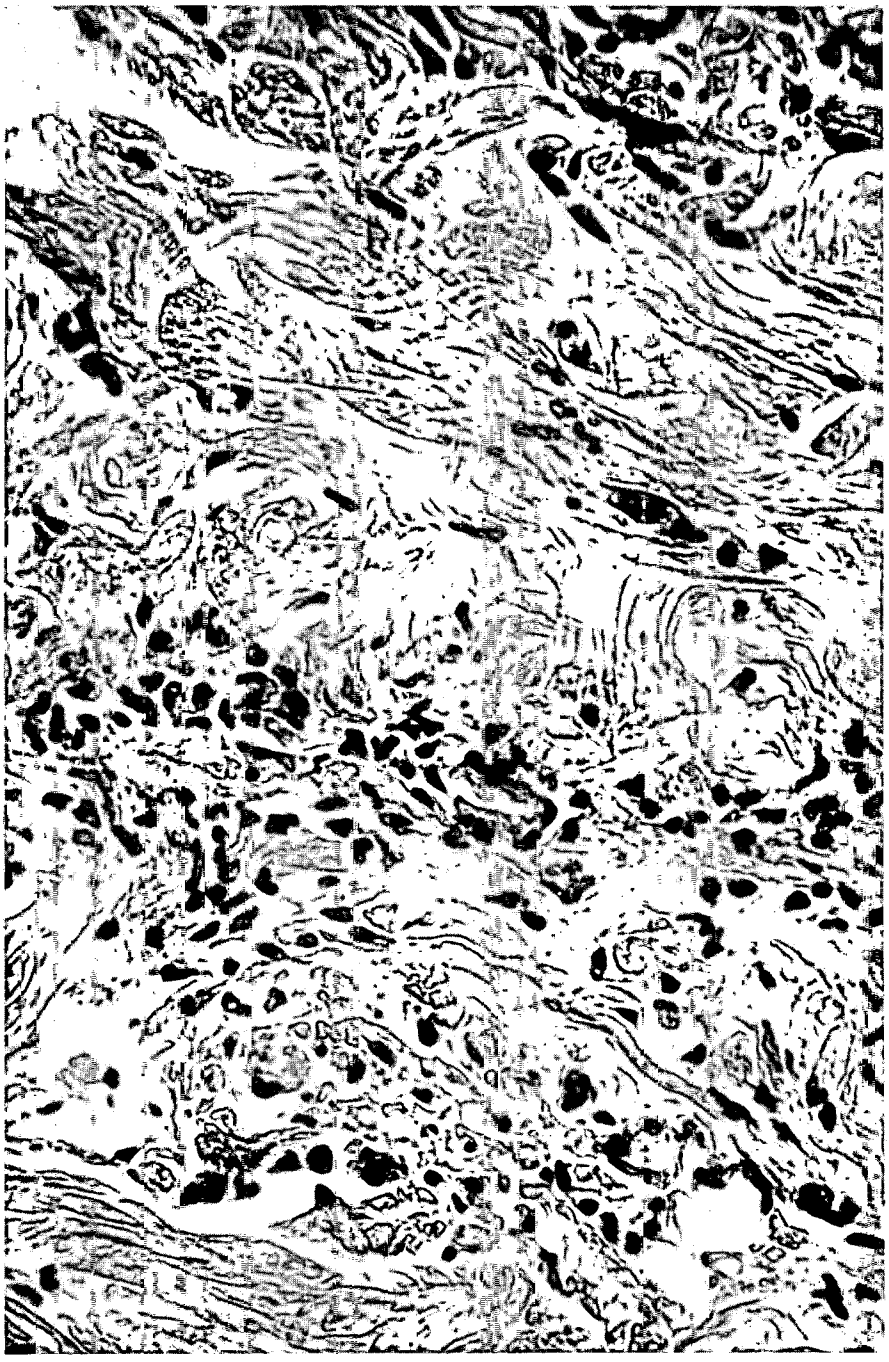

Figure 4 Transverse Section of a Wound from a Rat Pretreated with Histamine and Exposed to an EM Field (Test Group No. 4). (Note the Difficulty in Identifying the Wound as Compared to the Other Groups). (1200 X).

wound were not evident. Connective tissue fibres in the wound area were closely apposed and intertwined.

Inspection of the serial sections of tissue taken from the wound area 24 hours after treatment revealed that the incisional gap was narrowest at the surface of the skin and increased in width below the surface. This accounted for some variation in the time course of wound healing since the closer the apposition of the edges of a wound, the easier and quicker the defect is bridged and the entire wound healed.

The typical appearance of wounds treated (i) with histamine and EM field and (ii) with saline are as shown in Figure 5.

Figure 5 Typical Appearance of (I) Treated Wounds and (II) Untreated Wounds After 24 Hours.

Rats After 72 Hours

After three days, the incisional area in the rats pretreated with saline alone could be identified by collagen fibres in the wound lying parallel to the edges of the incision. In certain area, leukocytes, predominantly mononuclear cells, were observed to be clustered at one edge of the wound.

The edges of the wounds of rats pretreated with histamine alone were not as distinct as those of the control group treated with saline alone. Further, the collagen fibres were not as thick. The fibrin base of the wound appeared loosely woven together.

In each animal of the test group treated with histamine and the EM field, the incisional gap was very difficult to detect. Whereas in some parts of the incision the healing process was well advanced, in others there were signs of interference to healing revealed by marked infiltration of cells. This variation correlated with the presence of a blood clot.

Wounds treated with the EM field revealed incisional gaps much smaller than those of either control group. The wound area of the test group pretreated with saline and exposed to the EM field appeared as a very fine defect in a collagen and fibroblast stroma. Only by the infiltration of cells into the area was the wound detectable. The collagen was closely associated with, and predominantly oriented parallel to the incisional edges.

Dogs After 5 Days

Wounds in the dogs followed the same pattern of healing observed in the rats. The incision line was difficult to detect in the test animals after five days. Only the site of the lesion was discernible as a change in density of the hair.

Examination of the inner and outer surfaces of the excised skin specimens revealed that the incision had completely closed in the test animals but had failed to close on the inner surface in the controls. Samples of these sections have been stored for future histological examinations.

The results of the tensile tests are presented in Table 1. The average value for the test dogs is 530 gm compared to 141 gm for the controls. In the test dogs the cosmetic appearance of the wounds was superior to those of the controls throughout the 5-day period.

Discussion

Twelve hours after making the incisions there were marked differences between the control and test groups. In the control groups the distance between the edges of the wound was much greater than in the groups exposed to an EM field and the only sign of organization was the infiltration of acute inflammatory cells. Contrast this with the histamine-treated control group in which a greater number of fibroblasts and macrophages were seen, suggesting an advance in the healing process, perhaps related to the profound vasodilation and vascular permeability observed in these wounds.

In the test group treated with saline or histamine and exposed to an EM field for 15 min., the wound area was very difficult to identify except in certain areas where there was a resorbing blood clot or foreign body reaction.

Malapposition of the edges of an incision is a well known deterrent to wound healing [2]. It is understandable that if the edges of a wound are well apposed initially, with a very small gap between them, much of the delay in healing due to infiltration of acute inflammatory cells, removal of debris by macrophages and infiltration of fibroblasts, is obviated. Collagen required to bridge the gap and impact tensile strength to the healed wound is produced earlier. Also, the incisional area is smaller, thereby ensuring a smaller scar and better cosmetic appearance of the healed wound.

In a previous paper [1] it was noted that the edges of wounds treated with histamine and EM field are more manageable and more adhesive. This is very beneficial since closely apposed edges minimize the area in which

TABLE I
RESULTS OF TENSILE TESTS PERFORMED ON SKIN SPECIMENS FROM 10 BEAGLE DOGS

	Animal	Sex	Weight (kg)	Tensile Strength (gm)
Test	1	M	12.3	240
	2	M	13.2	500
	3	M	10.0	1205
	4	M	11.8	347
	5	F	11.6	360
Average Tensile Strength (Test) 530 gm				
Control	6	M	13.4	74
	7	F	11.9	264
	8	F	10.0	163
	9	F	7.8	150
	10	M	12.4	54

Average Tensile Strength (Control) 141 gm

healing occurs. At the present time, the role of histamine in wound healing is not fully understood. There is evidence that it stimulates the healing process by increasing capillary permeability [3] and it may also be an important factor in determining wound tensile strength [4].

It is presently known that the acute inflammatory reaction following injury is accompanied by degranulation of mast cells and release of histamine with subsequent increase in capillary permeability and swelling of the injured area. In our experiments, however, the opposite appeared to be true, namely swelling of individual cells after the application of histamine followed by vasolidation and increased permeability of the vessels. One may postulate that histamine acts on the cells membrane to make the cell more porous thereby depleting the extra cellular space (ECS) and leading to an increase in ECS osmotic pressure. Further, in response to the injury, fibroblasts and macrophages leave the vicinity of the vessels, denuding the vessel wall. They migrate to the

injured area, attracted by the increased concentration of toxic substances created by the loss of extracellular fluid. The vessels become more porous because of the loss of the surrounding fibroblasts and as a result the individual endothelial cells swell and expand. Fluid is drawn into the area by the difference in osmotic pressures, the increased porosity of the injured cells and the increased permeability of the capillaries.

Wounds treated with the EM field were observed to have less of a polymorphonuclear infiltrate than those not exposed to the radiation. In contrast, there were many more fibroblasts and macrophages in the incisions of the test groups than in those of the unexposed control groups. This would suggest that the test group wounds were an entire day ahead of the control groups if a comparison is made based on the sequence of events in normal wound healing [2].

Histological sections of the wounds in rats in the test group 24 hours after treatment with saline and EM field revealed that the collagen fibres were oriented parallel with the incision. The fibres appeared greater in number than in either control group. A similar observation of increase in collagen formation with EM field treatment was described in a previous paper [5] by the authors.

In the previous report [1] the authors presented evidence to show that wounds treated with an EM field were at least 24 hours ahead of the control groups in the healing process when compared with the sequence of events in normal wound healing 24 hours after incision (2). It was clear that the test wounds were better healed than those of the controls and that there would be a significantly smaller area of scar tissue. This was one of the major differences between the treated and untreated animals.

Tensile tests on dog skin specimens containing healed wounds 5 days old revealed a substantial improvement in the healed strength of those treated with histamine and irradiated with VHF. These wounds also presented a significantly superior cosmetic appearance. The compounding of improved strength and cosmetic appearance promises great potential benefit in a wide variety of clinical applications.

Summary

From histological analysis one may conclude that 12 hours after making the incisions, those treated with histamine and exposed to an EM field were smaller and more advanced in the healing process by comparison with the controls. After 24 hours, the healing process was greatly advanced with clearly identifiable parellel orientation of the collagen fibres. (Further experimentation may reveal that this is beneficial to the healing process.) After three days, the time rate of healing of the wounds exposed to an EM field was similar to those which were not. There was, however, a strong indication that the wounds exposed to the EM field would have a smaller scar.

One may conclude from the tensile tests on dog skin specimens that the benefits are not only improved mechanical strength and resistance to injury but also improved cosmetic appearance.

References

1 Romero-Sierra, C., Halter, S. and Tanner, J. A., "Effect of an Electromagnetic Field on the Process of Wound Healing," NRC, DME Control Systems LTR-CS-83, (National Research Council of Canada), Ottawa, Ontario, August 1972.
2 Ordman, L. J. and Gilman, T., "Studies in the Healing of Cutaneous Wounds. 1. The Healing of Incisions Through the Skin of Pigs." Arch. Surg. *3*(6): 857-882, 1966.
3 Peacock, E. E. and VanWinkle, W., *In*: *Surgery and Biology of Wound Repair,* W. B. Saunders Co., Philadelphia, 1970, p. 4.
4 Sandberg, N., "Time Relationship Between Administration of Cortisone and Wound Healing in Rats," Acta Chir. Scand. *119*: 367-371, 1964.
5 Romero-Sierra, C., Halter, S. and Tanner, J. A., "Effect of an Electromagnetic Field on the Sciatic Nerve of the Rat," *In*: *Nervous System and Electrical Currents,* (Vol. 2); *ed.* N. L. Wulfsohn and A. Sances, Jr., Plenum Press, 1971.

Reactions of Polymer Films with Active Species Produced in a Microwave Discharge*

J. T. Books† and J. P. Wightman‡

ABSTRACT

Films of polyethylene, polystyrene, "Teflon"—fluorocarbon resin, "Mylar"—polyester film, "Kapton"—polyimide film, pyronne and "Kodacel"—cellulose acetate butyrate film were exposed to the excited species produced in microwave discharges of NO, SO_2, N_2, H_2O and O_2. Water contact angles of the polymers decreased significantly after exposure to each of the discharge species. The predominant discharge species observed by emission spectroscopy on reaction with the polymers were CO^+, NO, CS, and S_2.

Introduction

Atom-solid reactions have been studied infrequently and represent a virtually unexplored area of chemistry. On the other hand, atom-solid reactions represent quite a significant area with a number of applications. For example, reactions of atomic oxygen may be used to simulate and gain insight into corrosion and combustion processes. Reactions of solids and molecules have been studied extensively. Unfortunately, one cannot extrapolate from reactions involving molecules and predict how atoms will react. The few atom-solid reactions which have been studied have been summarized elsewhere [1].

Previous work [2, 3] in this laboratory using a microwave discharge has been concerned with the study of the reaction between carbon and atomic oxygen with a major emphasis on the analysis of gaseous reaction products. It was felt that it would be of considerable interest to study reactions of other gases with different solids and to emphasize the measurement of changes in the solids on reaction. Polymer films are readily available, convenient to handle experimentally, and represent an interesting class of solids both theoretically and practically. The only study between polymer films and the gaseous products of a *microwave* discharge was reported by Greyson et al. [4]. Here the rate for the addition of N and O atoms to polystyrene was significantly lower than that for H atoms. On the other hand, a number of gas-polymer studies involved the use of other types of electrical discharges [5 - 15]. Most of these studies have been directed towards improving the adhesive properties of the polymer. Several patents [5, 8, 9, 13]

* Manuscript received August 9, 1974; in revised form October 21, 1974. Work supported in part by NSF Undergraduate Research Program under Grant GY-7270. Dr. L. K. Brice served as Grant Director.

†Undergraduate Research Participant.

Chemistry Department, Virginia Polytechnic Institute and State University, Blacksburg, Virginia 24061

‡ Author to whom inquiries for reprints and further information should be addressed.

have been issued concerning electrical discharge exposure to enhance adhesive strength of polymers.

Reactions between five (5) gases and seven (7) polymers have been studied in this work. Contact angles of water on each polymer film were measured before and after reaction. The emission spectra of each discharge was obtained with and without the polymer film present.

Experimental

Materials. The following gases (grade indicated) were obtained from Matheson: nitric oxide, sulfur dioxide (anhydrous grade), and nitrogen (pre-purified grade). These gases were used without further pretreatment. Oxygen was obtained from Airco, condensed at 77°K and the middle fraction collected.

The seven polymers used are listed in Table 1 with the source of the film and the thickness. The polymer films were pretreated by wiping with a solution of Tide XK followed by a distilled water rinse. A 9 × 55 mm sample was then cut for reaction in the discharge. A small adjoining piece was cut off for use as a reference in the contact angle measurements.

TABLE 1
POLYMER CHARACTERISTICS

Type	Source	Thickness (mil)
Polyethylene	Dupont	1
Polystyrene		1
"Teflon"-fluorocarbon resin	Dupont	
"Mylar"-polyester film	Dupont	1
"Kapton"-polyimide film	Dupont	1
Pyrrone-polyimidazopyrrolone film	NASA-Langley	0.6-0.7
"Kodacel"-cellulose acetate butyrate film	Tenn. Eastman Co.	1.6

Microwave Discharge. The controlled-flow, vacuum apparatus in which the polymer films were reacted with species produced in the microwave discharge is shown schematically in Figure 1. The sample was placed on a custom holder

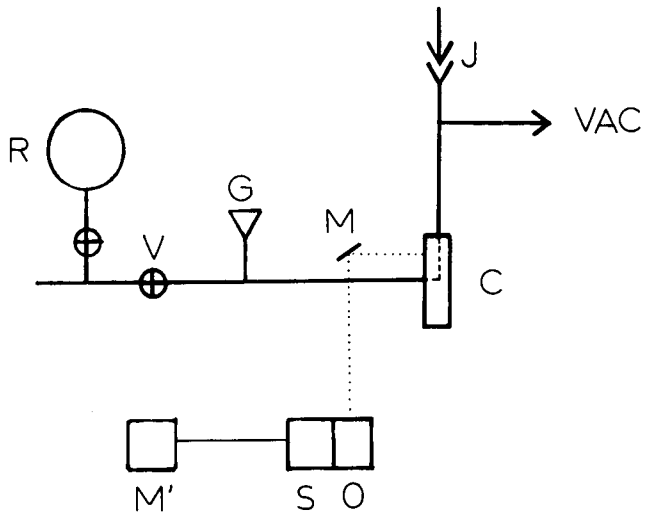

Figure 1 Schematic diagram of the reaction apparatus.

which was suspended on a filament of "Nylon" from the 24/40 joint (J). The sample holder was positioned 3 cm above the cavity (C); 4.5 cm in the case of water. The cavity was a Raytheon (Model FC-7097) NBS waveguide connected via a coaxial cable to a Raytheon (Model KV-104) generator. The generator was operated at 2450 MHz and at 10 - 15 watts. The apparatus was evacuated with a liquid nitrogen trapped oil diffusion pump and gas flow from reservoir (R) was regulated by means of a Nupro needle valve (V). The pressure in the discharge region was maintained at 0.2 Torr and was monitored with a Hastings thermocouple gauge (G). The discharge was initiated with a Tesla coil and was maintained for a period of thirty minutes. The films after removal from the discharge apparatus were exposed to the atmosphere and set aside for contact angle measurements and reflectance infrared spectroscopy. No attempt was made to fix the time between exposure and contact angle measurements. The contact angle measurements were made within 2 weeks and generally less than 5 days. The infrared reflectance were obtained several months later.

Emission Spectroscopy. Emission spectra of the discharges were obtained with and without the polymer films present. The emission spectra were obtained using a Beckman DU spectrophotometer (S) equipped with a photomultiplier tube whose output was read off of meter (M'). A mirror (M) was positioned to focus light from the discharge on the slit of the spectrophotometer.

Contact Angles. Water contact angle measurements were made using a Gaertner Scientific goniometer. The sample film was placed under a custom glass container fitted with a septum through which the tip of a 5 cc syringe was inserted. Drops of distilled water were placed on the film and a series of at least nine measurements were made. Reference and exposed samples were run concurrently.

Results and Discussion

The color of the discharge varied somewhat with the gas. Discharges of N_2, O_2, and NO all appeared pinkish whereas the discharge of H_2O was quite red. The SO_2 discharge gave a blue color and deposition of sulfur presumably was noted on the walls in the discharge region. The polymer films were initially placed directly in the discharge; however, severe film degradation was noted even for short exposure times. Thereafter, all films were positioned down-stream from the discharge. There were several obvious changes in some of the films after exposure to some of the discharges. A clear polyethylene film became cloudy and grainy on exposure to an O_2 discharge. A deposit was noted on the films of polyethylene, "Kapton" and polystyrene in a SO_2 discharge but not on the films of pyrrone and "Mylar".

Contact Angles. The average contact angles with the average deviation of the reference (unexposed) and films exposed to the indicated gases are listed in Table 2. The most obvious conclusion which can be drawn from the results shown in Table 2 is that there is invariably a decrease in the contact angle of water of any polymer film exposed to any discharge. The polymer film is more wettable after a relatively short exposure to the reactive species produced in a microwave discharge.

Related studies have been made by Blais et al. [10], and Westerdahl et al. [15]. Blais et al. [10] noted a decrease in the water contact angle (θ) from

TABLE 2
SUMMARY OF CONTACT ANGLE MEASUREMENTS ON POLYMER FILMS BEFORE AND AFTER EXPOSURE TO VARIOUS DISCHARGES

Gas	Contact Angle Reference	Contact Angle Exposed	Discharge Species
		Pyrrone	
O_2	42° ± 5°	19° ± 4°	
N_2	66 ± 4	23 ± 7	CN(452,745) NO(490)
SO_2	55 ± 5	33 ± 7	CS(254) S_2(337)
NO	45 ± 7	15 ± 2	
H_2O	49° ± 2°	26° ± 3°	CO^+(378)NO or CH(430)
		Polyethylene	
O_2	60° ± 8°	35° ± 7°	
N_2	68 ± 13	38 ± 2	
SO_2	57 ± 12	36 ± 6	CS(261,263) S_2(337)
NO	80 ± 7	33 ± 3	
H_2O	77° ± 8°	28° ± 4°	CO^+(468)
		Polystyrene	
O_2	62° ± 14°	10° ± 2°	
N_2	68 ± 9	32 ± 4	
SO_2	84 ± 6	67 ± 14	CS(247,254,261,262,267) S_2(476,480,485)
NO	77 ± 4	22 ± 4	NH(364)
H_2O	77° ± 3°	22° ± 3°	
		"Mylar"	
O_2	61° ± 7°	31° ± 4°	CO^+(380)
N_2	55 ± 8	36 ± 6	NO(281)
SO_2	61 ± 8	38 ± 5	
NO	62 ± 7	30 ± 2	CN(395)
H_2O	72° ± 6°	19° ± 2°	
		"Kapton"	
O_2	37° ± 5°	19° ± 2°	CO^+(380)
N_2	57 ± 12	31 ± 3	NH(364) NO(448)
SO_2	71 ± 23	31 ± 6	CS(254,261,262,267) S_2(337)
NO	48 ± 14	22 ± 3	
H_2O	74° ± 3°	27° ± 3°	CH or NO(430) CO^+(468) CO(519)
		"Kodacel"	
NO	64° ± 3°	40° ± 4°	
H_2O	77° ± 2°	34° ± 2°	CO(368)
		"Teflon"	
H_2O	102° ± 4°	65° ± 8°	

$85° \rightarrow 60°$ for polypropylene exposed to N_2 in a corona discharge. Westerdahl et al. [15] used a 13.56 MHz rf discharge. They report for an oxygen discharge a θ decrease from 96° to 41° for high density polyethylene film and a θ decrease from 88° to essentially 0° for polystyrene. These water contact angle results are certainly consistent with those for the similar systems shown in Table 2.

Considerable efforts were made in the present study to determine changes in surface groups by reflectance infrared spectroscopy. No discernible difference was noted in any of the multiple internal reflectance infrared spectra of the exposed compared to the reference polymer films. Apparently, the internally reflected beam penetrates too far into the sample and masks surface groups if indeed present.

Emission Spectroscopy. Wavelengths of lines occurring in the emission spectra of the discharges of the various pure gases without polymer films present were recorded. The wavelengths of new lines appearing when the polymer films were also recorded. Provisional assignments of new species appearing in the discharge when the polymer films were present are shown in Table 2. The numbers in parenthesis refer to the wavelengths in nanometers used to document the assignment [16 - 18]. Only the more intense lines are reported for each species. There are a variety of species produced on reaction between the polymer films and the reactive species generated in the microwave discharge. The species detected appear consistent with the composition of the gas phase and the polymer substrate. The predominant discharge species for all gases and polymers were CN, NH, CH, NO, CS, S_2, and CO^+.

The fact that new bands were observed when the polymer films were present was an indication of back diffusion. That is, the reaction products of the discharge species and the polymer film produced downstream diffused back into the discharge giving rise to new emissions.

Acknowledgements

The authors thank Dr. N. J. Johnston, NASA-Langley Research Center and Dr. W. C. Wooten, Tennessee Eastman Company for making available samples of some of the polymer films.

References

1 Wightman, J. P., Proc. IEEE, *62* 11 (1974).
2 Melucci, R. C. and Wightman, J. P., Carbon *4*, 467 (1966).
3 McGuffin, R. O. and Wightman, J. P. *Abstracts*, 19th Southeastern Regional Meeting, Amer. Chem. Soc., Atlanta, Ga. Nov. 1967.
4 Greyson, J., Ingalls, R. B. and Keen, R. T., J. Chem. Phys., *45*, 3755 (1966).
5 Mantell, R. M., U.S. Patent 3309299 (1967); Chem. Abstr., *66*, 106020j (1967).
6 Schonhorn, H. and Hansen, R. H., J. Appl. Polymer. Sci., *11*, 1461 (1967).
7 Chevillon, M. and Mahieux, F., C. R. Acad. Sci., Paris, Ser. C., *265*, 558 (1967).
8 Pouncy, H. W., Jr., U.S. Patent 3380870 (1968); Chem Abstr., *69*, 2468u (1968).
9 Kalle, A. G., Fr. Demande 2010 272 (1970); Chem. Abstr., *74*, 427v (1971).
10 Blais, P., Carlsson, D. J. and Wiles, D. M., J. Appl. Polymer. Sci., *15*, 129 (1971).
11 Virlich, E. E., Krotova, N. A., Stefanovich, N. N., Vilenskii, A. I., Radtsiy, V. A. and Vladykina, T. A., Plaste Kaut., *19*, 17 (1972); Chem. Abstr., *76*, 141641v (1972).
12 Yasuda, H., Lamaze, C. E. and Sakaoku, K., J. Appl. Polymer. Sci., *17*, 137 (1973).

13 Manion, J. P. and Davies, D. J., U.S. Patent 3740325 (1973); Chem. Abstr., *79,* 54321e (1973).
14 Dzhewarly, CH, M., Vechkhaizer, G. V. and Orlova, S. I., Elektron. Obrab. Mater., *29,* (1973), Chem. Abstr., *80,* 27469f (1973).
15 Westerdahl, C. A. L., Hall, J. R., Schramm, E. C. and Levi, D. W., J. Colloid Interf. Sci., *47,* 610 (1974).
16 Harrison, G. R., *"Wavelength Tables,"* John Wiley, New York, 1939.
17 Pearse, R. W. B. and Gaydon, A. G., *"The Identification of Molecular Spectra,"* John Wiley, New York, 1963.
18 Striganov, A. R. and Sventitskii, N. S., *"Tables of Spectral Lines of Neutral and Ionized Atoms,"* Plenum, New York, 1968.

Microwave Irradiation of Plant Roots in Soil*

D. H. Schrader† and D. D. McNelis‡

ABSTRACT

A theoretical analysis of the microwave irradiation process in an agricultural application shows that heat may be selectively generated in small objects such as weed seeds and weed roots in about the same ratio as that of the electrical conductivities of the object and the surrounding soil. The time required for conductive cooling of such small objects to the surrounding soil decreases approximately in proportion to the inverse square of their dimensions. These objects may be selectively heated if the conductivity ratio is favorable and if the irradiation is done at high intensity before appreciable heat loss can occur.

The power and energy required for necrosis in root tissue due to microwave irradiation are estimated. This estimate is based on an extrapolation of known relationships between exposure times and lethal environmental temperatures. It is concluded that the energy required for root tissue necrosis decreases with increasing radiation intensity.

Introduction

Selective irradiation of living tissue in soil by high-intensity, microwave fields is possible and its economic practicability should be carefully investigated (Davis, *et al.*, [5]; Menges and Wayland, [8]). A few examples of desirable uses which could be investigated are: killing insects inside a host plant, killing weeds or modifying the growth rates of plants, and killing plant pathogens or seeds in the soil. The physical situation must be modeled accurately to determine mathematically the selectivity and the economic feasibility of the microwave heating process in these applications. Although some of the effects of microwave irradiation possibly could be non-thermal in nature, we shall use the terminology and mathematics of a thermal model and extrapolate known electrical and thermal effects to this case. This requires a knowledge of the electrical and thermal properties of the target tissue and the surrounding medium over the full range of moisture conditions.

In order to illustrate the type of problem analysis which is required, we discuss the specific case of killing a plant root by high-intensity radiation. Our example treats the case of killing the root by a radiation source located above the air-soil interface. The analysis reported here is based on the use of 1 GHz. At this frequency, the penetration depth in moderately wet soil is about 11 cm.

* Manuscript received August 13, 1974; in revised form October 28, 1974.

† Department of Electrical Engineering, Washington State University, Pullman, Washington 99163, U.S.A.
‡ Systems Group of TRW, Inc., One Space Park, Redondo Beach, California 90278, U.S.A.

This depth suffices for many potential applications. Moreover, at 1 GHz the generation and directional control of adequate power levels is easily achieved.

Although the numerical results are only approximately correct, it is shown that (a) the rate of energy absorption in the root is significantly greater than in the soil under a wide variety of conditions, and (b) readily available power levels can be used to kill plant roots.

This example embodies the primary problems encountered in, and illustrates the principles governing, selective heating in agricultural applications.

Radiation Reflection at the Ground

One of the problems arising in such applications is that of causing the wave to radiate into the ground from a source located above the ground. There are values of angle of incidence of the radiation into the ground at which the reflected wave becomes minimal and almost all the radiation enters the ground. The geometry of the situation is shown in Figure 1.

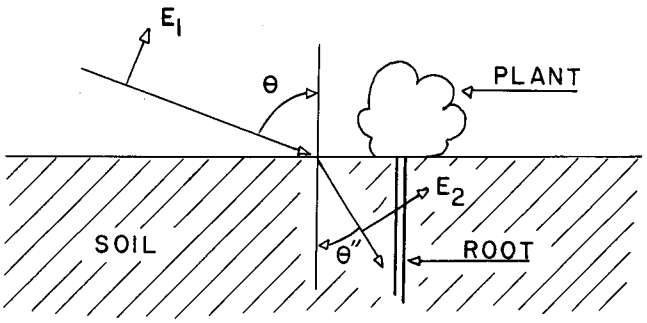

Figure 1 Irradiation Geometry for the Vertically Polarized Case. The Incident Wave, E_1, and the Reflected Wave (not shown) Make Equal Angles, θ, to the Vertical. The Transmitted Wave, E_2, Makes an Angle, θ'', to the Vertical as Discussed in Appendix A.

In evaluating the energy delivery which can be achieved with dielectric heating, the number and type of interfaces between the energy source and the target object must be considered. As discussed in *Appendix A,* two cases must be treated: (a) electric field in the plane of incidence (vertical polarization) as shown in Figure 1, and (b) electric field perpendicular to the plane of incidence (horizontal polarization).

Values of the voltage reflection coefficient for these two cases and for a typical air-soil interface are shown in Figure 2. In that figure the magnitude of the voltage reflection coefficient is plotted versus the angle of incidence. From observation of that figure, it may be seen that, for incidence angles between about 35° and 70° for dry soil and vertical polarization, the magnitude of the voltage reflection coefficient is less than 0.2. Since power varies as the square of the field intensity, the power transmitted across the interface is greater than $100 \times (1 - 0.2^2) = 96\%$ of the impinging power. For wet soil, the corresponding range of incidence angles is $71° - 82°$. Thus, there is always a significant range of angles over which very good transmission can be obtained.

It may also be noted that vertical incidence on dry soil yields a voltage reflection coefficient of 0.27, or a transmitted power which is 92.7% of the incident power. For many circumstances this may be an acceptable power transfer. In dry soil, the transfer will be at least this great for all incidence angles from 0° to 74°.

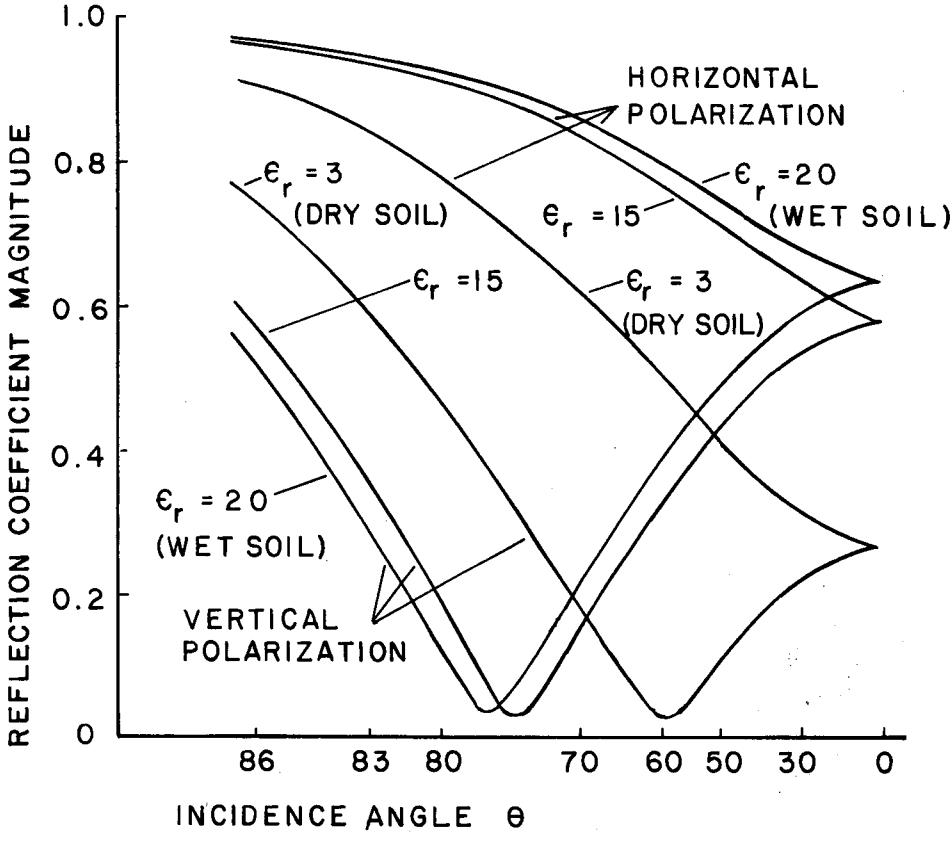

Figure 2 Magnitude of Reflection Coefficient vs. Angle of Incidence at an Air-Soil Interface

The energy which is transmitted across the air-soil interface propagates in the plane of incidence but at an angle to the vertical which differs from that of the impinging energy. For our example of killing a root in the soil we have taken the case of a vertically polarized wave incident upon the air-soil interface. In that case, significant components of the electric field usually will be present both parallel and perpendicular to a root element. Thus, one must solve the problem in two parts by considering these components separately. However, one can gain considerable insight by solving only one of these parts. Consequently we modeled the actual situation of the root in the ground by an infinitely long cylinder irradiated by a plane wave at 90° to the axis of the cylinder. Inside the cylinder we used values of conductivity and dielectric constant typical of a root and, in the surrounding medium, values commensurate with those for soil.

Thermal Relaxation Time

The irradiation process heats both the ground and the root. As discussed later, the root will be selectively heated and will rise to a higher temperature than will the surrounding soil. This temperature differential will cause heat to flow from the root into the ground. Heat will also flow up the root to the

surface of the ground and to the foliage of the plant. We are interested in the time in which heat conduction tends to cool the root. Let us consider the simpler problem in which a hot, cylindrical object is located in a medium with finite thermal conductivity. From the discussion in *Appendix B* we see that such an object cools in a way approximately characterized by an exponential solution. The exponent in the solution is $-Kt/(\tau a^2 \rho C)$, where K is the thermal conductivity, C is the heat capacity, ρ is the density, t is time, τ is the parameter in the family of solutions, and a is the radius of the cylinder. Consequently, we define the *thermal relaxation time* to correspond to that time at which this exponent is -1, or

$$t_d = \tau \rho C a^2 / K$$

We notice that a root or a seed located in the ground will have a thermal relaxation time which varies approximately with the square of its radius. For instance, if we assume a soil of sandy loam with a moisture content of 20% and an average density (soil and moisture) of 1.7 grams per cubic cm, we calculate that the average thermal conductivity and heat capacity are 0.046 Joules/sec/°C/cm and 1.34 Joules/gm/°C. For these constants and for seeds and roots in the range of 0.1 cm to 1 cm in radius we arrive at thermal relaxation times in the range of 0.2 sec. to 20 sec.

Since these thermal relaxation times are short with respect to the exposure times for which lethal temperatures are quoted in the literature (Curtis and Clark, [4]; Altman and Dittmer, [1]; Bursell, [2]), it becomes evident that a transient heat conduction problem must also be solved along with the electromagnetic radiation problem in order to model the process of killing a root by irradiation. In this problem, the dominant heat loss should occur radially through the root wall into the ground rather than along the root axis to the surface of the ground because the root radius is small with respect to its length. Consequently, we used the same model of an infinite cylinder in uniformly conducting ground as we used for the electromagnetic radiation problem.

Energy Absorption in the Root

We consider the incident radiation to be a plane wave at a large distance from the root. In the vicinity of the root the wave is not plane, since it is altered by the electrical properties inside the cylindrical volume of the root. The power absorbed by the root can be determined from a calculation of the actual field inside an idealized model of the root. Because the field equations are linear for most agricultural applications, the power absorbed by the root is proportional to the power density in the incident wave. This constant of proportionality is called the *absorbing cross section,* A_α, and is defined by the relation (Power dissipated in the target object)/(Power density in the incident wave).

The absorption cross section depends on the geometry and electrical properties of the root and the surrounding soil.

The absorption per unit volume in the root material may be calculated by the product of the current density times the electric field. Although the fields inside the root are not uniform in general, they will be approximately uniform for small radii. In that case, the absorption per unit volume is approximately equal to its average value given by the absorption cross section times the incident power density divided by the root volume: PA_α/root volume.

To evaluate the absorption cross section for a root, we solved the electromagnetic boundary value problem for our root model. Solutions which satisfy the cylindrical geometry are expressed as a series of terms, each term having the product of a constant coefficient, a Bessel function, and a sinusoidal function. The details of this series and of the solution are given in *Appendix C.*

The unique part of this solution was that the arguments of the Bessel functions were complex. The reason for this is that the root material is neither a good conductor nor a good insulator. In this case the loss tangent is of the order of magnitude of unity. This precludes the use of approximations which characterize most of the work in electromagnetic boundary value problems. Hence, a computer program was used for computing the required values of the Bessel functions because Bessel functions of complex argument are not well tabulated.

From the solution described in *Appendix C,* we have the expression for the electric field inside the root as given below.

$$E''_z = E[b_0 I_0(\gamma_2 R) + b_1 I_1(\gamma_2 R) e^{j(\phi)}] e^{-j\omega t}$$

In this expression the quantities are expressed in a cylindrical coordinate system where z is the axis of the cylinder (root), R is the radial distance, and ϕ is the azimuthal angle. We also used ω as the radian frequency of the applied wave, t as time, j as the square root of -1, I_0 and I_1 as modified Bessel functions of the first kind, γ_2 as the propagation constant inside the root, and E as the magnitude of the electric field of the incident plane wave. The quantities b_0 and b_1 are constants whose calculation is described in *Appendix C.*

The time-averaged power dissipated in the root volume is given by $P = (\frac{1}{2}) \int \underline{J}^* \cdot \underline{E}'' \, dv$, where $\underline{J}$ is the current density vector which is equal to $\sigma_2 \underline{E}''$, σ_2 is the conductivity in the root, and the asterisk indicates the complex conjugate. We computed the time-averaged power density in the incident wave by the formula $(\frac{1}{2}) \mathrm{Re}(\underline{E} \times \underline{H}^*)$, where $\underline{E}$ and $\underline{H}$ are the incident wave electrical and magnetic field intensity vectors. Evaluating the absorption cross section of the root from these formulas, we obtained

$$A_{\alpha R} = \sigma_2 \eta 2\pi L [(|b_0|)^2 \int_0^a |I_0(\gamma_2 R)|^2 R \, dR + (|b_1|)^2 \int_0^a |I_1(\gamma_2 R)|^2 R \, dR]$$

In this formula we assumed that $I_0(\gamma_2 R)$ is constant for the values of the argument corresponding to the values of R from 0 to 0.1 cm and for values of γ_2 used here. For that same range of R, $I_1(\gamma_2 R)$ is small enough to make the second integral negligible. The quantity η is the impedance of the soil to the incident wave, σ_2 is the conductivity of the root, a is the radius of the root, and L is its length.

For small values of a, the formula reduces to the approximate form $A_{\alpha R} = \sigma_2 \eta \pi a^2 L$. Since the optical cross section presented by the root to the incident wave is 2aL, we see that the absorption cross section decreases more severely than does the optical cross section as the radius of the root decreases.

The plane wave formula $P = (E^2/2\eta) \exp(-x\sigma\eta)$ watts per sq meter may be used to calculate the time-averaged power density of a plane wave as it propagates in the x direction in a lossy medium. Hence, the power per unit volume absorbed from the plane wave by losses in the soil is given by $-\partial P/\partial x = \sigma\eta P$, where σ is the conductivity of the soil and η is its wave impedance.

Selective Heating

The selectivity of the absorption process is described by the ratio of the absorbed power per unit volume in the root to that in the soil. Let the subscript s stand for quantities as measured in the soil. For small values of a, the ratio of the power absorption capability of the root to that of the soil is given by

$$(PA_{\alpha R}/\pi a^2 L)/(-\partial P/\partial x) = \sigma_2/\sigma_s$$

The interesting feature of this formula is that the selectivity is not dependent upon the ratio of the dielectric constants even though that ratio was not taken to be unity. It depends only on the electrical conductivities. This contrasts with the case where a plane wave propagates across a plane boundary between media of different electrical properties. In that case, the reflection process can materially reduce the power density in the transmitted wave, and then the ratio of the absorbed power in the two media will depend on the ratio of the dielectric constants as well as on the conductivities.

Power Required for Lethal Effects

The net result of the simultaneous process of energy absorption and conductive cooling determines the temperature rise and the effect on plant mortality. In order to estimate the time required to kill a root at intense radiation power densities, one must determine how the temperature rises in the root. To find this, one can use the model discussed above of a long cylindrical root located in a uniform medium. When such a root is subjected to irradiation it absorbs power and converts that to heat throughout the root. Since the usual electromagnetic radiator is operated at a constant output, this heat production term is also constant for its duration. Thus, one must solve the heat conduction equation

$$\rho C\,(\partial T/\partial t) = K\nabla^2 T + q$$

for a region having a cylindrical boundary. Inside the cylinder we can assume zero for the heat generation term, q, until the irradiation starts and then it can be assumed to remain constant. To further simplify the problem we can assume that the heat generation term is zero outside of the cylinder. This corresponds to assuming that the heat generated in the soil by absorption of the radiation is negligible. The assumption of $q = 0$ in the soil leads to an overestimate of the temperature difference between the root and the soil. Since the heat flow from the root to the soil is determined by this temperature difference, the computed value of heat conducted away from the root should be higher than actual. Consequently, the time, or energy (delivered to the root), required to kill the root should be less than estimated.

At the boundary between the cylindrical region representing the root and the outer region representing the soil, the conditions one uses to match the solutions inside and outside are that the heat flow field have a continuous normal component and that the temperature be continuous across the boundary. This last condition is based upon the assumption that there is intimate thermal contact between a root and the surrounding soil. Poorer thermal contact would lead to greater heating rates than those calculated here.

Although this problem has not been solved, a problem which is similar to it has been solved by Jaeger and reported in the literature (Jaeger, [6]). This is the problem of an electrical cable buried in the ground. Heat is generated

in the cable by electrical current. This heat is conducted to the surface of the cable and then it is conducted away through the soil. Although this problem is very similar to the one presented above, it is different in that the electrical cable was assumed to have perfect thermal conductivity, whereas the root does not. However, once again, such an assumption leads to an estimated energy requirement greater than the actual amount needed to kill the root. Consequently, we adapted the calculations of the buried electrical cable problem to our root problem and used the result as an upper limit.

Using the data in Table 2 of Jaeger's article [6], we calculated a curve, shown in Figure 3, of root temperature versus time for the assumed value of heat generation, q. To do this we assumed a thermal conductivity of the soil equal to 0.046 Joules/sec/cm/°C, a heat capacity of the soil equal to 1.34 Joules/gm/°C, a density of the soil equal to 1.7 gm/cm^3 (all of these corresponding to a sandy loam soil at a 20% moisture content), and assumed both the heat capacity and the density of the root equal to unity (corresponding to that of water). The curve thus represents the variation of temperature in the root for a power input per cm length of 10.5 W. Similar curves were obtained for other power inputs. These temperature variations were then used to compute the time and energy required to kill the root.

Rate Coefficient Model

The process of killing tissue apparently is similar in seeds, plants, and insects. In these cases the required exposure times, t_e, vary inversely with the temperature. However, the relationship is not linear. Experiments have determined that it is logarithmic over a considerable range of exposure times (Curtis and Clark [4]; Bursell [2]). The lethal exposure time decreases by a factor on the order of 100 with an increase of 10°C. This factor is usually referred to as the *temperature coefficient* (Curtis and Clark [4]). Temperature coefficients of this magnitude are found in the process of denaturation of some proteins.

In view of these facts, we assume that the process of killing the root with a minimum amount of heating is one with a *rate coefficient,* R, dependent only upon the temperature. This can be represented as an integral:

$$\int_o^{t_e} R\, dt = \text{constant}.$$

Considering the case when the temperature is held constant, one may integrate this equation and take the logarithm of the resulting equation to obtain the formula $\ell n(e_e) = -\ell n(R) + A$. However, inspection of the curves shown in Figure 11.1 on page 297 of the text by Curtis and Clark [4] shows that the curves of temperature versus exposure time are of the form $\ell n(t_e) = -B\,T + A$, where T is the temperature in °C, B is the slope of the curve, and A is the intercept. From these two equations we may determine that the rate coefficient is given by $R = \exp(BT)$ as a first approximation. One may then write the integral for calculating the exposure time as

$$\int_o^{t_e} e^{(BT-A)} dt = 1$$

in which the temperature can be any specified function of time such as the curve of temperature vs. time for the irradiated root shown above and in which the constants A and B can be determined from data given by Curtis and Clark [4].

They show data on pea seedling roots. Since these values are likely to be similar to those for other living plant tissue, they were used to make a realistic example of the calculations but not with the intention of designing a process to kill pea crops. The curve for pea seedlings was fitted with a straight line and values of $A = 23.955$ and $B = 0.403$ were determined from this approximation.

Numerical integration of the equation above when the temperature is a function of time as shown in Figure 3 and for three different rates of heat input into the seedling root yielded the following results:

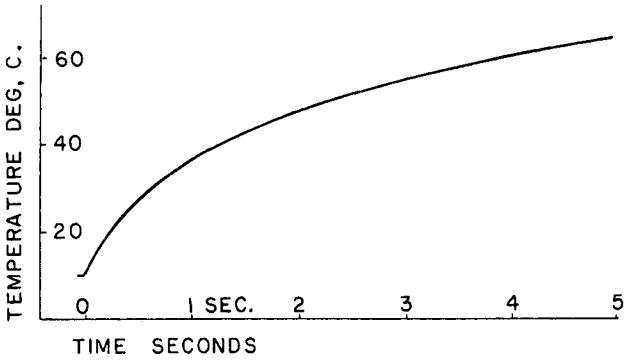

Figure 3 Heating Curve for a Heat Input of 10.5 Watts per cm of Root Length

(a) For the heat input, Q, of 10.5 W/cm of root length, we have $t_e = 4.5$ sec. and a total energy input, J, to the root of about 47 Joules/cm of root length.
(b) For $Q + 21$ W/cm, we have $t_e = 1$ sec. and $J = 21$ Joules/cm.
(c) For $Q = 50$ W/cm, we have $t_e = 0.3$ sec. and $J = 15$ Joules/cm.

Thus, the energy required to kill the root should decrease with increasing intensity of radiation.

Lethal Dosage at a Short Exposure Time

On the other hand, we notice that the data of Curtis and Clark [4] implies a decreasing lethal exposure time with increasing temperatures. If this curve may be extrapolated to very short exposure times, then the temperature required to kill at an exposure time which is much shorter than the relaxation time (0.2 sec.) should be higher than the temperature required to kill in six seconds.

We can estimate a lower bound for the energy required to kill at the very short exposure time by noticing that significant cooling does not occur if the exposure time is short with respect to the thermal relaxation time. Therefore, the energy required at these very short exposure times is that required to bring the temperature up adiabatically: $J = MC\Delta T$, where M is the mass of the root in grams, C is the specific heat in Joules/gram/°C, and ΔT is the change of temperature in °C. If we can assume that the temperature required at the very short exposure time is greater than the 55° required at six seconds, then the energy required will be greater than the 6 Joules per cm length which is required to adiabatically raise the temperature of the root from 10°C to 55°C.

Consequently, the energy required to kill the pea seedling root when the exposure time is short with respect to the thermal relaxation time should be greater than 6 Joules/cm of root length but less than the 15 Joules/cm of root length calculated in the previous section.

Electrical Parameters

The radiation power required to achieve those energy inputs in the time specified can be calculated by using the absorption cross section determined above. This formula depends upon the propagation constants in the plant root, the soil, and the radius of the root. In turn, the propagation constant depends upon the frequency, the dielectric constant, and the loss tangent of the material. These last two parameters have been used to characterize electrical properties of materials largely because they are less sensitive functions of frequency than some of the alternative parameters such as conductivity. However, they are highly dependent upon the water content and the salt content of the root material.

Using a laboratory setup similar to that described by S. O. Nelson [10], we have measured these parameters for dry and wet downey brome seeds and for 6-day-old downey brome seedlings at a frequency of 9.6 GHz. It appears that these parameters are the same in soil and in dry seeds but that they differ inside plant tissue. In particular, we arrived at a value of loss tangent of 0.9 and a relative dielectric constant of 27 when averaged over a region closely packed with 6-day downey brome seedlings.

Similarly, we must use values of these parameters typifying soil when calculating absorption cross sections. These values are available in the literature (Von Hippel [13]). We selected a typical value of relative dielectric constant as being 20 in soil and, similarly, a loss tangent of 0.2.

Using these parameters, the absorption cross sections for roots were calculated and are tabulated in Table 1.

TABLE 1
ABSORPTION CROSS SECTIONS OF ROOTS HAVING A LOSS TANGENT OF 0.9 AND A RELATIVE DIELECTRIC CONSTANT OF 27

Frequency	Absorption Cross Section	
	Root radius = 0.1 cm	Root radius = 0.5 cm
GHz	cm^2/cm length	cm^2/cm length
1	0.036	0.88
10	0.34	4.90

Lethal Energy and Soil Temperature with Exposure Time

From the calculations of the power required to heat a root to the lethal point in a given exposure time and the calculation of the root absorption cross section, we calculated the radiation intensity and then the soil temperature rise expected from the irradiation.

The radiation intensity was calculated by dividing the calculated lethal powers by the absorption cross section of a root with 0.1 cm radius at 1 GHz. Then we assumed that this radiation field was established over a square meter of soil surface and we used the corresponding exposure time to determine the radiation energy per square meter. We also determined what part of the total radiation energy would be converted into heat in the soil by calculations from the radiation intensity, the exposure time, and the loss per unit depth of soil. From this heat and the heat capacity of the soil we determined the average temperature to which the top 11 cm of soil would be raised during the exposure. The top 11 cm was used because that is the penetration depth of the 1 GHz radiation.

The results are shown in the graphs below. The first graph, Figure 4, is a plot of the radiation intensity required for lethality versus assumed exposure times. From this graph it appears that one would desire to use the less intense radiation. However, the more intense radiation allows an area to be treated more quickly and requires less total radiated energy, as is illustrated in the graph of Figure 5.

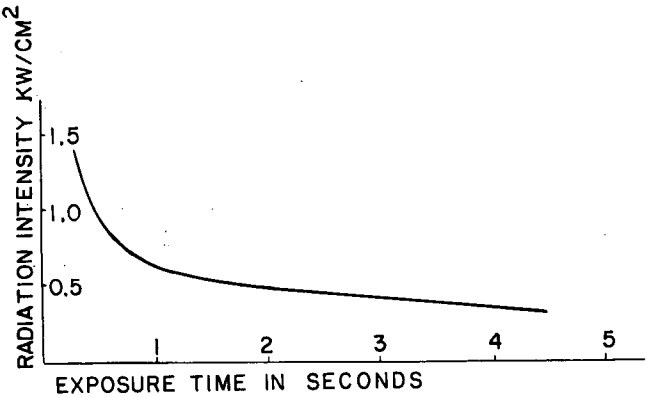

Figure 4 Radiation Power Density Required for Root Tissue Necrosis (0.1 cm Radius Root and 1 GHz)

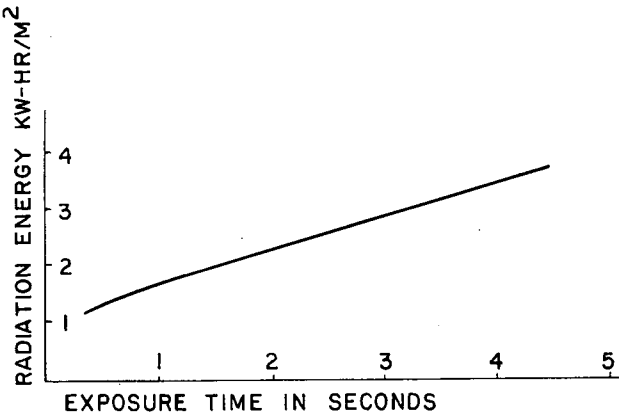

Figure 5 Radiated Energy Required for Root Tissue Necrosis (0.1 cm Radius and 1 GHz)

Assuming that the methods of analyzing the heat generation and transfer used above also apply to the soil organisms, the effect of the radiation on them can be calculated. Those having dimensions which are orders of magnitude less than the root dimensions would have thermal relaxation times far less than the exposure times considered here. Thus, heat conduction would tend to keep them near the temperature of the soil unless their electrical conductivity is several orders of magnitude higher than that of their environment.

Figure 6 below shows the temperature to which the soil is raised above the ambient temperature as a result of the radiation levels used to calculate the above graphs. Since the large volume of soil will not cool quickly, the organisms in the soil are subjected to this elevated temperature for a long period of time. Presumably their sensitivity to the elevated temperature is also described by a rate process characterized, as before, by a logarithmic relation. Consequently, the determination of whether they would be killed by the elevated environmental temperature should be made on the basis of the long period of time during which the soil is slowly cooling.

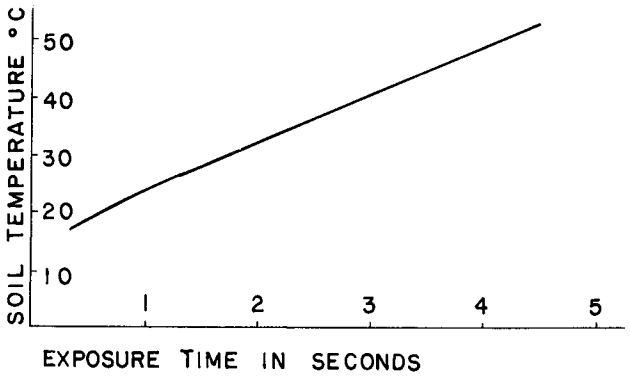

Figure 6 Maximum Soil Temperature vs. Exposure Time

Finally, note must be taken of the fact that one cannot extrapolate the graphs of this section to the case of the 0.5 cm radius root. That is because the thermal relaxation time of the larger root is 25 times longer than that of the 0.1 cm root. Since we have ignored the effect of the elevated temperatures upon the root during the cooling period, our analysis would result in calculated energy dosages much greater than the actual lethal energy dosages for these larger roots.

Acknowledgements

A computer program for evaluating the Bessel function of complex argument was supplied by M. Goldstein. We gratefully acknowledge the help of Professors T. J. Muzik and B. L. McNeal when determining dielectric constants of seeds, seedlings, and soils.

This work was supported in part by the National Science Foundation under grant GK40238.

APPENDIX A

Reflection and Transmission at a Plane Boundary

If the boundary between two media is the x-y plane and the impinging energy is in the form of a plane wave as shown in Figure 1, the portion of the incident energy which will be transmitted across the boundary may be readily computed following Stratton [12]. The air has a permittivity, ϵ_o, and a permeability, μ_o, the same as in the free space. The soil has a permittivity, denoted by ϵ_2, which increases with increasing soil water content. The soil also has a finite conductivity which increases with both water content and salt content. We account for the effect of the conductivity of the soil with the loss tangent, tan δ.

Both the horizontally and vertically polarized cases should be considered because every physical case of plane reflection by linear, isotropic dielectrics may be characterized as a combination of these two cases. In both of these cases the requirement that the incident, reflected, and transmitted waves have matching phase angles along the interface leads to the equation

$$\sin \theta'' = \{1 + [(\sin \theta)/\mathrm{Re}(B)]^2\}^{1/2}$$

where B is a complex number given by

$$B = \{(\epsilon_2/\epsilon_o) - \sin^2 \theta - j(\epsilon_2/\epsilon_o) \tan \delta\}^{1/2}$$

Then, in the case of vertical polarization, the requirement that tangential components of the fields be continuous across the boundary leads to the relation for the vertical polarization reflection coefficient below:

$$\rho_v = E_t/E_i = [(\cos\theta/\cos\theta'') - Z_3] / [(\cos\theta/\cos\theta'') + Z_3]$$

where

$$Z_3 = 1/(\sin\theta \sin\theta'' + B\cos\theta'')$$

Similarly, in the case of horizontal polarization, the requirement of continuous tangential components across the boundary leads to the relation for the horizontal polarization reflection coefficient below.

$$\rho_H = E_t/E_i = [(\cos\theta/\cos\theta'') - (1/Z_3)]/[(\cos\theta/\cos\theta'') + (1/Z_3)]$$

A plot of the magnitudes of ρ_v and ρ_H for various values of dielectric constant and for a loss tangent of 0.1 is shown in Figure 2.

APPENDIX B

Heat Conduction from a Long, Cylindrical Root

In essence the thermal relaxation time as it is defined here is the time required for a heated object embedded in a cooler environment to cool down by about 63 percent. For the case of a seed or a root located in the soil we would normally expect the object to have the same or a higher percentage water content than the surrounding soil. Because of this we would expect the heat capacity and the thermal conductivity to be greater in the object than in the surrounding soil. To simplify the problem of finding the thermal relaxation time we have assumed that the numerical value of these thermal properties in the object is the same as in the soil. The effect of this assumption on the overall problem solution is to obtain the case where the actual energy required will be less than the calculated energy.

The solution of the heat conduction equation is one of the classic problems of physics. The formula describing the heat conduction process is:

$$\rho C(\partial T/\partial t) = K\nabla^2 T + q$$

where T is the three-dimensional temperature distribution, K is the thermal conductivity, ρ is the density, C is the specific heat capacity, and q is the energy production density due to the irradiation process. If we take the case where a high, but uniform, value of temperature is established initially throughout a finite spherical or a cylindrical region and then the heat source is removed, the resulting solution involves error functions which are well tabulated. The integral solutions for these two cases are (Carslaw and Jaeger, [3]):

(a) For a right circular cylinder

$$T = (T_o\rho C/4\pi Kt) \iint_c \exp\{-[(x-x')^2 + (y-y')^2]\,\rho C/4Kt\}\,dx'dy'$$

(b) For a sphere

$$T = [T_o/8(\pi Kt/\rho C)^{3/2}] \iiint_v \exp\{-[(x-x')^2 + (y-y')^2 + (z-z')^2]\,[\rho C/4Kt]\}\,dx'dy'dz',$$

where the double integral is over the circular cross-section and the triple integral is over the spherical volume.

The temperature profile across the region does not stay constant in time; instead, it decays away to form a Gaussian-shaped curve. However, the temperature at the center of the region does decrease with an approximately exponential time

decay. Extrapolating values from plots of numerical solutions of these two integrals, we can determine to within 10 percent the thermal relaxation time of the spherical and cylindrical regions (Carslaw and Jaeger, [3]). In order to do that we determined values of the constants ρ, C, and K. We assumed a sandy loam at a moisture content of 20 percent, an average density (soil and moisture) of 1.7 grams per cubic cm, and calculated an average thermal conductivity and heat capacity of 0.046 Joules/sec/°C/cm and 1.34 Joules/gm/°C.

Upon performing these calculations for two different radii, 0.1 cm and 1.0 cm, we got the thermal relaxation times listed in Table 2. These values pertain to the temperature at the center of the object. The corresponding values for a point at $r = 0.7a$ where a is the radius of the object, are reduced to about 75 percent of the values at the center. The thermal relaxation time is related to the parameter, τ, in the family of solutions shown in the reference cited (Carslaw and Jaeger, [3], figure 4, p. 55), as: $t_d = \tau(a^2\rho C/K)$, where a is the radius of the object. Hence, we see that it varies with the square of the dimension of the object, for a given τ.

TABLE 2
THERMAL RELAXATION TIMES, t_d

Shape	0.1-cm radius	1.0-cm radius
Sphere	0.13	13
Cylinder	0.27	27

APPENDIX C

Radiation Field Determination in a Region Near a Long Cylindrical Conductor

To calculate the absorption of radiation power by a root we chose a model of a cylindrical root embedded in a uniform medium. At a distance far from the root the radiation was taken to be a plane wave. Then, in the vicinity of the root the radiation pattern is perturbed by components which have cylindrical symmetry. In order to determine these components it was necessary to make a full-wave solution of the problem.

Since the boundaries are cylindrical, the wave equation which was solved is that given in cylindrical coordinates for the case where the medium has appreciable conductivity, as shown below (Jordan and Balmain, [7]):

$$\partial^2 E_z/\partial R^2 + (1/R)\,\partial E_z/\partial R + (1/R^2)\,\partial^2 E_z/\partial\phi^2 + \gamma^2 E_z = 0$$

We assumed that there was no dependence upon the z variable because the cylindrical root was assumed to be long with respect to a wavelength of radiation. We also assumed that the radiation was sinusoidal in time. The constant, γ, is the propagation constant given by: $\gamma = \omega\sqrt{\mu\epsilon}\,\sqrt{1 - j\sigma/\omega\epsilon}$, where ω is the radian frequency, μ and ϵ are the permeability and permittivity, and σ is the conductivity.

Since the electrical parameters are different inside and outside of the root, there are two different solutions inside and outside of the root and these solutions have to match up at the boundaries. The solutions entail Bessel functions; consequently, the incident (plane) wave was expressed in terms of Bessel functions as below (Panofsky and Phillips, [11]):

$$E_z = E \sum_m j^m e^{j(m\phi - \omega t)}\, J_m(\gamma_1 R)$$

In this relation we have E as the magnitude of the applied field and $J_m(\gamma_1 R)$ as a Bessel function of the first kind of order m. The scattered wave outside of the root is of the form

$$E'_z = E \sum_m a_m K_m (\gamma_1 R)\, e^{j(m\phi - \omega t)}$$

where a_m are undetermined constants and $K_m(\gamma_1 R)$ are modified Bessel functions of the second kind. The wave inside the root is given by

$$E''_z = E \sum_m b_m I_m (\gamma_2 R)\, e^{j(m\phi - \omega t)}$$

where b_m are undetermined constants and $I_m(\gamma_2 R)$ are modified Bessel functions of the first kind.

These solutions must match at the boundary of the root as per the equation $E_z + E'_z = E''_z$. From that relation and from the orthogonality of the functions exp (jmϕ), we derived the relation between the undetermined constants shown below.

$$j^m J_m(\gamma_1 a) + a_m K_m(\gamma_1 a) = b_m I_m(\gamma_2 a)$$

Another independent relation between these constants was obtained by deriving the H fields from the E fields by using Maxwell's equation, $\nabla \times \underline{E} = -(\partial \underline{B}/\partial t)$, and by requiring that the tangential components of these H fields match at the boundary, R = a. This second relation is

$$\gamma_2 b_m I'_m(\gamma_2 a) = j^m \gamma_1 J'_m(\gamma_1 a) + a_m \gamma_1 K'_m(\gamma_1 a)$$

where the prime denotes differentiation with respect to the argument of the Bessel function. These two equation were then solved for the relation

$$b_m = j^m \frac{J_m(\gamma_1 a) K'_m(\gamma_1 a) - J'_m(\gamma_1 a) K_m(\gamma_1 a)}{I_m(\gamma_2 a) K'_m(\gamma_1 a) - (\gamma_2/\gamma_1) I'_m(\gamma_2 a) K_m(\gamma_1 a)}$$

These constants, b_m, are thus dependent on the propagation constant both inside and outside of the target material. The propagation constants in turn are proportional to the square root of the complex number, $1 - j\sigma/\omega\epsilon$, in which the loss tangent, $\sigma/\omega\epsilon$, is of the order of magnitude of unity. Hence the arguments of the Bessel functions in the above equation are complex. Because tables of only zero and first order Bessel functions of complex argument are available (Nat. Bur. Standards, [9]), these were evaluated numerically with a digital computer. They were evaluated at two frequencies, 1 and 10 GHz, for two values of root radius, 1 and 5 cm. The electrical parameters corresponded to a loss tangent and relative dielectric constant of 0.9 and 27, respectively, inside the root. These were assumed to be 0.2 and 20, respectively, outside the root. The two values of propagation constant, γ_2, inside the root which correspond to these frequencies

TABLE 3
ELECTROMAGNETIC FIELD COEFFICIENT, b_m

Radius / Frequency	1 cm		5 cm	
	b_0	b_1	b_0	b_1
1 GHz	0.9996/-0.013°	0.6460/-105°	0.9938/-0.22°	0.6428/-105°
10 GHz	0.9792/-0.73°	0.6440/-105°	0.7401/-0.92°	0.5995/-108°

and electrical parameters above are 10.353 $\angle 21°$ and 103.53 $\angle 21°$. The resulting constants, b_m, are given in Table 3. These values were then used in the expression (from the wave inside the root)

$$E''_z = E[b_0 I_0(\gamma_2 R) + b_1 I_1(\gamma_2 R) \exp(j\phi)] \exp(-j\omega t)$$

in which the higher-order terms have been dropped because the higher-order Bessel functions are essentially zero for the range of argument involved.

References

1 Altman, P. L. and Dittmer, D. S., 1966, Environmental Biology, Federation of Amer. Soc. for Env. Biol., Bethesda, Md.

2 Bursell, F., 1964, *The Physiology of Insecta, 1,* (ed. by M. Rockstein), Academic Press.

3 Carslaw, H. S. and Jaeger, J. C., 1959, *Conduction of Heat in Solids,* (2nd ed.), p. 55, Oxford Univ. Press.

4 Curtis, O. F. and Clark, D. G., 1950, *An Introduction to Plant Physiology,* (1st ed.), McGraw-Hill Book Co., Inc., p. 297.

5 Davis, F. S., Wayland, J. R. and Merkle, M. G., 1971, Science, *173,* pp. 535-537.

6 Jaeger, J. C., 1956, Aust. J. Phys., *9,* pp. 167-179.

7 Jordan, E. C. and Balmain, K. G., 1968, *Electromagnetic Waves and Radiating Systems,* (2nd ed.), p. 258, Prentice-Hall, Inc.

8 Menges, R. M., and Wayland J. R., 1974 Weed Science (in press).

9 National Bureau of Standards, 1943, "Table of Bessel Functions $J_0(z)$ and $J_1(z)$ for Complex Arguments"; Columbia Univ. Press.

10 Nelson, S. O., 1972, Trans. ASAE, *15,* pp. 1094-1098.

11 Panofsky, W. K. H. and Phillips, M., 1962, *Classical Electricity and Magnetism* (2nd ed.), p. 226, Addison-Wesley Pub. Co.

12 Stratton, J. A., 1941, *Electromagnetic Theory,* p. 500 McGraw-Hill Book Co., Inc.

13 Von Hippel, A. R., 1954, *Dielectric Material and Applications,* John Wiley and Sons, p. 314.

Dielectric Food Data for Microwave Sterilization Processing

Th. Ohlsson and N. E. Bengtsson†

ABSTRACT

Using a cavity perturbation method we have extended our earlier measurements on the dependence of dielectric food data on temperature at the microwave frequencies of 2800, 900 and 450 MHz to temperatures from +60°C up to +140°C for a number of food products. Such high temperature data are required for microwave sterilization studies.

The results obtained are in good agreement with previously reported data at the temperatures where such data are available.

At temperatures above +60°C, ϵ'_r decreases gently with temperature, whereas ϵ''_r clearly increases, particularly at lower frequencies and for salty foods. Penetration depths calculated from the data show a clear advantage for the two lower frequencies only at temperatures below about 50°C.

Application of the new data to computer simulations of microwave sterilization show that the resulting temperature depends to a large extent on the food composition as well as on the frequency.

Introduction

Owing to the slow heat penetration into solid foods, conventional canning requires long processing times to ensure bacteriologically safe products. The long exposure to high temperature causes overheating of the food surface and deterioration of the flavor of the products, as demonstrated by Persson and von Sydow [11] for canned beef. A considerable improvement in quality was obtained by heating to high temperatures for short times (HTST-treatment). With conventional heating techniques, HTST-treatment can be used only for thin samples. The unique properties of microwaves to penetrate into and directly heat the interior of foods offers a possibility to HTST-treatment of relatively thick solid food samples with improved sensory quality.

Experiments with microwave sterilization at 2450 MHz of foods in plastic pouches with overriding air pressure have been reported by Kenyon *et al.* [7] and Ayoub *et al.* [1]. Other experiments with microwave sterilization of foods in plastic pouches have briefly been presented by Stenström [14].

Fundamental studies of microwave sterilization require dielectric food data over the temperature and frequency range of practical interest. The literature

* Manuscript received December 17, 1974; in revised form January 25, 1975.

† Swedish Institute for Food Preservation Research, SIK, Fack, 400 21 Göteborg 16, Sweden.

contains only few data on temperatures above +65°C and none above +80°C. We therefore extended the range of our previous measurements [2, 9] at 450, 900 and 2800 MHz, in the temperature range −20 to +60°C to include measurements from +40°C up to +140°C. In addition, a large number of industrially prepared food products and special type of foods were evaluated at 2800 MHz in the temperature range of +50°C to +125°C. From the measured values of ϵ'_r and ϵ''_r, penetration depths were calculated in some foods and the temperature distribution during microwave sterilization were calculated by a computer program based on a previously described method [8].

Methods and Materials

Measuring method

The measurements were made with the cavity perturbation technique described in detail by Risman and Bengtsson [12] for 2800 MHz and by Ohlsson *et al.* [9] for 900 and 450 MHz. The measuring frequencies were chosen close to the three ISM-frequencies of main practical interest for food heating applications; 2450 MHz, 915 (896) and 434 MHz [16]. The sample preparation technique and measuring and evaluation procedures were the same as those for our earlier measurements. A slightly modified instrumental setup was necessary. The plastic materials in the cavities were replaced by high temperature stable plastics or by quartz glass. In the first series of measurements at 2800 MHz coaxial cables rated for use up to 150°C were used. In the 900 and 450 MHz series and the second 2800 MHz series the cables were replaced by 50 ohm rigid copper coaxial air lines. The outer copper tube had an inner diameter of 14 mm and the inner tube an outer diameter of 6 mm. The coaxial lines were connected to the cavities with regular N-type connectors. Those parts of the coaxial lines extending from the thermostated cabinet were cooled by a water jacket in order to protect the measuring equipment.

In principle, the measuring procedures is as follows. An empty glass sample tube is inserted into the cavity, the generator is tuned to the proper resonant frequency and the signal transmitted through the cavity is adjusted to the same power level at each measuring run using a SWR-meter. A filled sample tube is then inserted and the shift in resonant frequency and in attenuation is determined, from which ϵ'_r and ϵ''_r are calculated from precalibrated graphs. Errors in attenuation due to non-linearity of the crystal detector are then minimized, and the deviations from non-linearity at different power levels are included in the measured values at the calibrations.

Since measurements on foodstuffs above 100°C involve work at overpressure, the sample tubes had to be fitted with a pressure-proof metallic cap. This closure should not interfere with the dielectric measurement. This was ensured by positioning the cap in areas of near zero field intensities in the 2800 MHz TM_{012} cavity, and in the TM_{010} cavities used at 450 and 900 MHz the metallic caps of the sample tubes extended well outside the cavities.

Since the cavity perturbation technique is not an absolute measuring method, it must be calibrated with the use of suitable reference liquids. Calibration required a very high loss liquid in addition to the reference data reported earlier [12, 9]. An absolute measurement was therefore made on 0.7 M NaCl-water solution by another Swedish laboratory. The values for the dielectric

constant (ϵ'_r) and loss factor (ϵ''_r) were 63 ±6 and 120 ±10 at 900 MHz and 65 ±10 and 230 ±12 at 450 MHz respectively.

With the above mentioned reference values, evaluation charts were constructed for each frequency. For high loss materials, the correction for ϵ'_r given by Risman and Ohlsson [13] was used. For loss tangent ($\tan \delta = \epsilon''_r/\epsilon'_r$) values above about 1.5 only approximate ϵ'_r values can be given, due to the low Q-factor of the loaded cavity.

Scope of measurements, materials and sample preparation

Four different series of measurements were made. The first three series cover measurements on basic foodstuffs at the temperatures +40, +60, +80, +100, +120 and +140°C for the frequencies 2800, 900 and 450 MHz. The fourth series included measurements at 2800 MHz on 16 different industrially prepared foods at temperatures of +50, 75, 100 and 125°C. In all the measuring series sample were taken from each preparation for determination of water and fat content by the methods described previously [9].

Series 1 - 3—The following substances were included in all the comparative measurements at the three frequencies: raw lean beef, precooked cod, gravy and distilled water. As seen from Tables 1, 2 and 3, measurements at 2800 MHz were made for a further 5 - 6 materials and at 450 and 900 MHz for one more material.

Precooking of beef and cod and the preparation and insertion of solid samples (cork bore technique) and disintegrated samples (syringe injection) were performed in the way described by Bengtsson and Risman [2]. At both 900 and 450 MHz the cooked cod samples were prepared by injecting raw fish tissue into the sample tubes and cooking in a water bath. Glass tubes of 1 mm wall thickness and of 5 mm inner diameter were used at 2800 and 900 MHz, and of 7 mm inner diameter at 450 MHz. Two separate preparations were made for each of the foods except for liver paté and 0.1 M NaCl where only one was made. Out of each preparation 3 to 4 sample tubes were prepared. The density of the sample in each tube was checked.

Series 4—In the fourth series at 2800 MHz some of the foods differed markedly in composition compared to those in the first three series. The 16 foods measured are grouped into basic (8), combined (5), and special (3) food products as specified in Table 4. A number of the solid foods (French fried potatoes, frankfurters, beef steak and filet of turbot) were prepared by the cork bore technique. To facilitate insertion of the sample plug, sample tubes with metallic caps at *both* ends were used. Only one preparation including 3 - 4 sample tubes was made for each food.

Results and Discussion

The results of the dielectric measurements of Series 1 - 3 at 2800, 900 and 450 MHz are given in Tables 1 - 3 together with the proximate compositions of the various samples. Since the differences between different batches and sample preparations of the same material were only small, the data were pooled and grand means were calculated together with their 95% confidence limits, as computed from the error variance. Table 4 gives the means for ϵ'_r and ϵ''_r as well as proximate compositions of the 16 food products measured at 2800 MHz in Series 4.

TABLE 1

APPROXIMATE COMPOSITION AND DIELECTRIC PROPERTIES OF FOODS AT 2800 MHz AND TEMPERATURES FROM +40 TO +140°C. MEAN VALUES FROM 1-3 BATCHES AND 3-4 REPLICATES GIVEN WITH 95% CONFIDENCE INTERVALS.

	Water %	Fat %		+40°C		+60°C		+80°C		+100°C		+120°C		+140°C	
				ϵ'_r	ϵ''_r	ϵ'_r	ϵ''_r	ϵ'_r	ϵ''_r	ϵ'_r	ϵ''_r	ϵ'_r	ϵ''_r	ϵ_r'	ϵ_r''
Beef, raw	74.9	1.3	Mean	45.2	12.5	44.4	12.0	42.6	13.1	41.2	13.7	40.1	14.9	40.5	16.0
			±△	0.5	0.7	0.5	1.1	0.8	0.4	0.9	0.3	1.7	0.8	7.6	5.7
Fish, cooked	77.2	0.2	Mean	45.0	11.9	43.8	12.0	42.6	12.7	41.3	13.4	40.5	14.4	39.9	16.8
			±△	0.3	0.2	0.5	0.3	0.2	0.1	0.4	0.4	0.3	0.3	0.3	0.5
Gravy	89.8	4.4	Mean	76.4	24.1	75.5	26.6	73.6	26.2	70.4	26.3	70.0	27.5	68.7	28.8
			±△	1.9	0.5	2.7	1.1	2.4	0.6	2.9	1.1	2.8	0.6	4.4	0.4
Water	—	—	Mean	72.8	6.5	66.9	4.0	61.8	3.2	56.7	2.4	52.5	2.0	48.1	1.5
			±△	0.5	0.3	0.5	0.2	1.0	0.2	0.8	0.1	1.1	0.1	0.7	0.1
Mashed potatoes	81.3	0.9	Mean	60.6	17.4	56.3	16.5	54.2	16.5	52.9	15.8	48.4	16.3	44.7	15.0
			±△	3.5	1.1	1.5	0.4	1.2	0.6	0.4	0.4	3.5	2.3	1.9	0.4
0.1M NaCl	—	—	Mean	71.1	13.7	67.7	14.0	63.5	14.8	59.2	15.6	55.0	16.5	51.9	17.4
			±△	0.8	0.1	0.4	0.0	0.7	0.1	1.0	0.2	0.9	0.1	0.9	0.2
Beef, precooked 60°	72.4	1.4	Mean	44.1	11.3	43.1	11.4	41.6	11.7	40.7	12.5	39.8	13.5	39.1	15.0
			±△	0.7	0.5	0.8	0.7	0.5	0.8	1.5	0.7	1.1	0.6	1.0	1.0
Beef, precooked 75°	68.1	1.3	Mean	43.0	10.9	41.8	11.0	40.7	11.3	39.6	11.9	38.9	12.8	38.7	14.8
			±△	1.2	0.4	1.4	0.5	1.2	0.8	1.0	0.7	1.5	1.0	2.0	2.0
Liver paté	55.0	20.0	Mean	41.4	16.5	41.0	17.4	38.9	18.4	38.3	18.8	38.1	19.7	38.7	20.7
			±△	0.5	0.6	0.3	0.5	0.5	0.9	0.6	1.3	1.3	2.5	2.5	1.3
Peas, cooked	78.6	—	Mean	60.8	12.6	55.6	10.8	50.5	9.7	46.6	9.1	43.0	8.9	41.2	8.9
			±△	1.4	0.7	2.2	0.6	1.6	0.4	1.2	0.5	0.3	0.5	0.3	0.9
Carrots, cooked	83.1	—	Mean	70.1	11.8	65.5	11.8	61.8	12.5	58.0	13.4	43.0	11.0	41.5	11.0
			±△	0.9	0.8	0.8	0.4	1.3	0.4	3.0	1.3	0.7	0.9	0.5	0.2

TABLE 2

APPROXIMATE COMPOSITION AND DIELECTRIC PROPERTIES OF FOODS AT 900 MHz AND TEMPERATURES FROM +40 TO +140°C. MEAN VALUES FROM 2 BATCHES AND 3 - 4 REPLICATES GIVEN WITH 95% CONFIDENCE INTERVALS.

	Water %	Fat %		+40°C		+60°C		+80°C		+100°C		+120°C		+140°C	
				ϵ'_r	ϵ''_r	ϵ'_r	ϵ''_r	ϵ'_r	ϵ''_r	ϵ'_r	ϵ''_r	ϵ'_r	ϵ''_r	ϵ_r'	ϵ_r''
Beef, raw	72.7	2.7	Mean	49.2	25.6	47.0	31.7	44.2	38.0	42.5	46.6	42.2	57.3	37.6	72.1
			± △	1.1	0.5	1.0	0.8	0.9	0.6	1.4	1.0	0.5	1.9	2.1	2.9
Fish, cooked	81.3	0.6	Mean	52.0	27.4	49.8	33.6	47.0	37.5	46.3	46.9	44.1	59.1	39.7	80.4
			± △	0.7	1.7	1.4	1.9	1.2	1.8	1.8	2.5	1.4	3.9	2.6	4.4
Gravy	89.8	4.8	Mean	51.5	52.2	42.6	68.3	~38	87.2	~35	100	~35	122	~35	144
			± △	1.1	0.2	1.4	0.5	1.6	0.6	2.4	2.2	3.5	1.3	5.1	2.4
Water	—	—	Mean	67.8	1.36	61.3	1.09	56.8	0.69	52.1	0.52	47.1	0.43	43.7	0.3
			± △	1.3	0.1	0.5	0.03	0.6	0.04	0.3	0.02	1.0	0.0	0.7	0.0
Potato, cooked	79.2	0.3	Mean	53.2	20.8	48.9	25.0	45.7	28.8	42.4	34.8	39.6	40.5	36.2	47.6
			± △	1.0	0.5	1.4	1.2	2.1	1.2	1.4	1.5	2.2	1.7	1.4	1.6

TABLE 3

APPROXIMATE COMPOSITION AND DIELECTRIC PROPERTIES OF FOODS AT 450 MHz AND TEMPERATURES FROM +40 TO +140°C. MEAN VALUES FROM 2 BATCHES AND 3 - 4 REPLICATES GIVEN WITH 95% CONFIDENCE INTERVALS.

	Water %	Fat %		+40°C		+60°C		+80°C		+100°C		+120°C		+140°C	
				ϵ_r'	ϵ_r''	ϵ_r'	ϵ_r''	ϵ_r'	ϵ_r''	ϵ_r'	ϵ_r''	ϵ_r'	ϵ_r''	ϵ_r'	ϵ_r''
Beef, raw	73.8	2.1	Mean	~50	58.3	~44	72.4	~42	87.3	~40	105	~40	126	~40	137
			±△	1.1	3.5	1.3	4.2	0.5	2.4	1.2	3.0	1.7	1.7	1.9	10.9
Fish, cooked	81.5	0.6	Mean	~53	54.2	~48	69.6	~45	83.6	~43	103	~42	118	~40	158
			±△	0.9	0.3	1.5	0.6	0.9	1.3	1.1	1.2	0.8	8.0	0.7	4.0
Gravy	89.5	5.0	Mean	~50	126	~50	160	~47	184	~48	227	~45	268	~42	303
			±△	1.6	4.2	1.6	3.9	1.3	2.4	2.0	1.1	3.6	1.2	1.7	1.5
Water	—	—	Mean	69.2	1.18	63.0	1.00	58.4	0.83	54.2	0.75	49.7	0.70	45.4	0.68
			±△	0.3	0.04	0.3	0.04	0.7	0.03	0.2	0.01	0.3	0.04	0.2	0.02
Potato, cooked	78.7	1.2	Mean	~54	57.6	~49	70.4	~44	82.9	~42	99.5	~38	122	~34	139
			±△	0.5	3.2	0.8	4.3	1.5	2.4	0.8	2.0	0.9	2.1	1.6	3.1

TABLE 4

APPROXIMATE COMPOSITION AND DIELECTRIC PROPERTIES OF FOODS AT 2800 MHz AND TEMPERATURES FROM +50 TO +140°C. MEAN VALUES OF 3 - 4 REPLICATES.

		Water %	Fat %	50°C		75°C		100°C		125°C	
				ϵ'_r	ϵ''_r	ϵ'_r	ϵ''_r	ϵ'_r	ϵ''_r	ϵ'_r	ϵ''_r
BASIC FOODS	Peanut butter	—	48.5	3.1	4.1	3.2	4.4	3.5	5.0	4.0	6.7
	Frankfurters	50.7	31.9	39.0	26.9	44.3	23.5	51.8	24.8	58.8	25.4
	Ground beef patties	55.7	25.4	31.7	10.4	32.2	11.5	31.7	12.6	31.5	14.7
	Concentrated orange juice	57.6	—	54.1	15.7	53.5	15.2	52.0	15.7	49.9	16.9
	Beef steak, cooked	60.8	19.6	37.0	10.6	35.6	11.6	33.6	12.6	31.0	12.9
	Ham	69.1	4.7	66.6	47.0	87.4	57	101	60	106	63
	Pork chop	70.0	6.2	49.8	18.3	47.3	18.8	44.5	19.4	43.1	20.9
	Filet of turbot	83.5	4.3	53.6	14.1	51.1	15.2	48.3	16.9	46.2	18.5
COMBINED	Ham salad	54.8	27.3	38.7	26.8	42.1	29.5	76.5	50	99	65
	Potato salad	77.7	3.8	56.4	22.7	55.4	25.0	52.4	26.4	54.1	31.3
	Macaroni and cheese	78.2	3.0	54.5	20.7	56.5	24.7	59.2	27.4	61.8	30.2
	Chicken à la King	80.8	4.6	54.9	19.9	54.9	22.5	56.8	25.8	59.0	28.4
	Sea food Newburg	81.8	4.9	53.1	21.4	51.3	23.1	50.8	25.3	52.2	28.2
SPECIAL	Pizza, baked dough	10.3	26.4	4.6	0.6	5.4	0.7	6.2	0.9	6.5	1.0
	Pizza stuffing	16.6	21.6	10.1	3.1	11.5	4.1	12.4	4.9	12.5	5.7
	French fried potatoes	27.2	18.5	12.4	4.6	14.4	5.3	16.3	6.6	15.1	6.4
	Pineapple, pieces	79.7	0.9	62.0	11.0	56.5	8.9	51.4	8.5	46.0	8.4
	Pineapple, syrup	—	—	67.8	11.6	63.5	9.8	57.1	9.2	51.4	9.1

Precision and accuracy

The composition of the different batches and preparations of the same food material differed by less than ±2% in water content. Differences in ϵ'_r and ϵ''_r between different batches and preparations were less than ±3% in ϵ_r' and ±5% in ϵ''_r, except at +140° and at 450 MHz, where differences in ϵ''_r were up to ±7%. For the three to four sample tubes measured in each run the differences in ϵ'_r and ϵ''_r as well as density did not, as a rule, exceed ±2.5%. The 95% confidence limits of the mean values were larger for temperatures above 100°C.

It should be pointed out that the ϵ'_r values of most foods at 450 MHz and of gravy at 900 MHz are only approximate. Accurate calculations of the ϵ'_r values for materials with very high losses ($\tan \delta > 1.5$) require a more complete analysis of the theory of the cavity perturbation method, an analysis extending beyond the scope of the present work. However, the inaccuracy in ϵ'_r has little influence on the calculated penetration depth. For raw beef at 434 MHz and 120°C a 5 unit change in ϵ'_r results in only a 2% change in penetration depth.

In the first series (at 2800 MHz) disturbances occurred in the form of double and extended resonance peaks when measuring high-loss food products, such as mashed potatoes and gravy. The reasons were probably discontinuities and reflection in the coaxial cables and small displacements in the antennas in the TM_{012} cavity. These difficulties were eliminated by improved soldering of the antennas and, later on, by the use of rigid coaxial conductors.

The accuracy can be estimated by comparison with literature data. However, such data are available only for temperatures up to +65°C. For raw beef good agreement was found with our earlier measurements at 2800, 900 and 450 MHz as shown in Table 5. Our values are lower for raw beef, and higher for cooked beef than those given by To *et al.* [15] for raw beef and cooked beef at 2450 MHz. These differences are probably largely due to differences in water content and measuring frequency. At 915 MHz our data are in very good agreement with theirs.

TABLE 5
COMPARISON BETWEEN OUR PRESENT AND EARLIER DIELECTRIC DATA FOR RAW LEAN BEEF AT +40 AND +60°C FOR 2800, 900 AND 450 MHz.

		2800 MHz		900 MHz		450 MHz	
		ϵ'_r	ϵ''_r	ϵ'_r	ϵ''_r	ϵ'_r	ϵ''_r
+40°C	present	45.2	12.5	49.2	25.6	50	58.3
	earlier	46.0	12.6	55.0	25.9	53.5	63.7
+40°C	present	44.4	12.0	47.0	31.7	44	72.4
	earlier	39.5	11.5	50.9	31.2	50.4	84.8

At 2800 MHz the agreement with our earlier data [2] for cod, peas, potatoes and water is fully acceptable since it is within ±2 units in both ϵ'_r and ϵ''_r. For carrots the deviations can be explained by a difference in composition.

Compared to our previous data [9] higher values of both ϵ'_r and ϵ''_r were found at 900 MHz for cooked cod in our present investigation because of a difference in the preparation of the sample. The deviation in the ϵ'_r values for gravy at 900 MHz can be related to the earlier discussed measuring difficulties for high loss materials. Different preparation techniques resulting in different densities can also explain the differences in the ϵ'_r values for the cooked potato samples at 900 and 450 MHz. Finally, the ϵ'_r values now given for distilled water at 900 and 450 MHz deviate from our earlier data [9] and literature data [4] by at most 5 units in ϵ'_r for which no ready explanation can be offered.

Influence of temperature and frequency and composition

Raw beef, cooked codfish, gravy and distilled water were included in the measurements at both 450, 900 and 2800 MHz and thus give a basis for comparisons between the three frequencies up to the temperature region above 100°C.

The influence of temperature and frequency on the dielectric data up to +60°C is in agreement with our previous data [9]. From +60°C up to sterilization temperatures the trends are much the same. However, at 2800 MHz the loss factor values are minimal at about +60°C, after which they increase slightly with temperature. It appears that for most foods a doubling of the ϵ''_r value occurs going from 2800 to 900 MHz, and again from 900 to 450 MHz.

Figures 1 - 3 give the penetration depths for water, raw beef and gravy at the ISM-frequencies of 2450, 915 and 434 MHz. Since these frequencies differ little from the actual measuring frequencies, the dielectric data were assumed to be about the same. It is often claimed in the literature that the penetration depths at different frequencies are roughly proportional to the wavelengths. This is also the case for distilled water, where the penetration depths are very much greater at the two lower frequencies as illustrated in Figure 1. With increasing temperature the penetration depth in water increases considerably because of decreasing values for the loss factor. For raw beef, however, the loss factor increases so much when going to lower frequencies, that calculated penetration depths remain quite close at the three frequencies (Figure 2). Our data indicate a smaller penetration depth at 915 MHz than at the two other frequencies for temperatures above 80°C.

For gravy the differences in penetration depth between frequencies are greater than for beef owing to the large differences in ϵ''_r values caused by the high salt content of the gravy (Figure 3). Also for gravy the penetration depth is lower at 915 than at both 2450 and 434 MHz.

It has already been shown that the composition of the foods both with regard to water and salt content have a dominating influence on their dielectric properties. The almost linear dependence on water content of the ϵ'_r values is clearly demonstrated by comparing the ϵ'_r values for the five different beef samples in Tables 1 and 4. This also explains the change in penetration depth due to the water loss during the cooking of beef.

The dramatic influence of added and natural salts is obvious, e.g. from comparison of Figures 1, 2 and 3. The penetration depth at 2800 MHz as a function of temperature is shown in Figure 4 for a number of foods of widely

varying composition. Large penetration depths are obtained for foods with low or no salt content and low penetration depths for foods with added salt, e.g. ham and the ready-to-serve foods such as macaroni and cheese. This underlines the importance of using the proper dielectric data corresponding to the actual composition of a product in the evaluation and analysis of microwave heating of different foods.

Significance of data with regard to microwave sterilization

From the data on the dielectric properties and penetration depth in relation to composition, temperature and frequency it is apparent that all these factors have influence on the heating performance in a microwave sterilization operation.

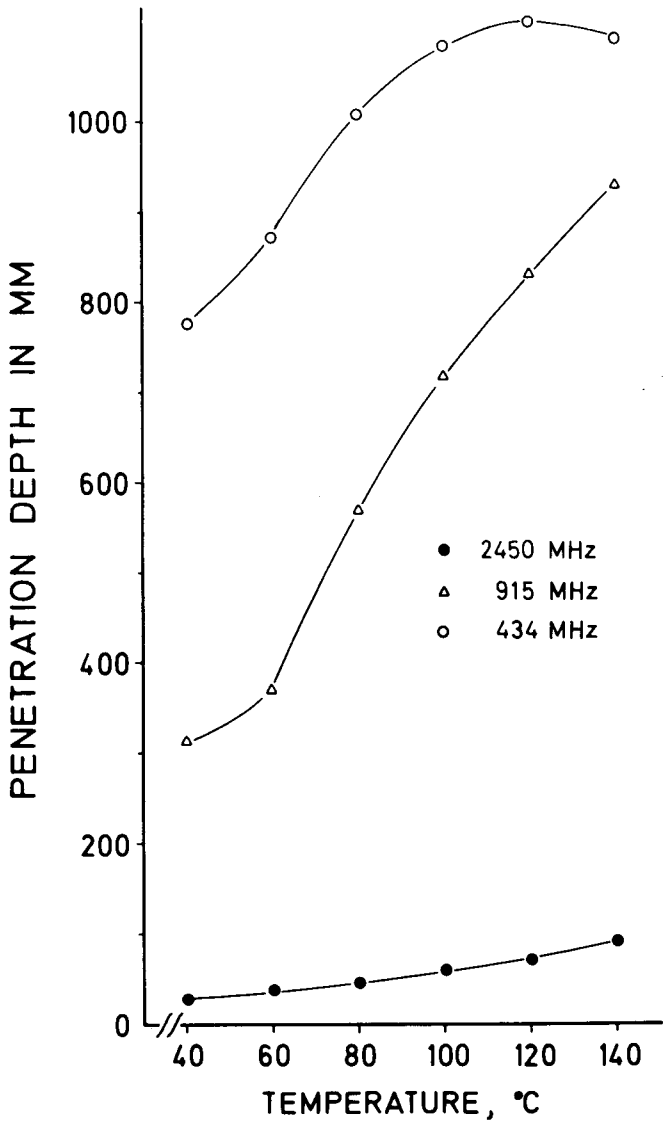

Figure 1 Penetration depth in distilled water at 2450, 915 and 434 MHz from +40 to +140°C.

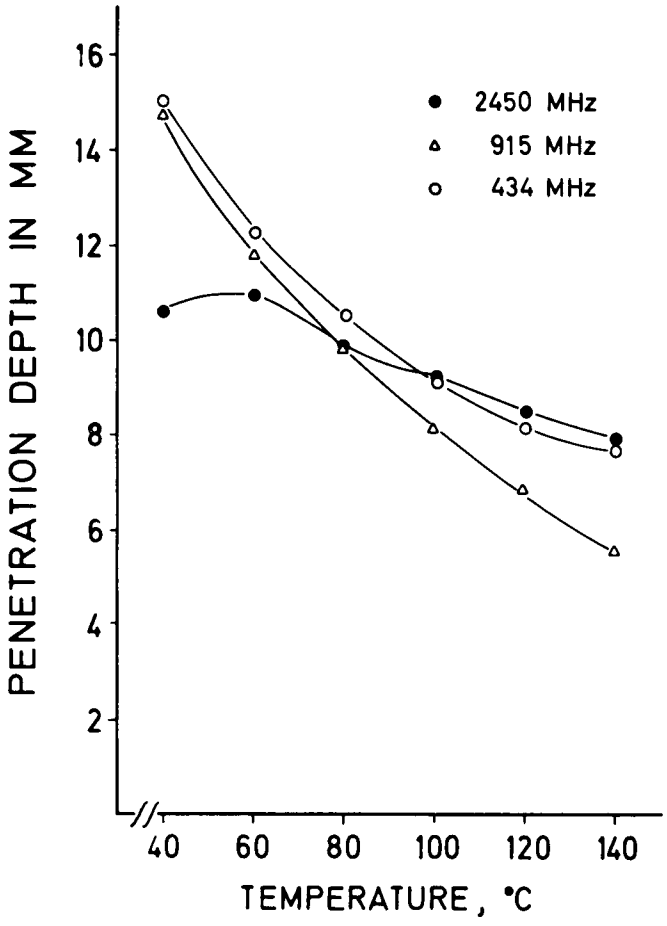

Figure 2 Penetration depth in raw beef at 2450, 915 and 434 MHz from +40 to +140°C.

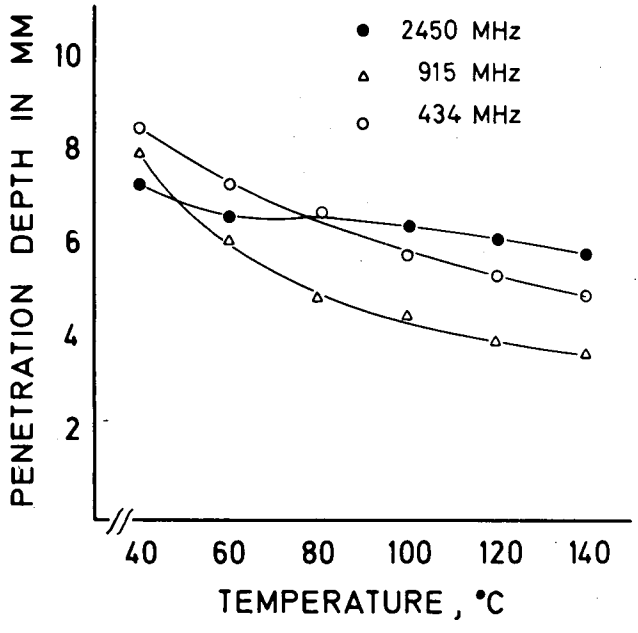

Figure 3 Penetration depth in gravy at 2450, 915 and 434 MHz from +40 to +140°C.

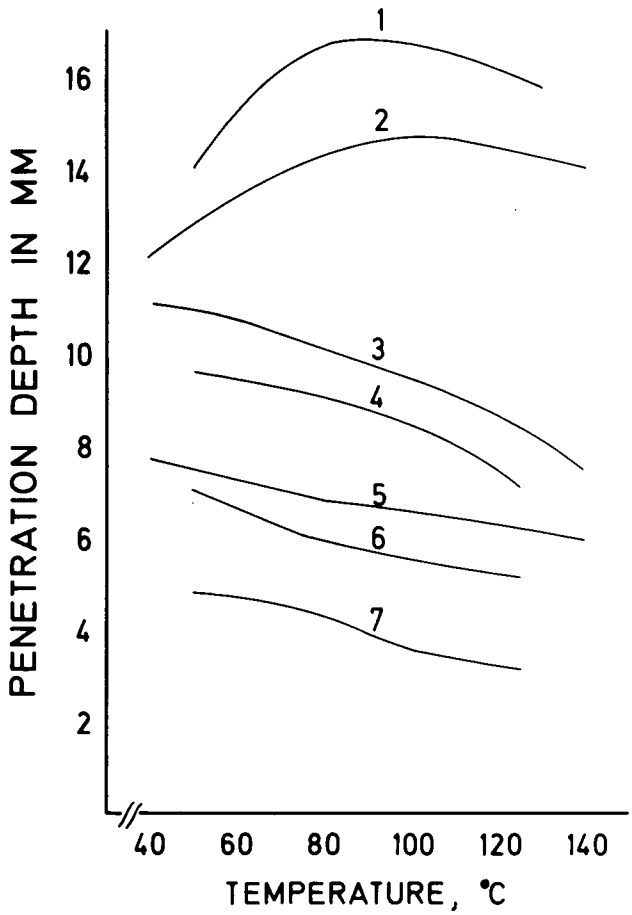

Figure 4 Penetration depth at 2450 MHz at elevated temperatures in foods of different composition. 1. Pineapple pieces, 2. Cooked peas, 3. Cooked cod, 4. Peanut butter, 5. Liver paté, 6. Macaroni and cheese, 7. Ham salad.

It is clear from our data on ϵ''_r that the temperature dependence, and consequently the "run-away" heating tendency, should increase with falling frequency, as well as that the differences in penetration depth between the three ISM-frequencies become surprisingly small with increasing temperature.

Knowledge of the dielectric properties of foods and their variation with composition, temperature and frequency is of great importance. In actual heating experiments, the thermal properties of the food material to be heated also influence the resulting temperature distribution in the food, as demonstrated by Bengtsson and Ohlsson [8].

To study the combined influence of all these factors on temperature development during simulated microwave sterilization of foods, a computer program was constructed, on the same principles as those given by Ohlsson and Bengtsson [8]. An explicit, finite—difference calculation method is used combined with a finite difference exponential decay of the impinging microwave power. The program also permits the calculation of accumulated sterilization values[1] at

1 The sterilization value, or F value, is a measure of the degree of assurance against survival of pathogenic microbial spores, and is expressed in equivalent minutes at the reference temperature of 121.1°C (250°F). It is time-temperature dependent according to the equation:

$$F = \int_0^t 10^{-[121.1 - T(t)]/10} dT,$$ where T(t) denotes the time dependent temperature of the food sample.

preselected locations in the food. HTST sterilizations of solid foods of 20 mm thickness were simulated. Starting from 60°C, foods were microwave heated for 130 sec. followed by air-cooling during 70 sec. and subsequent cooling in cold water. The processing conditions were chosen to give a final F-value of 6 at the sample centre. The microwave power surface density was 2.0 W/cm^2 at each side of the food sample. In Figure 5, the time temperature development at the surface and at the centre are illustrated for raw beef, cooked peas and liver paté. Also the corresponding F-values are given. In the calculations our own dielectric data and literature data [5, 6, 10] for the thermal properties of the respective foods were utilized.

The importance of the dielectric properties of foods to the result of heating is clearly illustrated in Figure 5. Large differences in the respective F-values for the different food products are demonstrated. Compared with conventional steam sterilization, surface heat treatment should be considerably less severe in microwave processing of beef and peas, but not of liver paté. A simulation of an identical sterilization for beef using steam of 121°C only, results in an F-value of 14.4 at the surface for 6.0 at the centre. The processing time is 4 times longer than for the microwave processing.

Simulations for raw beef samples at the three frequencies 2450, 915 and 434 MHz, are illustrated in Figure 6. The earlier observed lower penetration depth at 915 MHz, as compared with 2450 and 434 MHz, corresponds to a much higher surface F-value and lower centre F-value at 915 MHz. This also indicates that the risks of run-away heating at edges and corners should be greater at 915 MHz than at 2450 MHz. The findings imply that the 2450 MHz frequency should be advantageous for microwave sterilization of foods.

Conclusions

It is concluded that the dielectric properties of foods and their dependence on temperature, frequency and composition greatly influence the temperature distribution developed during microwave sterilization. Except for foods containing added salts, the temperature dependence of the penetration depth is moderate. The influence of different water content and salt content is, however, large. This is especially true at 450 and 900 MHz.

While dielectric loss at 2800 MHz decreases with rising temperature between 0°C and +60°C, a gradual increase occurs between 60 and 140°C. At 900 and particularly at 450 MHz, there is a clear increase in ϵ''_r over the entire temperature range.

At the three different frequencies investigated the penetration depths for normal foods show surprisingly small differences. On the other hand, the process simulation work indicates a disadvantage of 915 MHz in surface heating. It must be borne in mind, however, that these calculations do not take into account the possible development of reflections and standing wave patterns in the food which will depend on both frequency, sample dimensions and dielectric properties. It is evident, however, that the dielectric data and their temperature dependence of the actual foods must be determined, and that data cannot be extrapolated from lower temperatures up to the sterilization region.

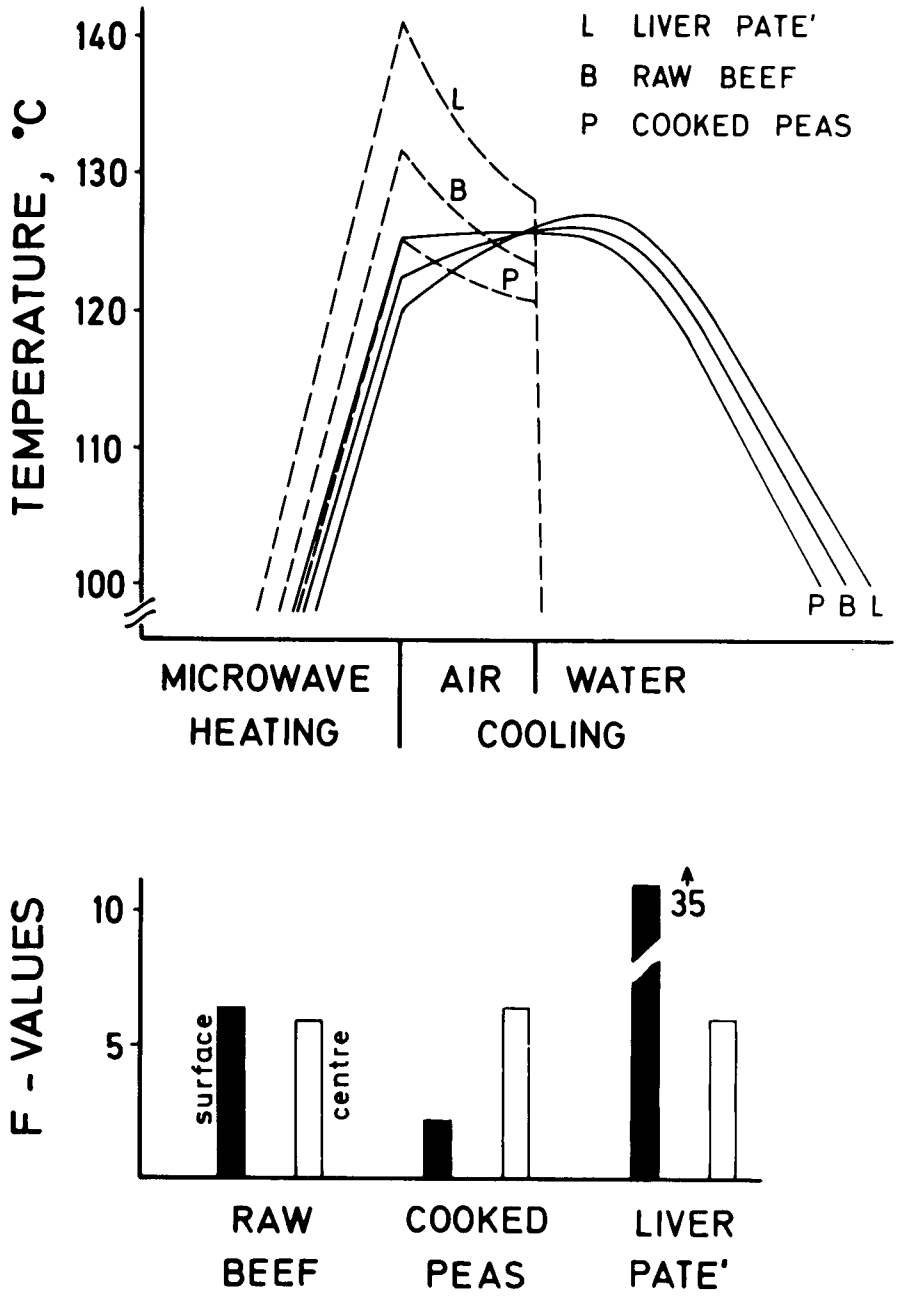

Figure 5 Computer simulated microwave sterilization at 2450 MHz of "infinite" slabs of 20 mm thickness of raw beef, peas and liver paté. Surface power densities were 2.0 W/cm² at both surfaces. Time-temperature distributions for centre (solid lines) and surface (broken lines) and corresponding F-values are shown.

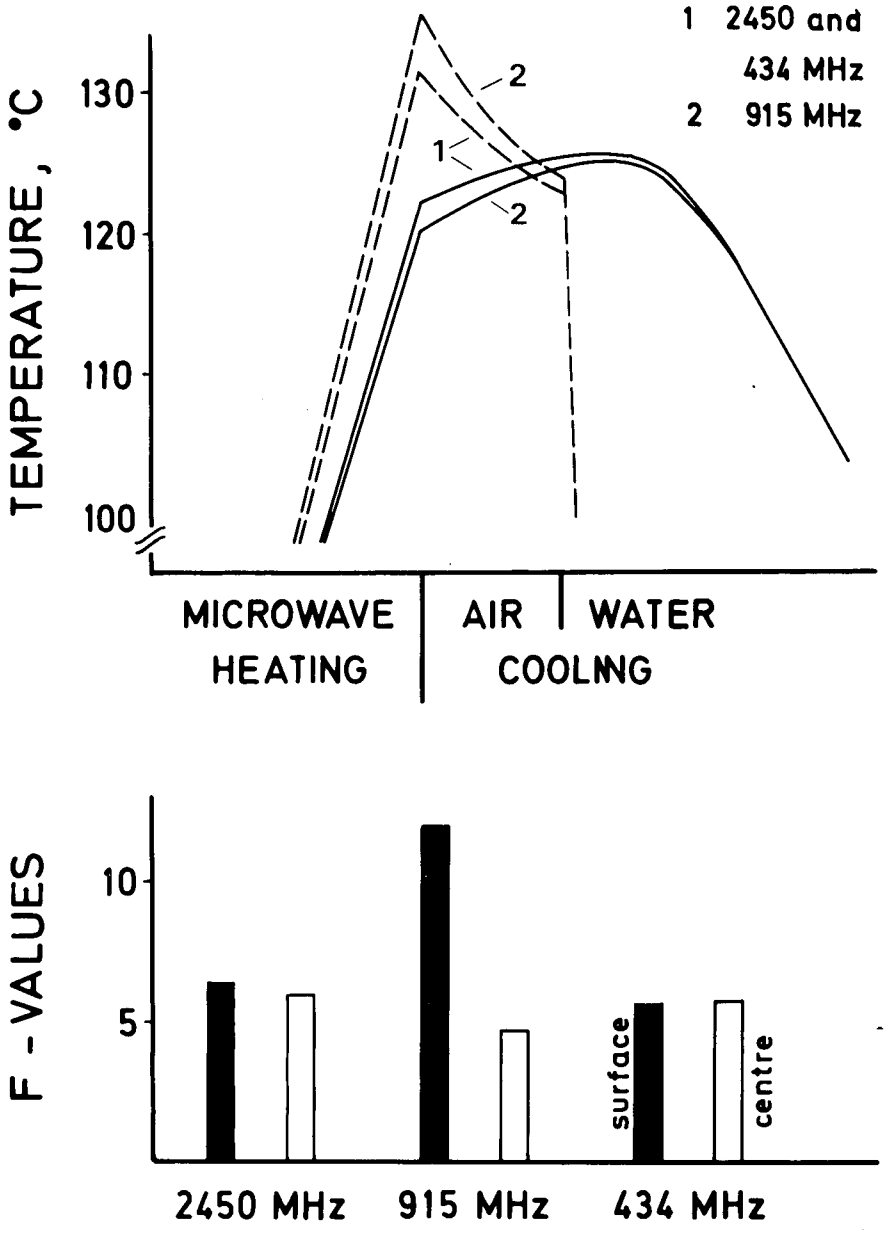

Figure 6 Computer simulated microwave sterilization of "infinite" slabs of 20 mm thickness of raw beef at 2450, 915 and 434 MHz. Surface power densities were 2.0 W/cm² at both surfaces. Time-temperature distributions for centre (solid lines) and surface (broken lines) and corresponding F-values are shown.

Acknowledgements

Thanks are due to Per Engwall and Karl Remi, *SIK*, who performed much of the experimental and computational work. The authors are indebted to the *Alfa-Laval Company of Tumba, Sweden* and the *Husqvarna Company of Husqvarna, Sweden* for permission to publish the 2800 MHz data. The invaluable assistance of P. O. Risman, *Husqvarna AB* for discussion and help with the measuring equipment and for the construction of the rigid copper conductors is gratefully acknowledged.

References

1 Ayoub, J. A., Berkowitz, D., Kenyon, E. M. and Wadsworth, C. K., 1974, "Continuous microwave sterilization of meat in flexible pouches," J. Food Sci. *39*, 309.

2 Bengtsson, N. E. and Risman, P. O., 1971, "Dielectric properties of food at 3 GHz as determined by a cavity perturbation technique. II. Measurement on food materials," J. Microwave Power, *6*(2), 107.

3 Bengtsson, N. E. and Ohlsson, Th., 1974, "Microwave heating in the food industry," Proc. IEEE *62*(1), 44.

4 Hasted, J. B., 1972, "Liquid water: Dielectric properties," *in "Water—comprehensive treatise."* (Ed. F. Franks), Plenum Press, New York 1972.

5 Jasper, W., 1962a, "Berechnung der Abkühl- und Gefrierzeiten von Schweine- und Rinderhälften," Der Fleischermeister *16*(3), 61.

6 Jasper, W., 1962b, "Berechnung der Abkühl- und Gefrierzeiten von Schweine- und Rinderhälften. II Das Gefrieren der abgekühlten Tierkörper," Der Fleischermeister *16*(4), 91.

7 Kenyon, E. M., Westcott, D. E., La Casse, P. and Gould, J. W., 1971, "A system for continuous thermal processing of food pouches using microwave energy," J. Food Sci. *36*, 289.

8 Ohlsson, Th. and Bengtsson, N. E., 1971, "Microwave heating profiles in foods," Microwave Energy Applications Newsletter, *4*(6), 3.

9 Ohlsson, Th., Bengtsson, N.E. and Risman, P. O., 1974, "The frequency and temperature dependence of dielectric food data as determined by a cavity perturbation technique," J. Microwave Power, *9*, 129.

10 Ohlsson, Th. and Svensson, S. G., 1974, "Calculation of heat transfer and enzyme inactivation in blanching of peas," *presented at* IV Int. Congr. of Food Sci. and Techn., Madrid Sept. 23-27 (Paper 6.4).

11 Person, T. and von Sydow, E., 1974, "The aroma of canned beef: Processing and formulation aspects," J. Food Sci. *39*, 406.

12 Risman, P. O. and Bengtsson, N. E., 1971, "Dielectric properties of food at 3 GHz as determined by a cavity perturbation technique. I. Measuring technique," J. Microwave Power, *6*(2), 101.

13 Risman, P. O. and Ohlsson, Th., 1973, "Dielectric constants for high loss materials. A comment on earlier measurements," J. Microwave Power *8*(2), 185.

14 Stenström, L.A., 1972, "Taming microwaves for solid food stabilization"; *Presented at* the IMPI Symposium, Ottawa, Canada, May 24-26, (Paper 7.4).

15 To, E. C., Mudgett, R. E., Wang, D. I. C., Goldblith, S. A. and Decareau, R. V., 1974, "Dielectric properties of food materials," J. Microwave Power *9*(4), 303.

16 Voss, W. A. G., 1969, "Advances in the use of microwave power," *Presented at* US Dept. Health, Education and Welfare Seminar, April 25, (Paper 008.)

Brief Communication

Microwave Bean Roaster*

M. A. K. Hamid, N. J. Mostowy† and P. Bhartia‡

ABSTRACT

This paper describes an application of microwave power for the roasting of beans (soybeans, rapeseeds, coffee beans, sunflower seeds, pumpkin seeds, sesame seeds, peanuts and the like) for the sake of destroying the anti-tripsin enzyme (or growth inhibitor) and thus facilitating safe nutritional consumption by humans and animals. A leaky waveguide applicator developed for this purpose is described and analyzed while representative results of bean roasting are presented to illustrate the improvement in efficiency and lowering of cost relative to present techniques.

Introduction

Destruction of the anti-tripsin[1] enzyme (growth inhibitor) in soybeans and other seeds and beans is a primary reason for their roasting for animal and human consumption. The process has conventionally been carried out using hot air, and in this work a microwave applicator which is faster and economic is described for the same purpose. The mode of operation and the field analysis of the applicator are given below, together with some experimental results. The applicator is shown to be practical and economical.

The Microwave Applicator

The proposed device for this application is shown schematically in Figures 1 and 2 and consists of a hopper, a perforated low loss dielectric tube for propagation of microwave energy, and a double walled cylindrical cavity (with hot air exhaust perforations in the inner wall). The beans are guided between the inner cavity wall and the outside of the dielectric tube down towards a holding bin and a metering device (auger). The latter discharges the beans into a packaging device or conveyor belt, depending on the actual type of application.

Figure 2 shows a detailed breakdown of the applicator. The cylindrical cavity constructed of aluminum consists of an outer cylinder wall and inner perforated cylinder. The top of the cylindrical cavity is terminated with an

1 Anti-tripsin is a substance in soybeans and other beans which, when ingested, limits the production of tripsin (an enzyme which digests protein).

* This paper was presented at the International Microwave Power Institute Symposium, May 1974 at Marquette University, Wisconsin. Manuscript received October 24, 1974.

† Department of Electrical Engineering, University of Manitoba, Winnipeg, Manitoba, Canada.
‡ Faculty of Engineering, University of Regina, Regina, Saskatchewan, Canada.

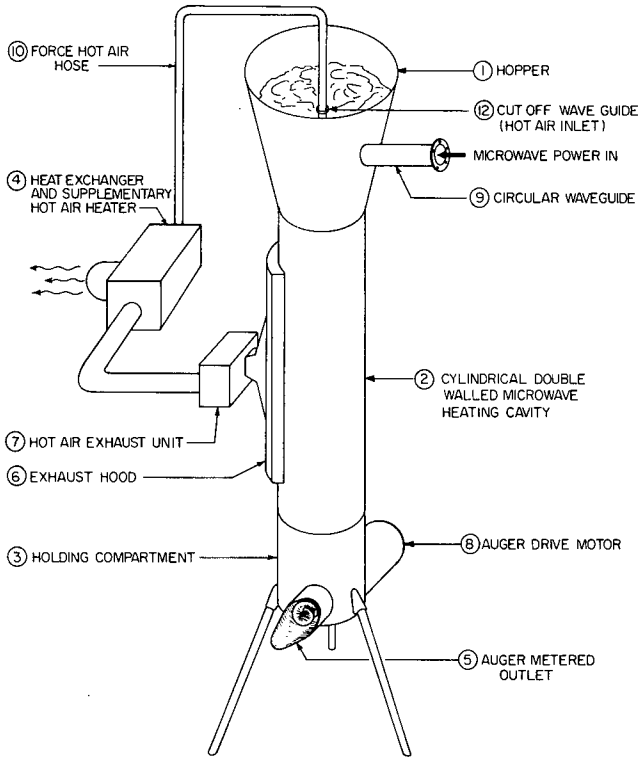

Figure 1 Microwave bean roaster system assembly.

end plate assembly consisting of an upper centre tube support, a waveguide to dielectric transition and a microwave radiation skirt. A dielectric tube mount, lower center tube support and a short circuit reflecting cone with tapered rim form the bottom terminator. A cylindrical double-walled holding compartment with a metering attachment consisting of an outlet spout, an auger and a variable speed motor is mechanically attached to the bottom of the main cylindrical cavity. The cavity assembly is mounted vertically. An outer wall exhaust hood is attached to the outer cylindrical wall to facilitate attachment of the hot air exhaust unit, which is then connected to the heat exchanger and the supplementary hot air heater. The hopper assembly consists of a 90° bent waveguide with a cut-off waveguide positioned at the center of the bend and at 90° in relation to the horizontal position of the circular input power waveguide. A forced hot air hose joins the cut-off waveguide and the heat exchanger hot air supply. Microwave power is fed through a circular waveguide in the dominant TE_{11} mode and is propagated through the dielectric tube into the applicator, the fields there being essentially hybrid EH_{11} mode type.

Mode of Operation

The bean roaster is operated in the vertical position with the beans being gravity fed. With the beans compacted around the dielectric tube due to gravity flow, a uniform dimensioned hole array is now available for propagation of microwave energy. The dielectric tube is transparent to the microwave energy due to the higher dielectric constant and loss factor of the surrounding beans in the manner of a leaky waveguide. The energy reaching the end of the

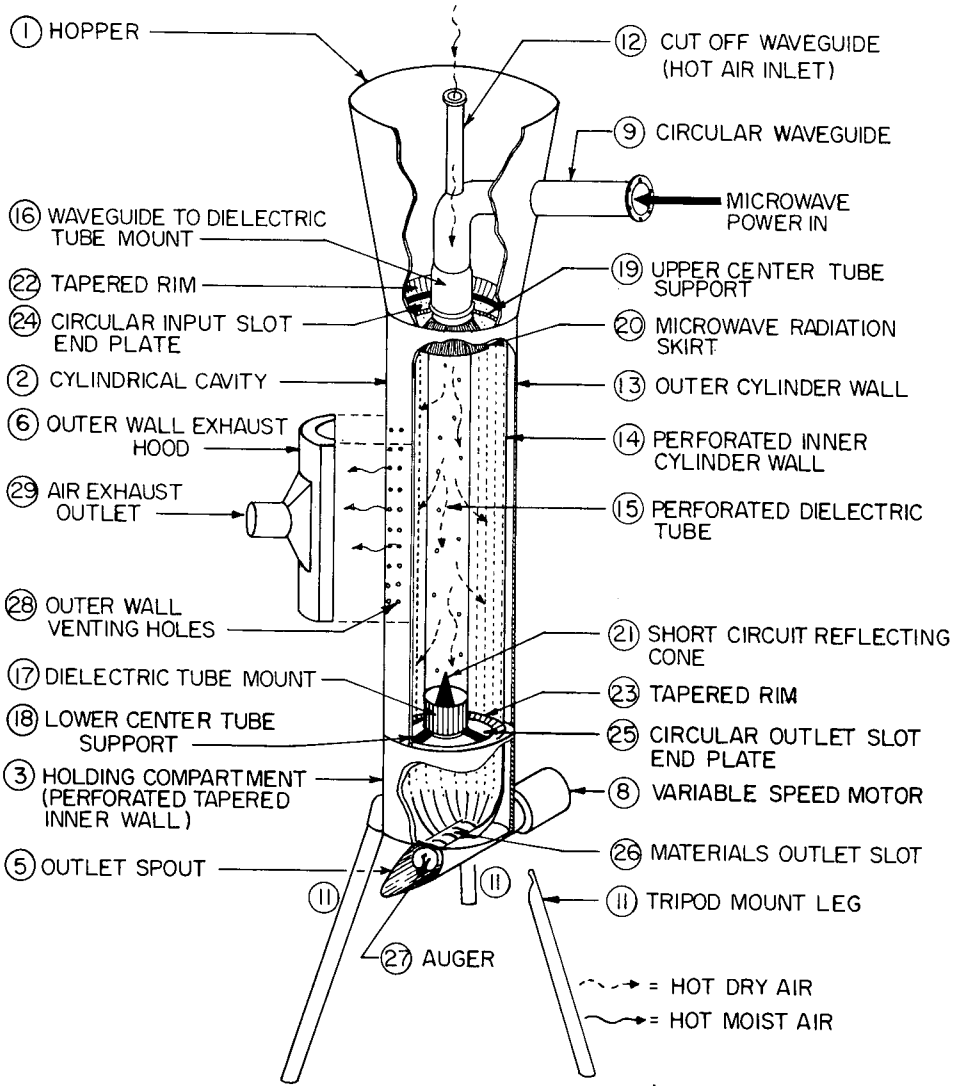

Figure 2 Microwave bean roaster assembly cut-away section view.

dielectric tube is reflected back to the load due to the short circuit reflecting cone.

As the microwave energy affects heating, removal of the hot moist air is affected with perforated inner cylinder wall and an exhaust suction system. The heat contained in this hot moist air is recovered (prior to discharge) by thermal transfer to the incoming fresh air (already heated in the magnetron power supply). This is injected into the system through the cut-off waveguide attached to the input power circular waveguide.

Moisture and temperature can be continuously monitored by strategically placed sensors which feed information to a control system to adjust power

level, flow rates, etc., necessary for a satisfactory quality and nutritious product. The holding compartment also maintains temperatures for a time period necessary to complete the thermal kill of the enzymes and any insects present.

Other systems for the heating of seeds have been developed [1 - 3], but the present applicator should provide a more efficient system due to the method of energy distribution.

Field Analysis of the Applicator

Since the inner hollow cylinder has a low dielectric constant, the propagating field may be obtained by analyzing the geometry in Figure 3. Thus, the structure can be analyzed as a cylinder of radius "a" and dielectric constant ϵ_1 surrounded by a medium of dielectric constant ϵ_2 in a metal waveguide of radius "b".

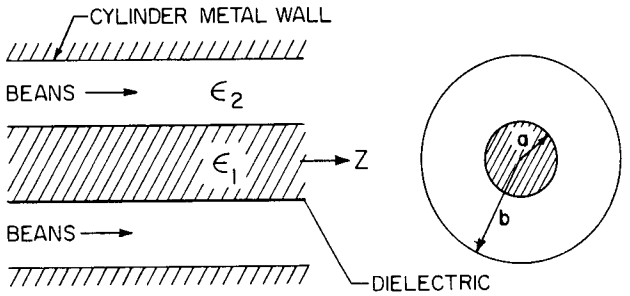

Figure 3 Schematic diagram of the applicator used in the field analysis.

The modes in this structure are hybrid [4 - 6] and contain coupled components of electric and magnetic fields in the z direction. They can be expressed as

$$e_{zm} = \begin{cases} J_1(\alpha_m r)\cos\phi, & 0 \leq r \leq a \\ \dfrac{N_1(\beta_m b)\,J_1(\beta_m r) - J_1(\beta_m b)\,N_1(\beta_m r)}{N_1(\beta_m b)\,J_1(\beta_m a) - J_1(\beta_m b)\,N_1(\beta_m a)}\,J_1(\alpha_m a)\cos\phi, & a \leq r \leq b \end{cases} \tag{1}$$

$$h_{zm} = \begin{cases} A_1 \sin\phi \left\{ N'_1(\beta_m b) J_1(\beta_m a) - J'_1(\beta_m b) N_1(\beta_m a) \right\} J_1(\alpha_m r), & 0 \leq r \leq a \\ A_1 \sin\phi \left\{ J_1(\beta_m r) N'_1(\beta_m b) - J'_1(\beta_m b) N_1(\beta_m r) \right\} J_1(\alpha_m a), & a \leq r \leq b \end{cases} \tag{2}$$

where

$\alpha_m^2 = \omega^2 \mu_o \epsilon_1 - \gamma_m^2$

$\beta_m^2 = \omega^2 \mu_o \epsilon_2 - \gamma_m^2$

γ_m is the mode propagation constant while $J_1(x)$, $N_1(x)$ are the Bessel and Neumann functions and A_1 is given by

$$A_1 = \frac{[\gamma_m/\omega\mu_o a]\left\{(1/\beta_m^2) - (1/\alpha_m^2)\right\}}{\dfrac{J'_1(\alpha_m a)}{\alpha_m J_1(\alpha_m a)}\left\{N'_1(\beta_m b) J_1(\beta_m a) - J'_1(\beta_m b) N_1(\beta_m a)\right\}} - -$$

$$- - \frac{}{-\dfrac{1}{\beta_m}\left\{N'_1(\beta_m b) J'_1(\beta_m a) - J'_1(\beta_m b) N'_1(\beta_m a)\right\}} \tag{3}$$

The eigenvalues γ_m, and hence α_m and β_m, may be obtained from an application of the boundary conditions for the electric and magnetic fields at the radii a and b. These result in the transcendental equation

$$\frac{1}{\beta_m}\{N'_1(\beta_m b)J'_1(\beta_m a) - N'_1(\beta_m a)J'_1(\beta_m b) - \frac{J'_1(\alpha_m a)}{\alpha_m J_1(\alpha_m a)}$$

$$[N'_1(\beta_m b) - J_1(\beta_m a) - J'_1(\beta_m b)N_1(\beta_m a)]\}\{\frac{1}{\beta_m}[N_1(\beta_m b)J'_1(\beta_m a)$$

$$- J_1(\beta_m b)N'_1(\beta_m a)] - \frac{\epsilon_1}{\epsilon_2}\frac{J'_1(\alpha_m a)}{\alpha_m J_1(\alpha_m a)}[N_1(\beta_m b)J_1(\beta_m a)$$

$$- J_1(\beta_m b)N_1(\beta_m a)]\} - \frac{\gamma_m^2}{\omega^2\mu_o\epsilon_2 a^2}\left(\frac{1}{\beta_m^2} - \frac{1}{\alpha_m^2}\right) \times$$

$$[J_1(\beta_m a)N_1(\beta_m b) - J_1(\beta_m b)N_1(\beta_m a)] \times$$

$$[N'_1(\beta_m b)J_1(\beta_m a) - J'_1(\beta_m b)N_1(\beta_m a)] = 0 \qquad (4)$$

Solving this equation, the fields can be determined everywhere in the applicator and comparison with measurements made to illustrate the validity of the theory used to optimize the design.

For the designed structure with $a = 1.4''$, $b = 3.5''$ and the roaster filled with peanuts of dielectric constant $2.24 + j\,0.14$ at 4.6% moisture content (dry weight basis) and the dielectric tube being assumed to be teflon ($\epsilon = 2.1$), the first four eigenvalues for γ are given in Table 1.

TABLE 1
TYPICAL VALUES OF γ FOR THE CASE OF PEANUTS BEING PROCESSED WHICH HAVE A DIELECTRIC CONSTANT $(2.28 + j\,0.14)$ AT 46% MOISTURE CONTENT CONSIDERING THE DIELECTRIC TUBE TO BE TEFLON OF RELATIVE PERMITTIVITY 2.1 ($a = 3.5''$, $b = 1.4''$)

Eigenvalues for m	γ
1	$0.7 + j\,0.00129$
2	$1.38 + j\,0.0531$
3	$3.77 + j\,0.284$
4	$7.35 + j\,0.173$

Experimental Results

Samples of soybeans were treated in this applicator and satisfactory results were obtained. As an example, for Anti-Tripsin destruction by conventional methods, the soybeans must be heated to over 105°C (220°F) and maintained at that temperature for 2 - 5 min. Samples of soybeans treated in the applicator gave the results in Table 2. It should be noted that the time taken was the total time in raising the sample from the initial temperature of 19.5°C (67°F) as compared to the conventional system where it must be raised to and then

maintained at 105°C for 2 - 5 min. Thermal calculations indicate that the total heat energy required for the microwave process is approximately 66% of that required by the conventional process.

Finally, the applicator was examined for microwave energy leakage and no noticeable deflection was observed on a Narda 8100 monitor.

TABLE 2

Sample No.	Power Level W	Exposure Time (Min)	Initial Temp. °C (°F)	Final Temp. °C (°F)	% Anti-Tripsin Destroyed
1	1250	2	19.5 (67)	116 (240)	75
2	1250	3	19.5 (67)	137 (280)	85
3	1500	3	19.5 (67)	153 (308)	100

Conclusions

A microwave applicator for the destruction of the anti-tripsin enzyme in beans and seeds has been developed and analyzed. The applicator is shown to be a practical and economically viable unit.

Acknowledgement

This research was supported by Farmatic Ltd., Gorrie, Ontario, Canada and the National Research Council under Grants A3326 and A8863.

References

1 Johnson, R. M., "Circular waveguide microwave applicator," U.S. Patent No. 3,715,555, (Aprli 1972).
2 Gorakhpurwalla, H. D., "Continuous microwave grain cooker," U.S. Patent No. 3,626,838, (Dec. 1971).
3 Day, J. A., "Construction for tuning microwave heating applicator," U.S. Patent 3,509,202.
4 Yaghjian, A. D., "Hybrid modes and the dielectric rod antenna," Ph.D. dissertation, Brown University, Providence, R.I., (June, 1970).
5 Angulo, C. M. and Chang, W. S. C., "The excitation of a dielectric rod by a cylindrical waveguide," IRE Trans., MTT-6, pp. 389-393, (Oct. 1958).
6 Clarricoats, P. J. B. and Taylor, B. C., "Evenescent and propagating modes of dielectric loaded circular waveguide," Proc. IEE, Vol. III, pp. 1951-1956, (Dec. 1964).

Volume 9 (1974) Index for the Journal of Microwave Power by Authors and Subject

AUTHORS

SUBJECTS

Agriculture

Biological Effects

Drying

Economics

Food

Instrumentation and Measurement

FANSLOW, G. E., Liquid Crystal Mapping of Slotted Waveguide Fields; *9*, (3), 173-175.

KASHYAP, S. C., LEWIS, J. E. and STEEVES, M. H., A Surface-Wave Method for Measuring Moisture Content of Sheet Materials; *9*, (1), 13-21.

KRASZEWSKI, A., Determination of the Strength of Water Suspension Using Microwave Bridge Technique; *9*, (4)), 295-302.

KRASZEWSKI, A., KULIŃSKI, S. and CHEÇIŃSKI, K., Measurement of Moisture Content in Granular Ammonium Phosphate by Microwave Method; *9*, (4), 361-372.

McAFEE, R. D., CAZENAVETTE, L. L. and SHUBERT, H. A., Thermistor Probe Error in an X-Band Microwave Field; *9*, (3), 177-180.

McREE, D. I., Determination of Energy Absorption of Microwave Radiation Using the Cooling Curve Technique; *9*, (3), 263-270.

METAXAS, A. C. and DRISCOLL, J. L., A Comparison of the Dielectric Properties of Paper and Board at Microwave and Radio Frequencies; *9*, (2), 79-89.

OHLSSON, T., BENGTSSON, N. E. and RISMAN, P. O., The Frequency and Temperature Dependence of Dielectric Food Data at Determined by a Cavity Perturbation Technique; *9*, (2), 129-145.

RO, B., EHLERT, T. C. and ISHII, T. K., Sensitivity of Microwave Double Impedance Bridge for Fluid Analysis and Monitoring; *9*, (4), 373-380.

ROZZELL, T. C., JOHNSON, C. C., DURNEY, C. H., LORDS, J. L. and OLSEN, R. G., A Nonperturbing Temperature Sensor for Measurements in Electromagnetic Fields; *9*, (3), 241-249.

RZEPECKA, M. A. and HAMID, M. A. K., Modified Perturbation Method for Permittivity Measurements at Microwave Frequencies; *9*, (4), 317-328.

RZEPECKA, M. A. and PEREIRA, R. R., Permittivity of Some Dairy Products at 2450 MHz; *9*, (4), 277-288.

TIURI, M., LIIMATAINEN, P. and REINAMO, S., A Microwave Instrument for Measurement of Small Inhomogeneities in Supercalendar Rollers and Other Dielectric Cylinders; *9*, (2), 117-121.

TO, E. C., MUDGETT, R. E., WANG, D. I. C., GOLDBLITH, S. A. and DECAREAU, R. V., Dielectric Properties of Food Materials; *9*, (4), 303-316.

WYSLOUZIL, W. and VAN KOUGHNETT, A. L., An Attenuation Based Microwave Moisture Gauge for Sheet Materials; *9*, (2), 91-98.

Lumber

KASHYAP, S. C. and LEWIS, J. E., Microwave Processing of Tree Seeds; *9*, (2), 99-107.

Microwave Oven and Applicator Design

Microwave Power Generation

Paper

Regulations, Leakage and Safety

PUBLICATION POLICY - 1975

THE JOURNAL OF MICROWAVE POWER

Articles Submitted must comply with the procedure outlined below for rapid review and publication. Whereas no author will ever be penalized on publication preference for inability to comply with any of the procedures, it is anticipated that exceptions will be few. *Articles Submitted* should comply with the following procedure when submitted, and be in the form of a Paper, a Brief Communication or a Letter:

Copy: Typewritten, original plus two carbons or Xerox copies (for review) on white bond, 8½″ × 11″ or 10½″, double spaced. When correcting copy, authors are requested to use standard notations (The Author's Handbook and 'Preparing a Technical Manuscript', McGraw Hill Book Co., 1955).

Readers: Authors must have their manuscripts read by at least one colleague, who is not one of the authors, before submitting their manuscript, giving his name and address with the letter submission of the manuscript. (This procedure has been found to reduce significantly the publication time and overhead costs).

Referees: Authors may, if they wish, propose the names (giving full address) of two suitable reviewers. Either or both of the reviewers named may be consulted. Normally authors and the Editors will have the benefit of the opinions of four reviewers, but the names of the actual reviewers are never disclosed to anyone.

Style: No style Manual is accepted in toto. The style of the Canadian Journal of Physics and Forest Science (two examples) is preferred. Tables, figures, etc., should conform to the Style Manual of Biological Journals (American Institute of Biological Sciences, Second Edition, 1964). Abbreviations should conform to those given in the Word List of Scientific Periodicals, 1964 Edition. Symbols where possible, should comply with the I.E.E.E. recommended usage.

Abstracts must be concise, not more than 150 words. (Summaries will, in general, be unnecessary).

Units SI (others in brackets afterwards if necessary). Manuscripts that do not honor this requirement will be returned.

Tables must be numbered in sequence, typewritten on a separate sheet, with a title. Numerical designations should be used for footnotes to tables.

Data: Tabulated raw data is preferred; graphs should either be used to illustrate effects, or should have points labelled with actual numerical values. A combination of table (separate or inlaid) and graph is preferred, with either the standard deviation or the standard error shown. Papers presenting new significant experimental data will have preference in review and, if accepted, preference in publication space.

Methods must be given in such a way that the reader could repeat the experiment reported by the author. Attention to detail in this respect is demanded of papers in the area of microwave biology.

Illustrations and Figures: All drawings must be made on 8½" × 11" tracing paper, film or cloth. Lettering and lines are to be made with black India ink. Lettering must be of *letterguide quality* and with a *minimum height of 4 mm.* Both lettering and drawing should consist of lines of *0.4 mm minimum thickness.* Graphs should show as few reference or grid lines as possible. Blueprints, photostats, pencil drawings, or mimeographed copies are not suitable. Deviation from any of the above requirements will result in a *service charge.* A print of any form may be used for the second and third copies.

Photographs should be high quality 8" × 10" black and white glossy prints with *strong contrasts.* Photographs with the original should be mounted on sturdy 8½" × 11" card and should not be rolled, bent or fastened by paper clips. *The author's name* must appear in faint pencil on the back of the *mounted* photographs. Unmounted, unnamed copies should be attached to the carbon copies.

Captions: All photographs and illustrations must be *identified* and the relevant legends listed on a separate sheet.

Literature Cited: In the text 'Jones *et al.* (1964)' and under Literature Cited (after Acknowledgements, if any) Jones, K. O. and Burgen, P. 1964. Title of Journal, Volume No., Pages, is preferred. However, the author may use the alternative styles if he wishes.

Commercial Devices, Organizations: Full information on special commercial devices should be given in footnotes wherever possible.
Compliance with the above procedures will ensure rapid publication of accepted manuscripts and reduce publication costs to the Journal.

Review Papers are generally invited by the editors. If a writer wishes to submit a review paper to the Journal, he should write to the editor first.

Translations: Abstracts may, in 1975, be translated into French, German, Polish and Russian by the Institute.

Reprints (with covers) must be ordered at the time of publication to obtain the minimum price. Forms are sent out ahead of time.

Page Charges and Reprints: A voluntary page charge of twenty-five dollars ($25) per printed page is imposed on all articles accepted for publication in the Journal of Microwave Power. This voluntary page charge applies only to papers and brief communications and does not apply to letters.

Reprints of published articles will be furnished to authors only if specifically requested by authors in advance of printing. Fifty reprints with covers will be supplied without charge to authors who honor the voluntary page charge. Charges for requested reprints will be supplied to authors before publication at the prevailing rate. At present the rate is approximately $0.50 per copy of an average article.

Address all manuscripts to: The Editor, The Journal of Microwave Power, Division of Biomedical Engineering and Applied Sciences, Faculty of Graduate Studies and Research, Room 247 CE Bldg., The University of Alberta, Edmonton, Canada T6G 2E1.

Consider, for example, our TH 2054 klystron. There's never been a microwave-heating tube quite like it. Specifically designed for industrial and scientific applications, it gives a CW output of up to 50 kW in the 2450-MHz ISM band, at a money-saving electrical efficiency of better than 60 %. An extremely rugged tube, the TH 2054 is capable of operating into processing loads whose RF impedance may vary over quite a wide range. To lower amortization costs, we built-in such long-life features as a dispenser cathode and an ion pump.

If your requirements don't quite call for a 30-50 kW klystron, THOMSON-CSF still has the tube for you.

Our F 1123 and MCF 1327 magnetrons each deliver up to 5 kW of 2450-MHz microwave power. Both tubes are also available in handy, ready-to-use power packs.

So whatever the size of your microwave-heating job, look to THOMSON-CSF to supply the tube you need. For complete information on all these tubes, just circle the appropriate number on the Reader's Service Card, or contact us directly.

In search of a microwave-heating tube? You've come to the right place!

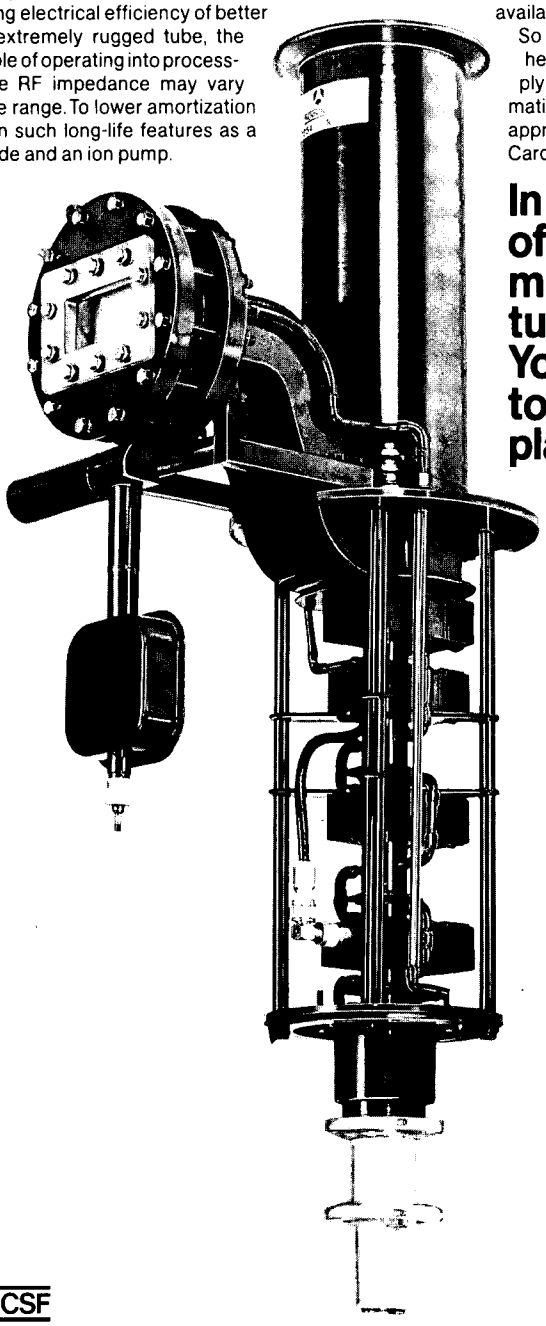

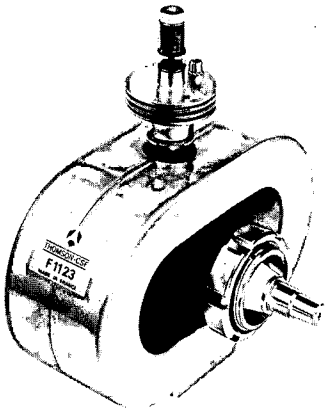

THOMSON-CSF

THOMSON-CSF ELECTRON TUBES. INC.
750 BLOOMFIELD AVENUE / CLIFTON NJ 07015 / TEL. (201) 779.1004 / TWX : 710 989 7149

France - THOMSON-CSF Groupement Tubes Electroniques / 8, rue Chasseloup-Laubat / 75737 PARIS CEDEX 15 / Tél. (1) 566 70.04
Germany - THOMSON-CSF Elektronenröhren GmbH / Am Leonhardsbrunn 10 / 6 FRANKFURT/MAIN / Tel. (0611) 70 20.99
Italy - THOMSON-CSF Tubi Elettronici SRL / Viale degli Ammiragli 71 / ROMA / Tel. (6) 38 14.58
Japan - THOMSON-CSF Japan K. K. / Kyosho Building / 1. 9. 3. Hirakawa-cho / Chiyoda-ku / TOKYO 〒 102 / Tel. (03) 264.6341
Spain - THOMSON-CSF Tubos Electronicos SA / Alcala 87 / 7° Dcha / MADRID 9 / Tel. (1) 226 76.09
Sweden - THOMSON-CSF Elektronrör AB / Box 27080 / S 10251 STOCKHOLM 27 / Tel. (08) 22 58.15
United Kingdom - THOMSON-CSF Electronic Tubes Ltd / Ringway House / Bell Road / Daneshill / BASINGSTOKE RG24 OQG / Tel. (0256) 29155